30 SMOKE EXCEPTIONAL EVENTS: April 5 – July 11, 2011

30.1 Summary of Events

2011 saw a very active fire season in Arizona, New Mexico and Mexico. Readings at the SPCY $PM_{2.5}$ Partisol monitor were elevated above the annual NAAQS of 12 µg/m^3 repeatedly beginning in early April and continuing through early July, corresponding with the fire season. Table 30-1, below, shows the dates and concentrations of $PM_{2.5}$ in µg/m^3 for which NMED believes smoke impacted the area and 24-hour average.

Date of exceedance	SPCY $PM_{2.5}$ Partisol 24-Hour Average (µg/m^3)
4/5/2011	23.7
4/12/2011	16.5
4/17/2011	19.9
4/21/2011	15.9
4/22/2011	16.8
4/25/2011	31.6
4/30/2011	23.0
5/1/2011	25.4
5/5/2011	33.1
5/6/2011	16.5
5/16/2011	16.4
5/17/2011	21.8
5/19/2011	20.9
5/26/2011	16.5
5/27/2011	18.3
5/30/2011	17.7
5/31/2011	20.8
6/2/2011	16.4
6/3/2011	18.8
6/7/2011	18.0
6/8/2011	19.5
6/11/2011	25.3
6/12/2011	21.3
6/16/2011	17.8
6/18/2011	22.7
6/20/2011	16.7
6/22/2011	30.9
6/26/2011	19.3
6/27/2011	23.4
7/7/2011	24.5
7/10/2011	21.4
7/11/2011	24.8

Table 30-1. Dates impacted by smoke during 2011.

In effect, New Mexico was surrounded by wildfires, several of them quite large (over 10,000 acres), for most of this time period. The following screenshots (Figures 30-1 to 30-32), one for each date listed in Table 30-1, are from Weather Underground's Wundermap® showing satellite-detected fires as red-orange flame icons. Satellites reporting fire detects include GOES-EAST, GOES-WEST, MODIS TERRA, MODIS AQUA, AVHRR METOP-02, AVHRR NOAA-15, AVHRR NOAA-18 AND AVHRR NOAA-19. Times of day vary because satellite coverage times vary. The yellow star superimposed on each map indicates the approximate location of the SPCY Partisol monitor.

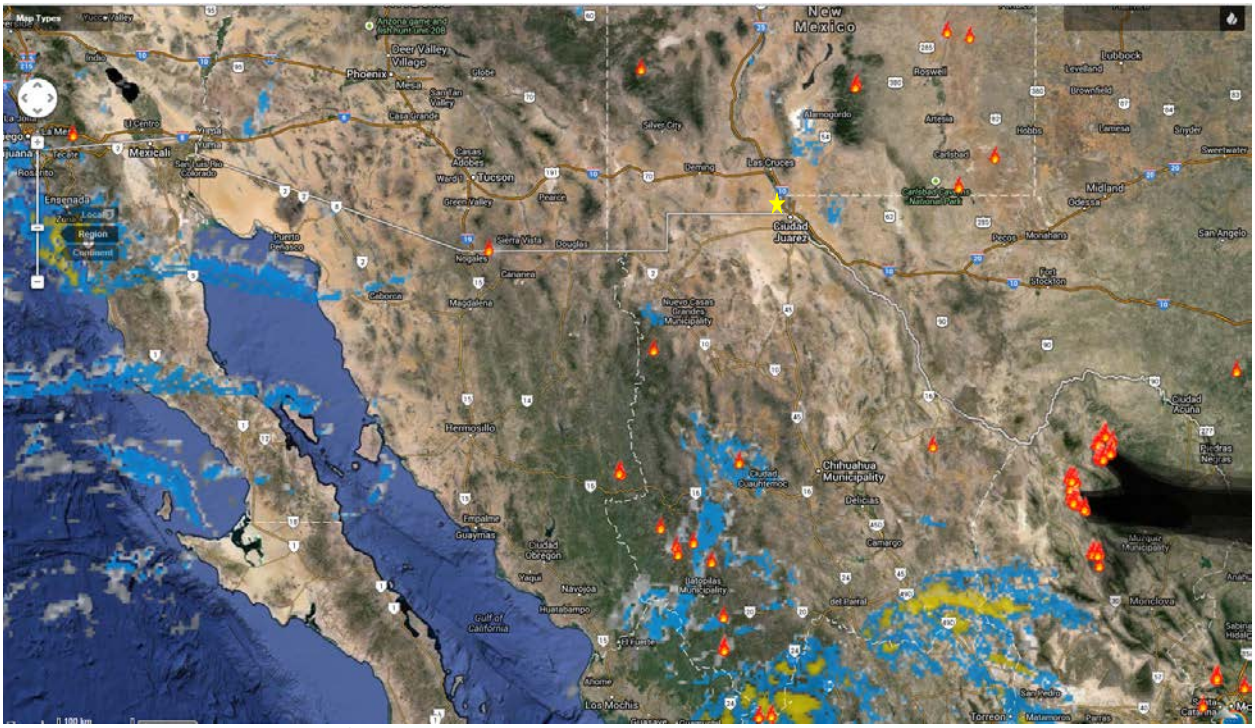

Figure 30-1. Satellite-detected active fires April 5, 2011, 1400 hr.

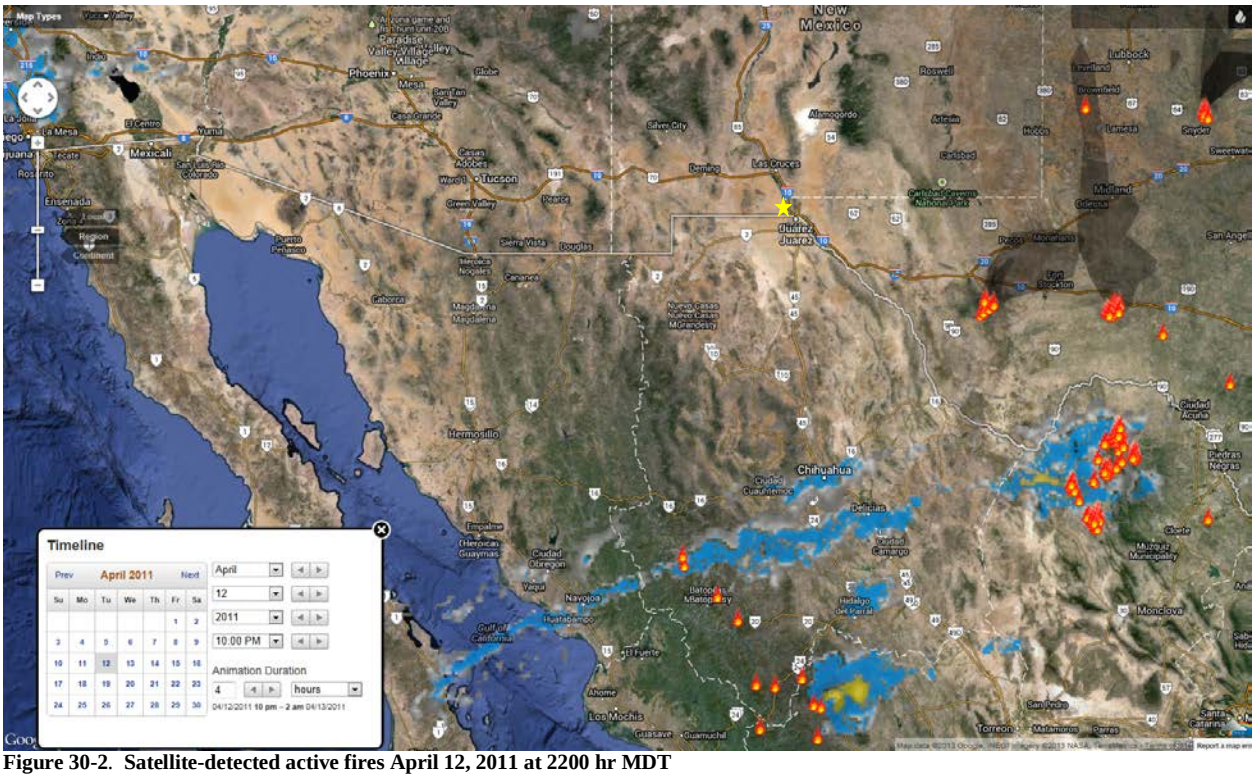

Figure 30-2. Satellite-detected active fires April 12, 2011 at 2200 hr MDT

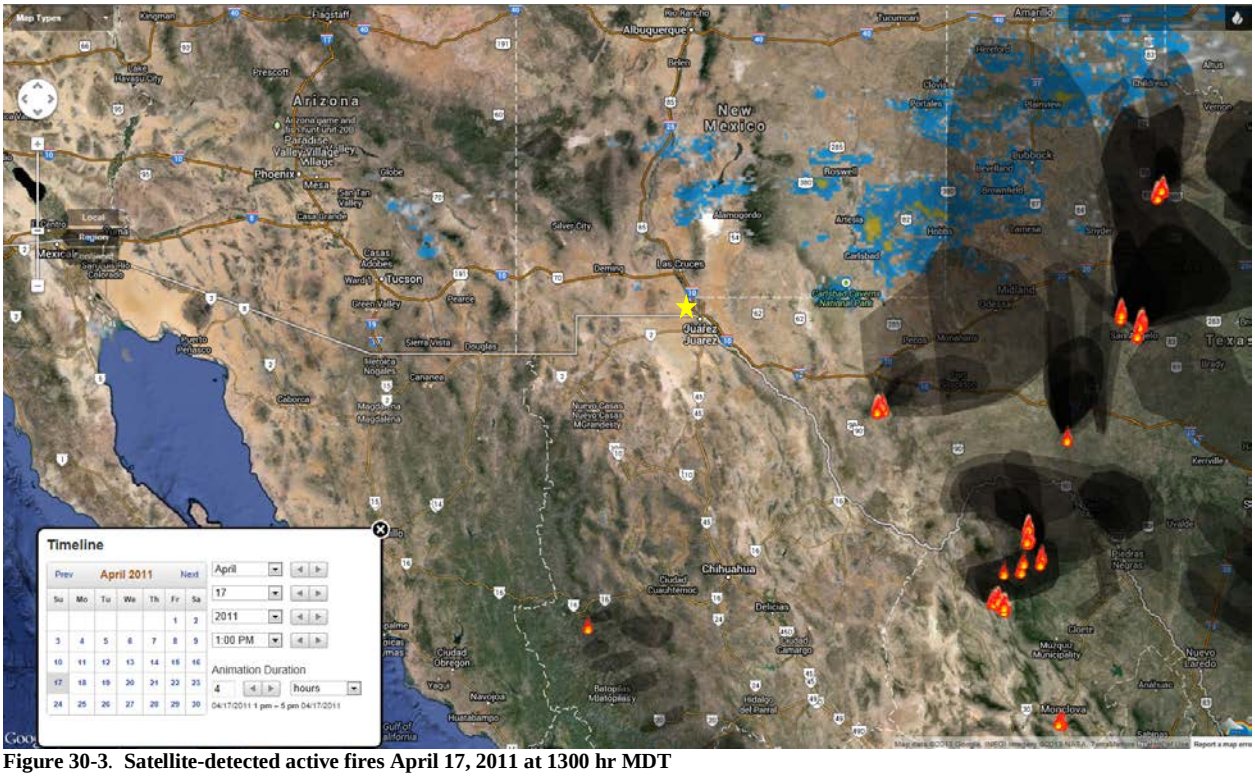

Figure 30-3. Satellite-detected active fires April 17, 2011 at 1300 hr MDT

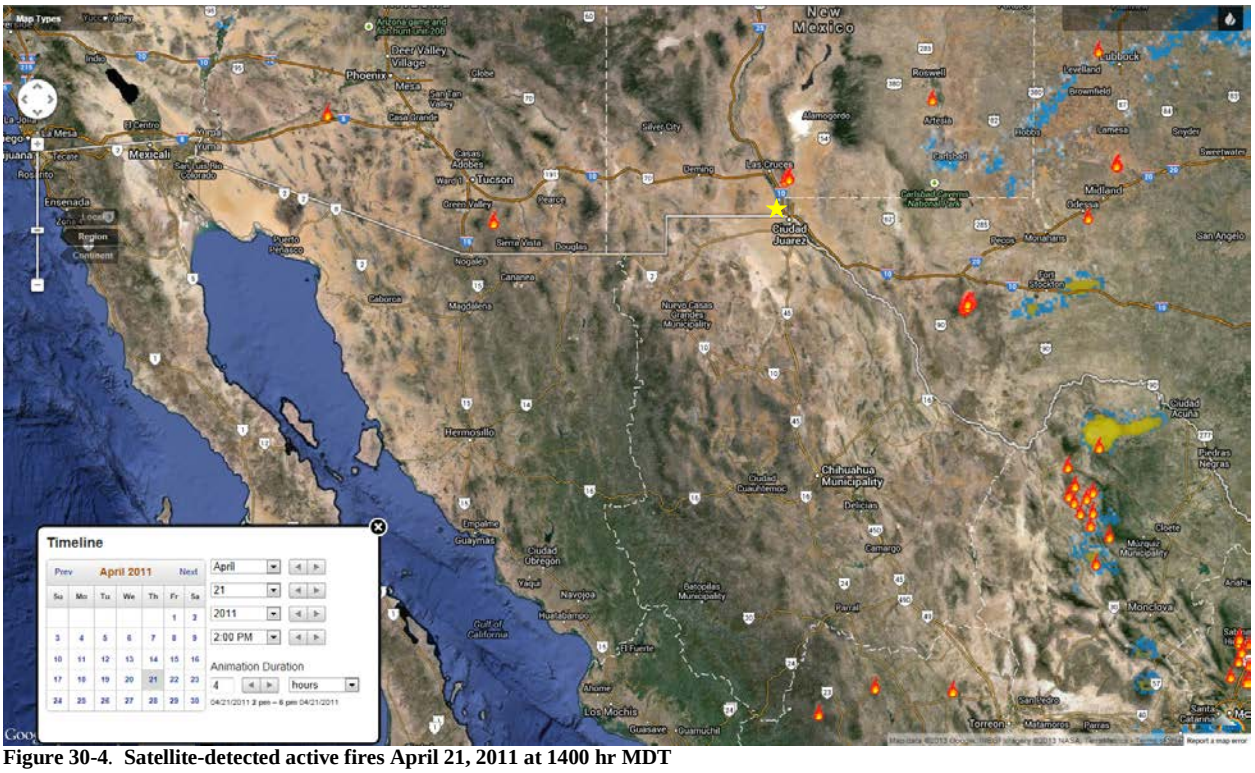

Figure 30-4. Satellite-detected active fires April 21, 2011 at 1400 hr MDT

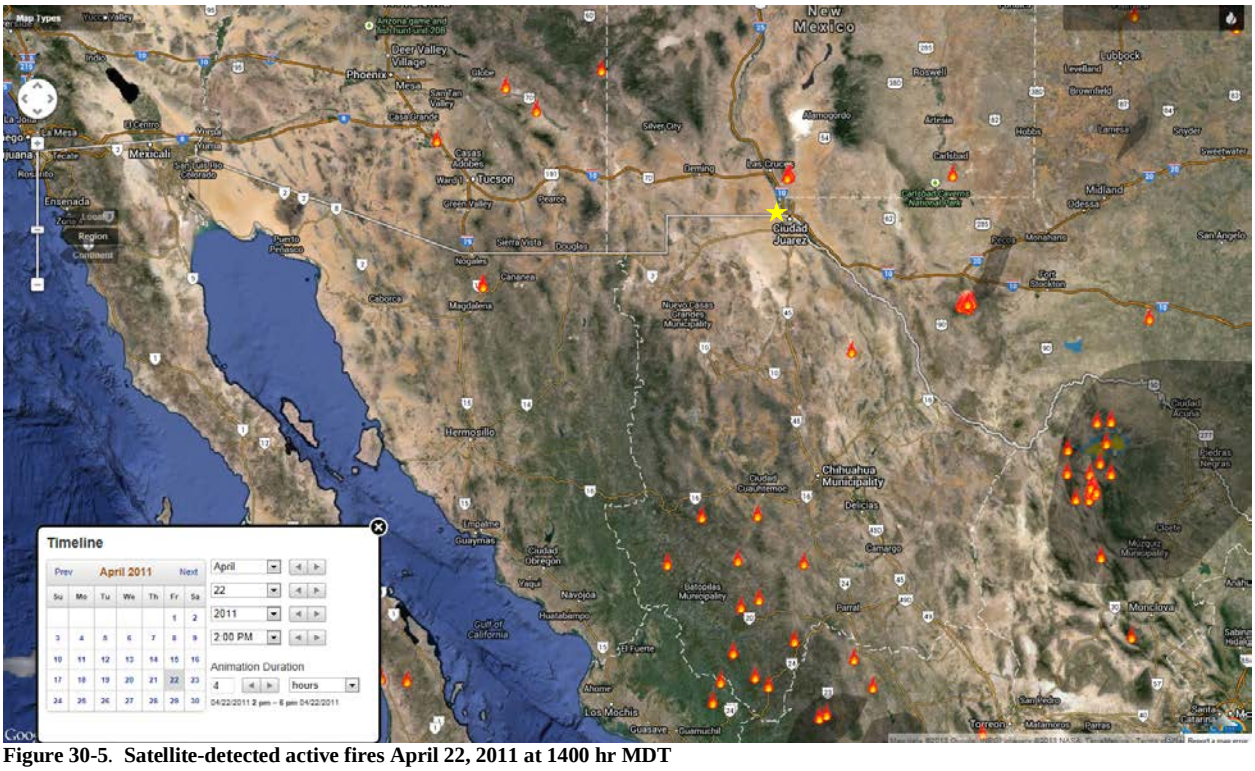

Figure 30-5. Satellite-detected active fires April 22, 2011 at 1400 hr MDT

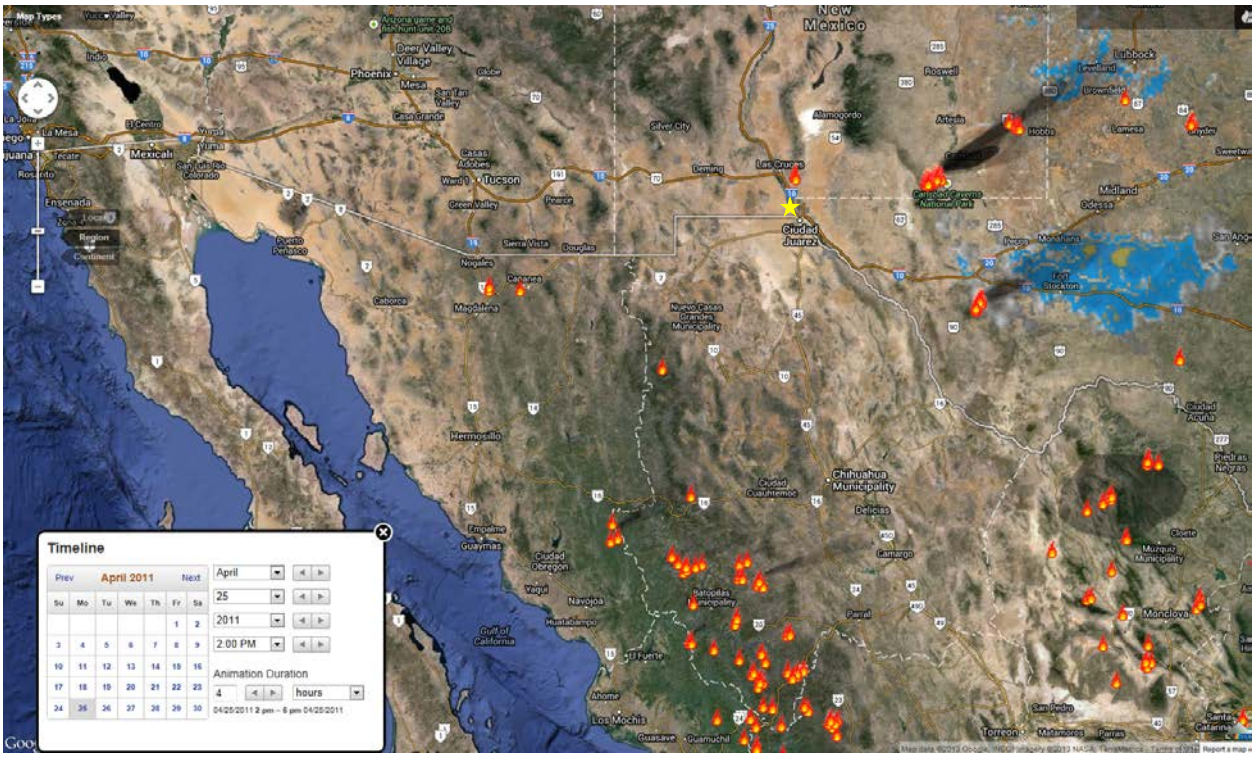

Figure 30-6. Satellite-detected active fires April 25, 2011 at 1400 hr MDT

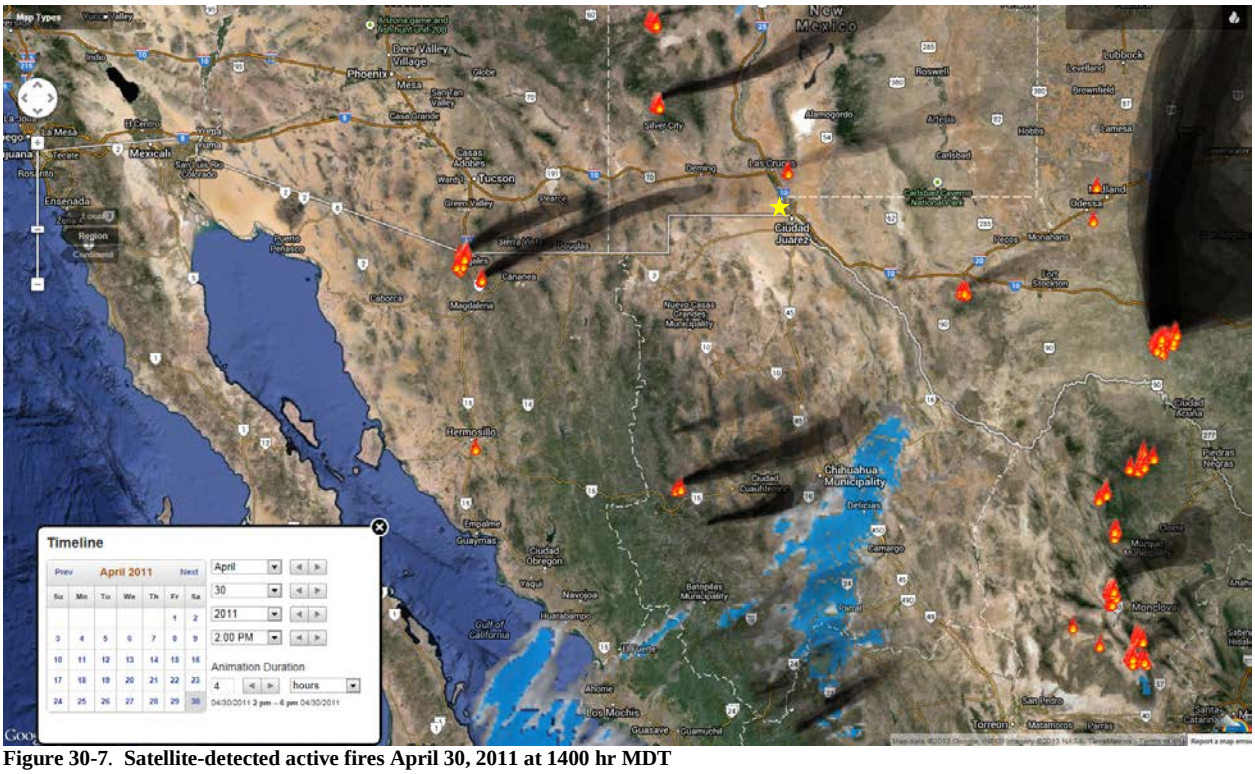

Figure 30-7. Satellite-detected active fires April 30, 2011 at 1400 hr MDT

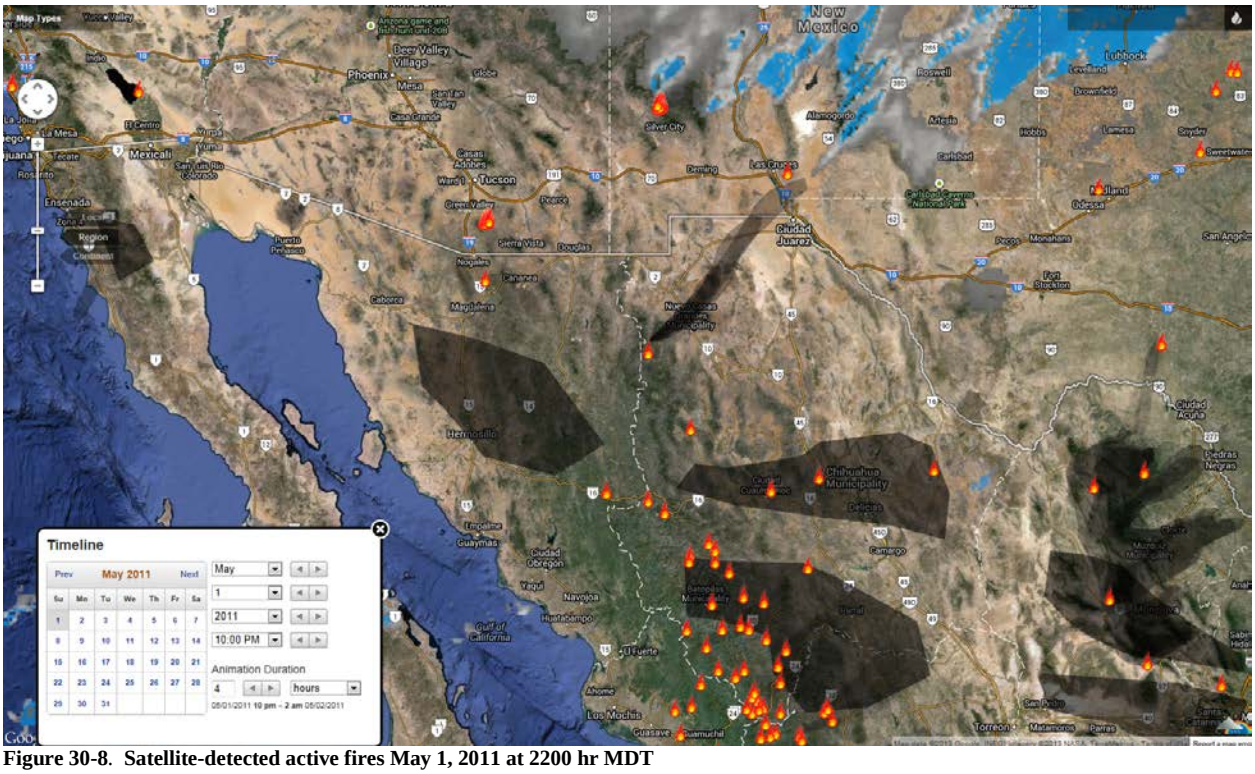

Figure 30-8. Satellite-detected active fires May 1, 2011 at 2200 hr MDT

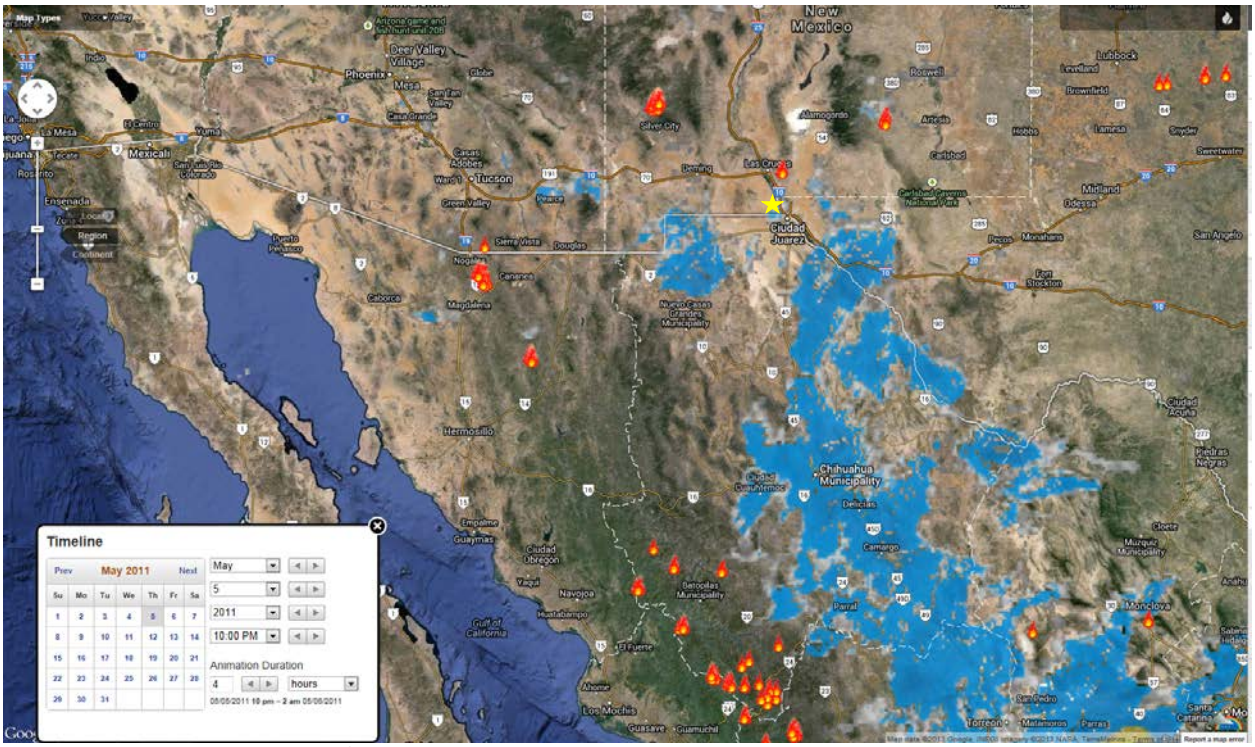

Figure 30-9. Satellite-detected active fires May 5, 2011 at 2200 hr MDT

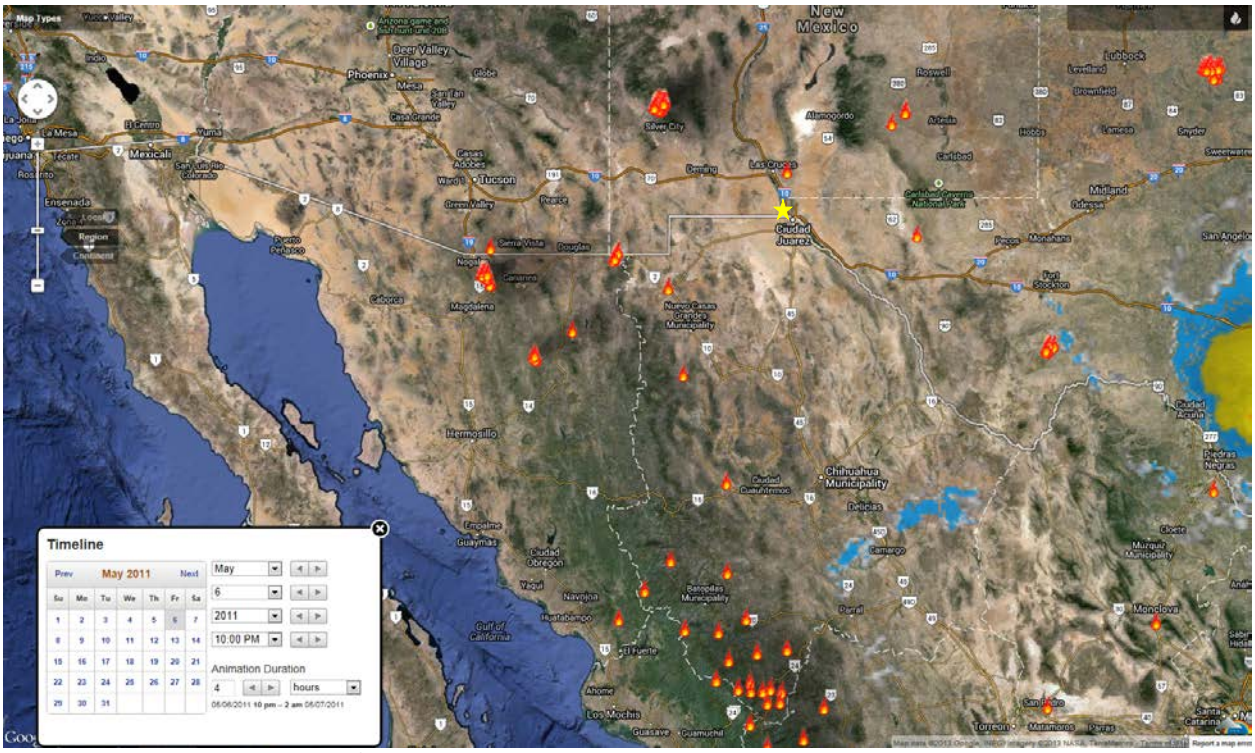

Figure 30-10. Satellite-detected active fires May 6, 2011 at 2200 hr MDT

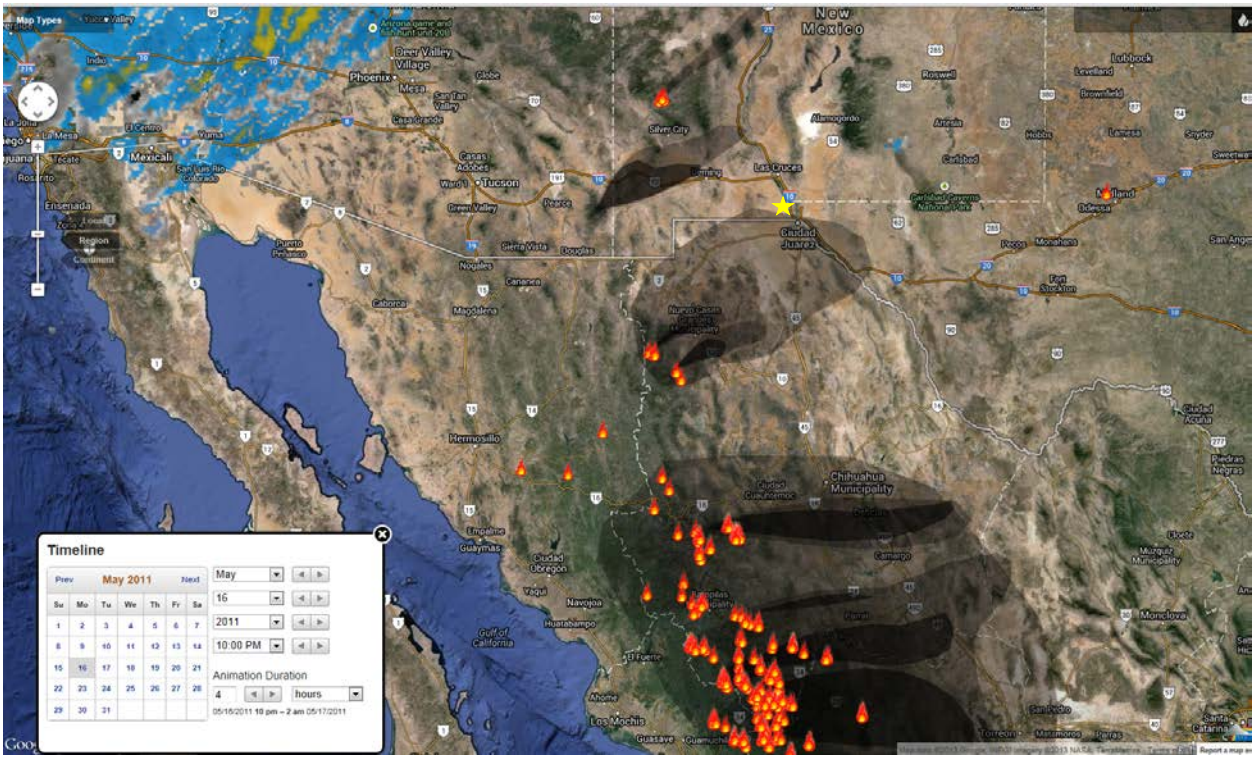

Figure 30-11. Satellite-detected active fires May 16, 2011 at 2200 hr MDT

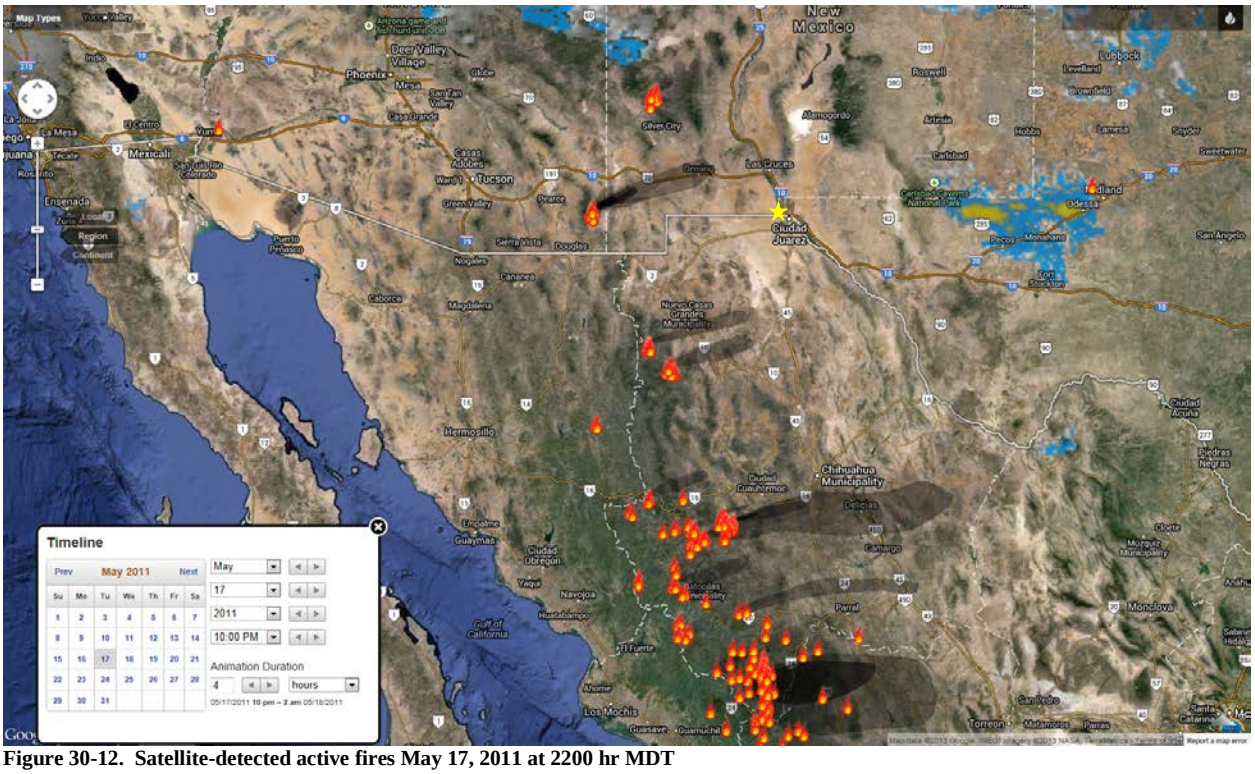

Figure 30-12. Satellite-detected active fires May 17, 2011 at 2200 hr MDT

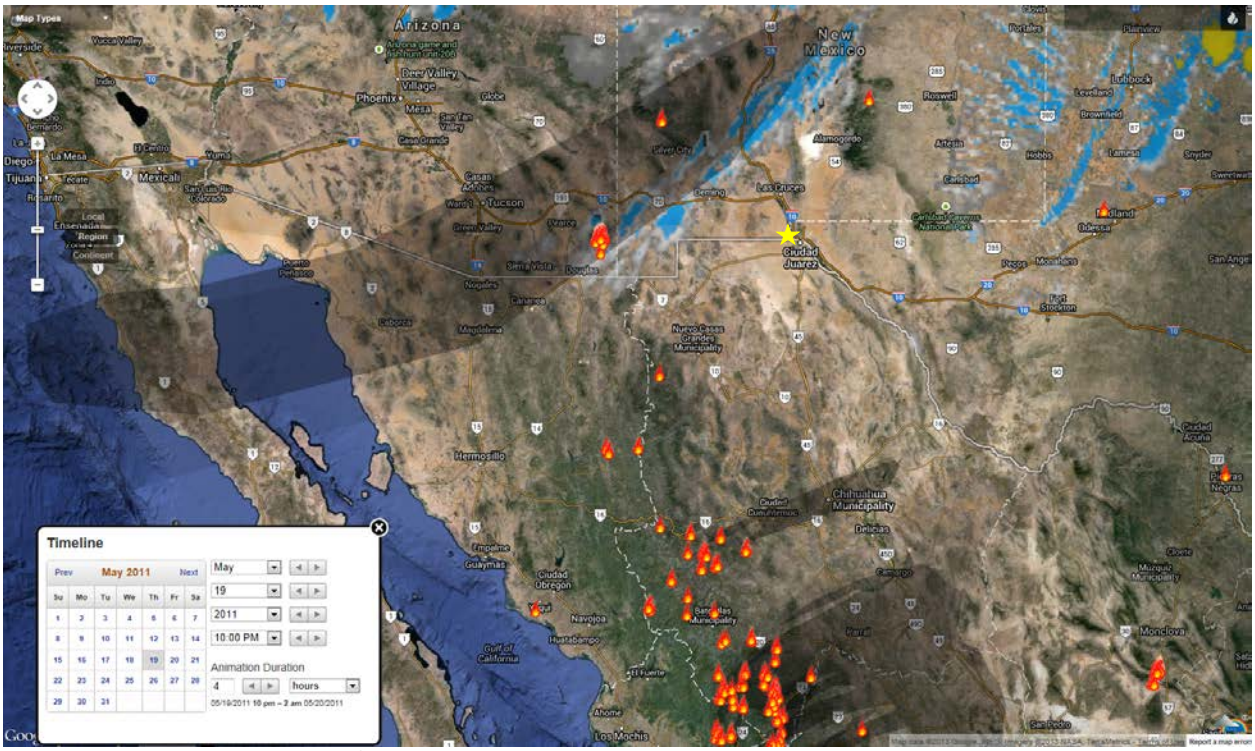

Figure 30-13. Satellite-detected active fires May 19, 2011 at 2200 hr MDT

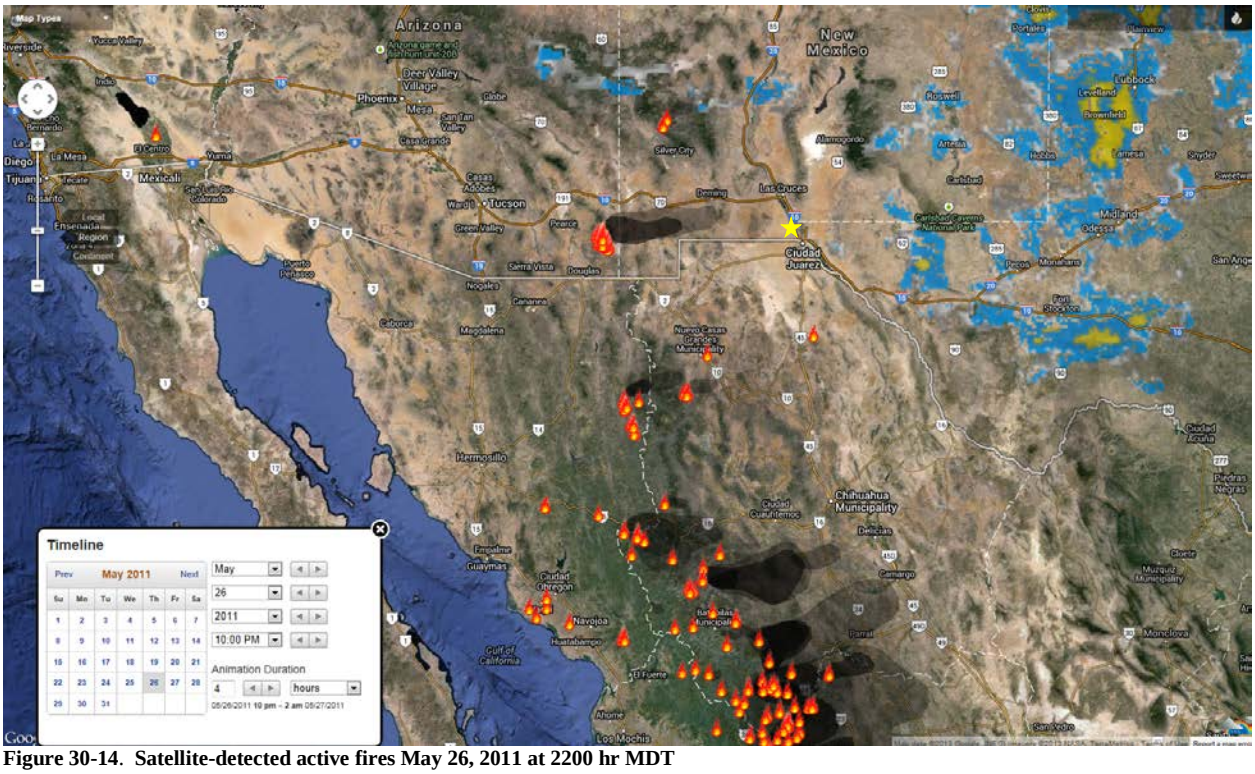

Figure 30-14. Satellite-detected active fires May 26, 2011 at 2200 hr MDT

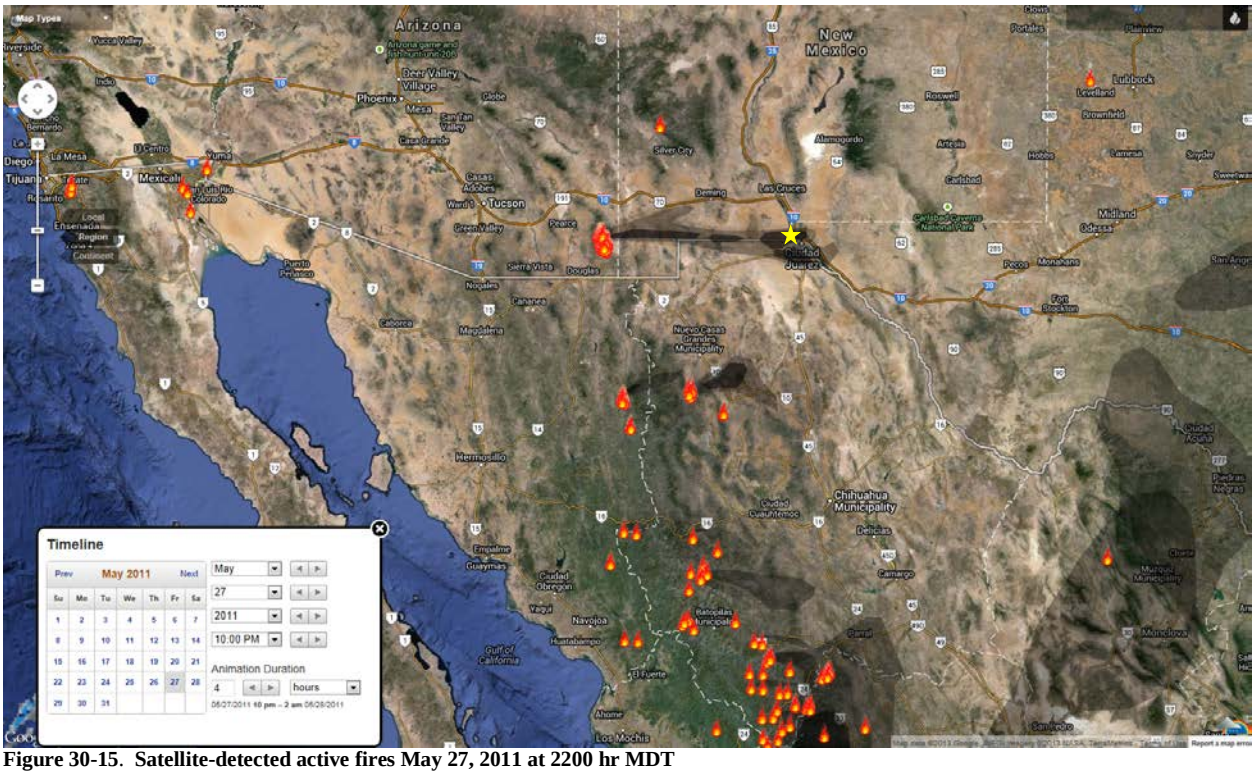

Figure 30-15. Satellite-detected active fires May 27, 2011 at 2200 hr MDT

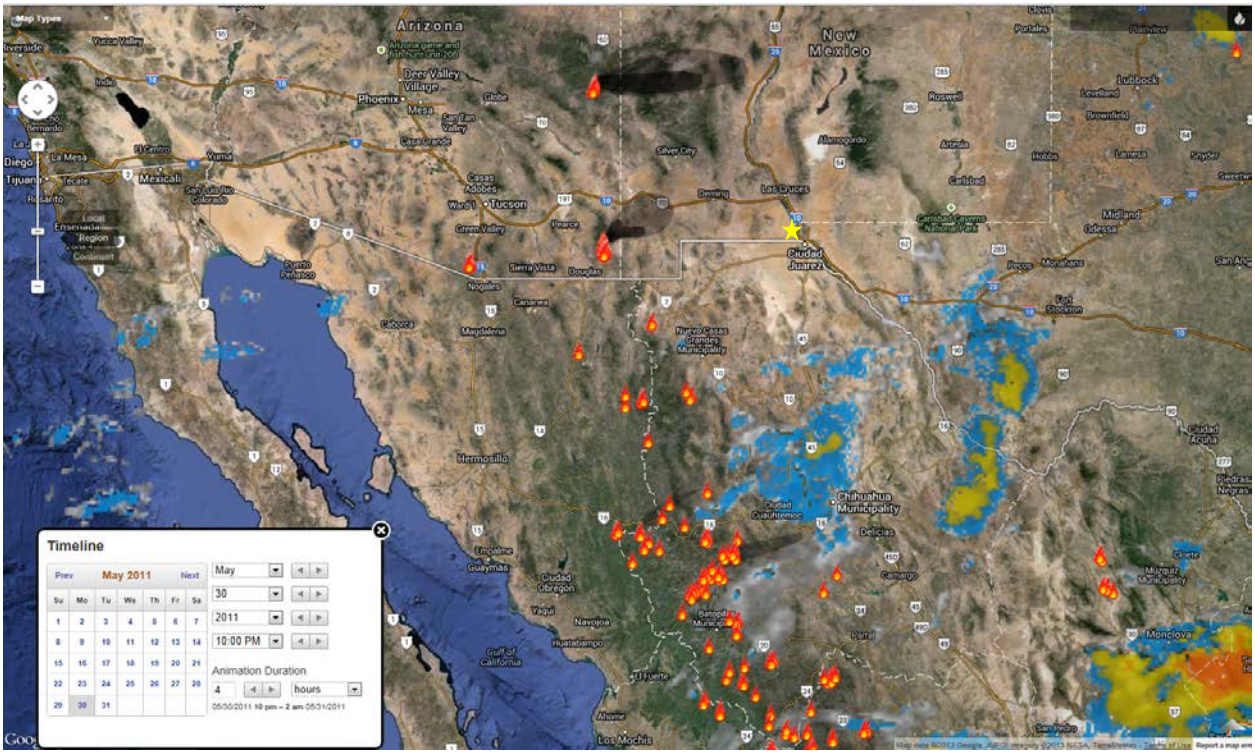

Figure 30-16. Satellite-detected active fires May 30, 2011 at 2200 hr MDT

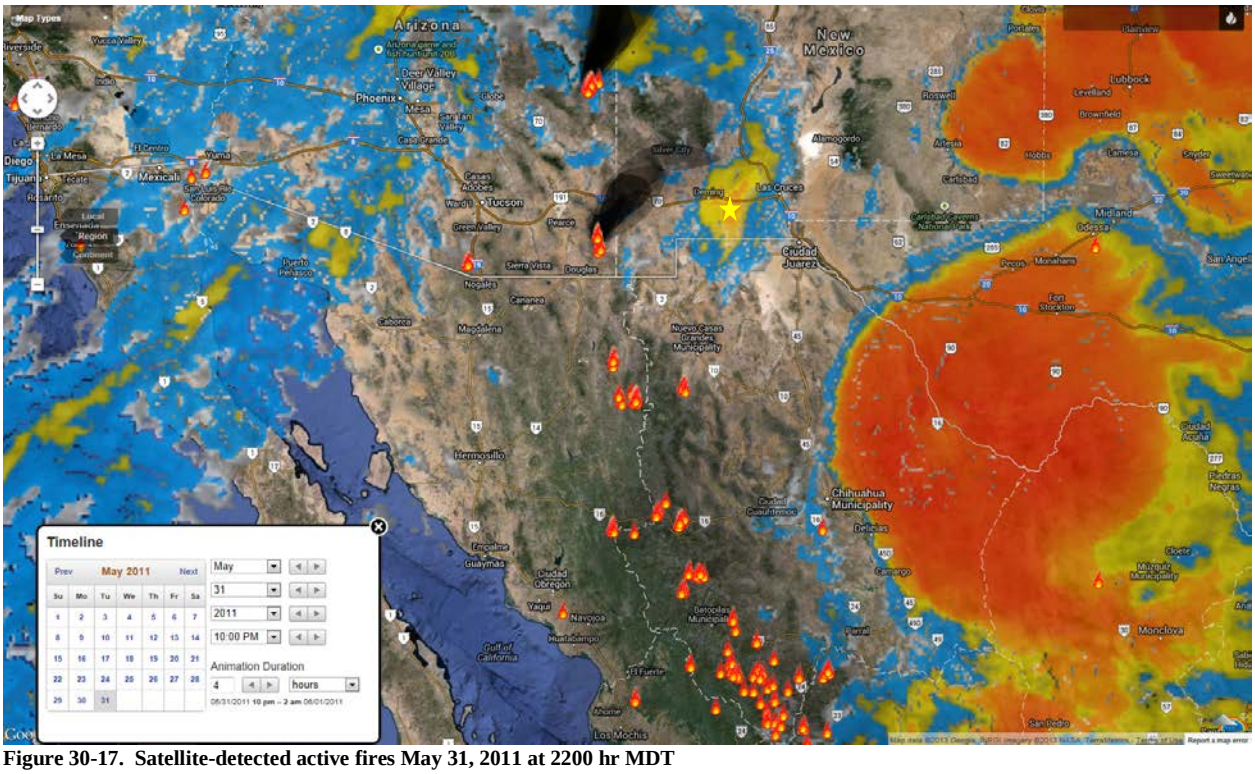

Figure 30-17. Satellite-detected active fires May 31, 2011 at 2200 hr MDT

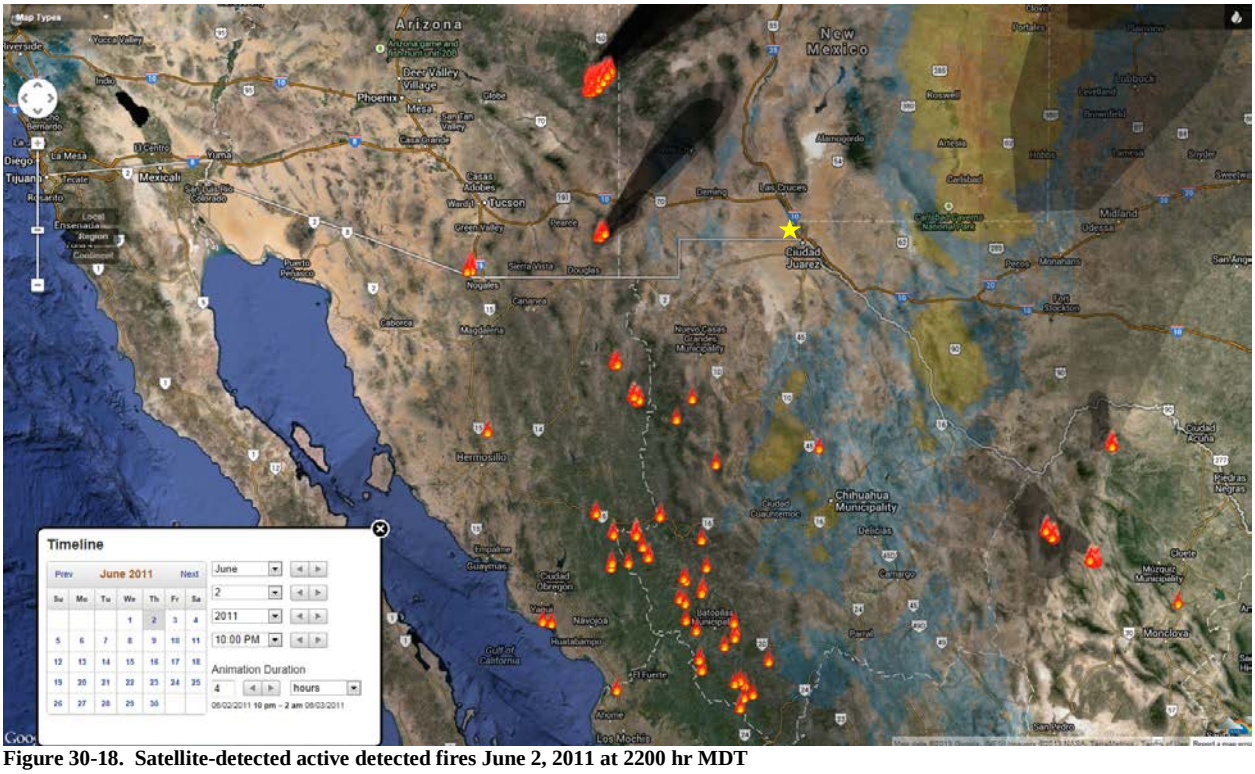

Figure 30-18. Satellite-detected active detected fires June 2, 2011 at 2200 hr MDT

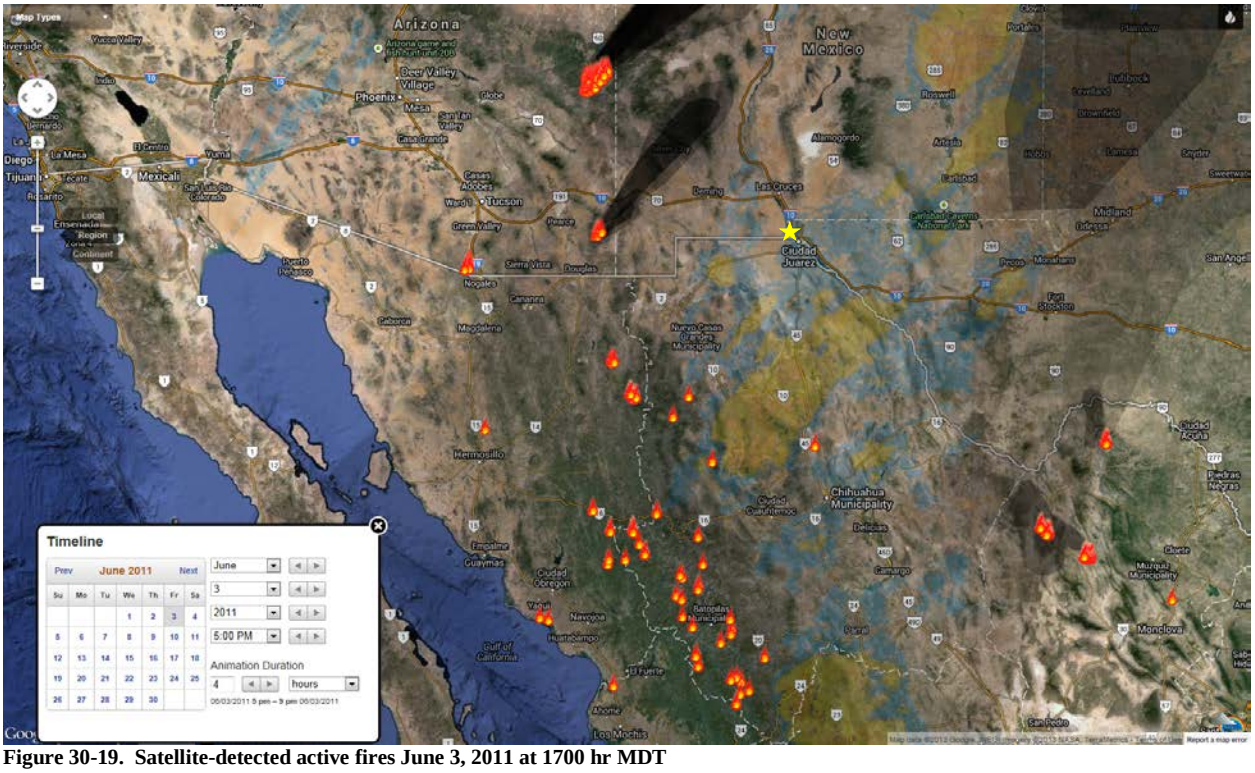

Figure 30-19. Satellite-detected active fires June 3, 2011 at 1700 hr MDT

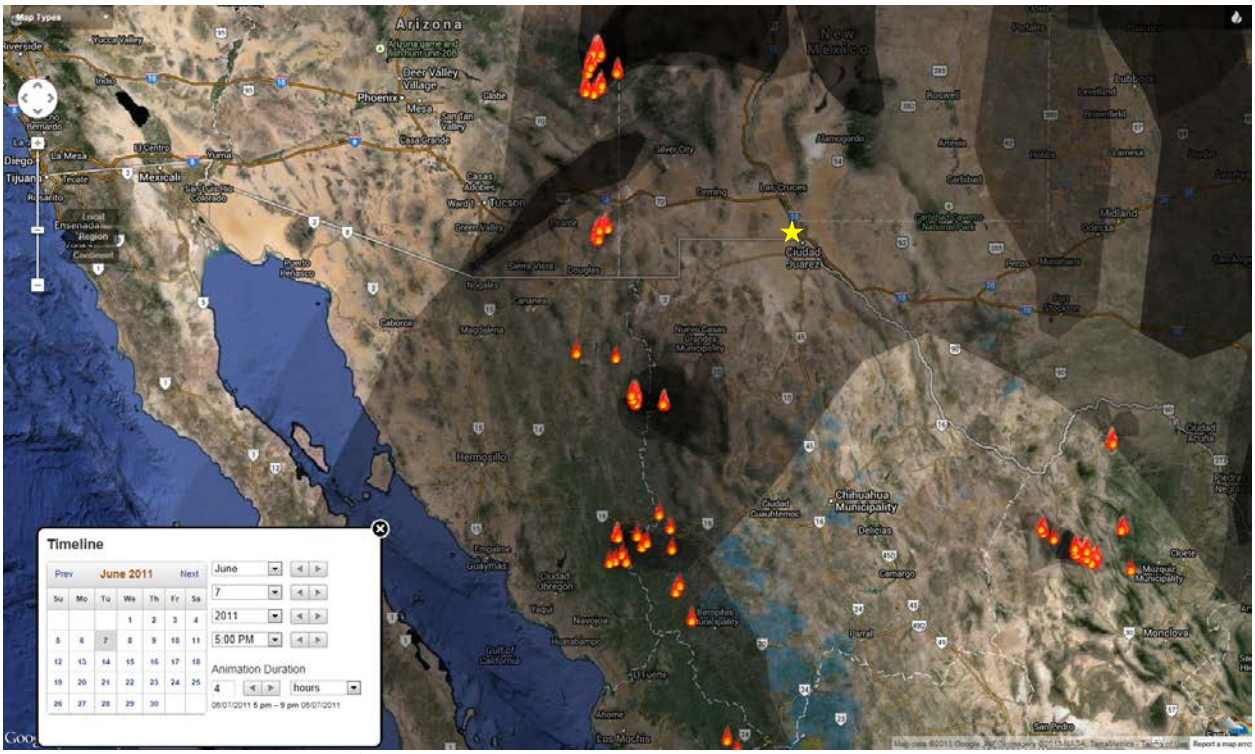

Figure 30-20. Satellite-detected active fires June 7, 2011 at 1700 hr MDT

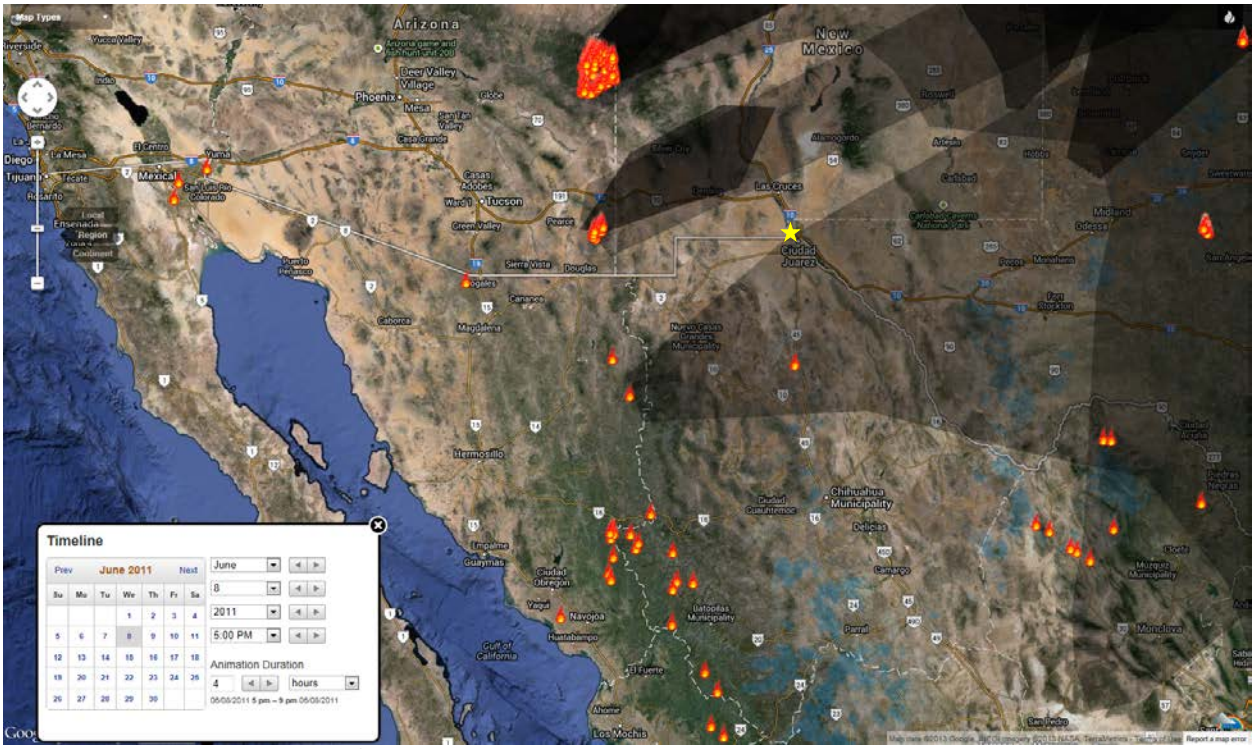

Figure 30-21. Satellite-detected active fires June 8, 2011 at 1700 hr MDT

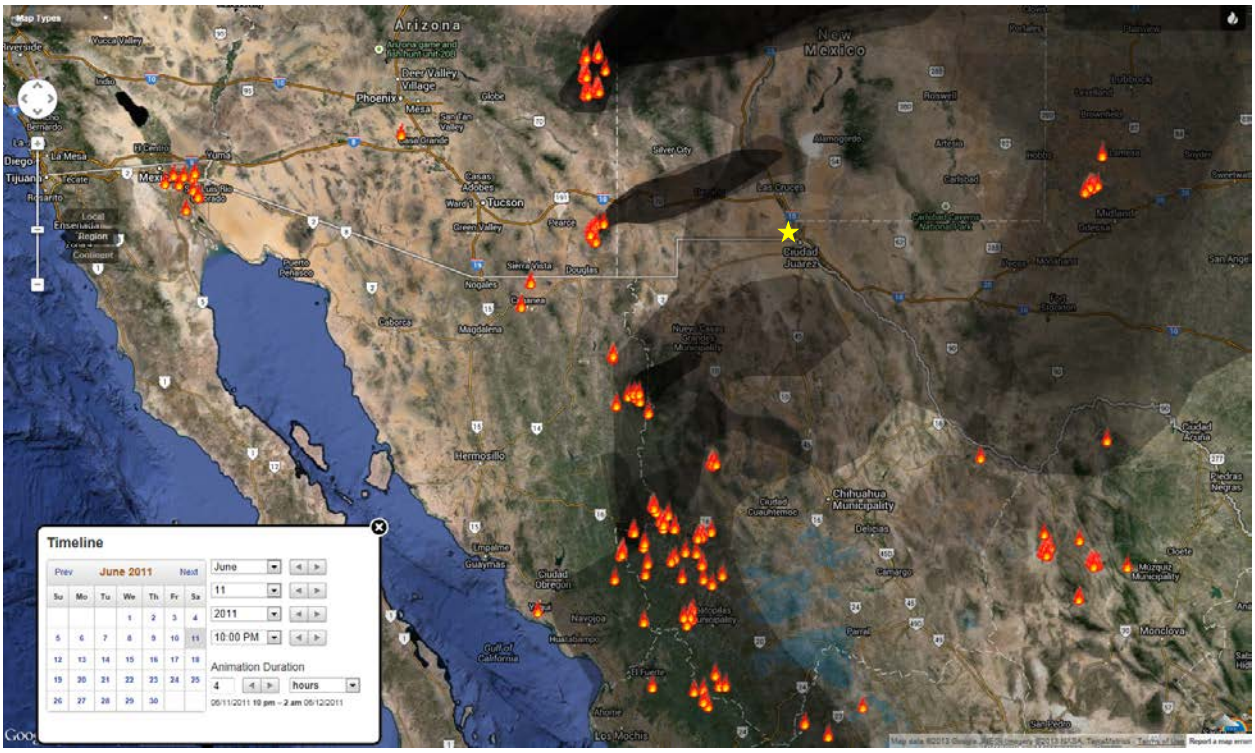

Figure 30-22. Satellite-detected active fires June 11, 2011 at 2200 hr MDT

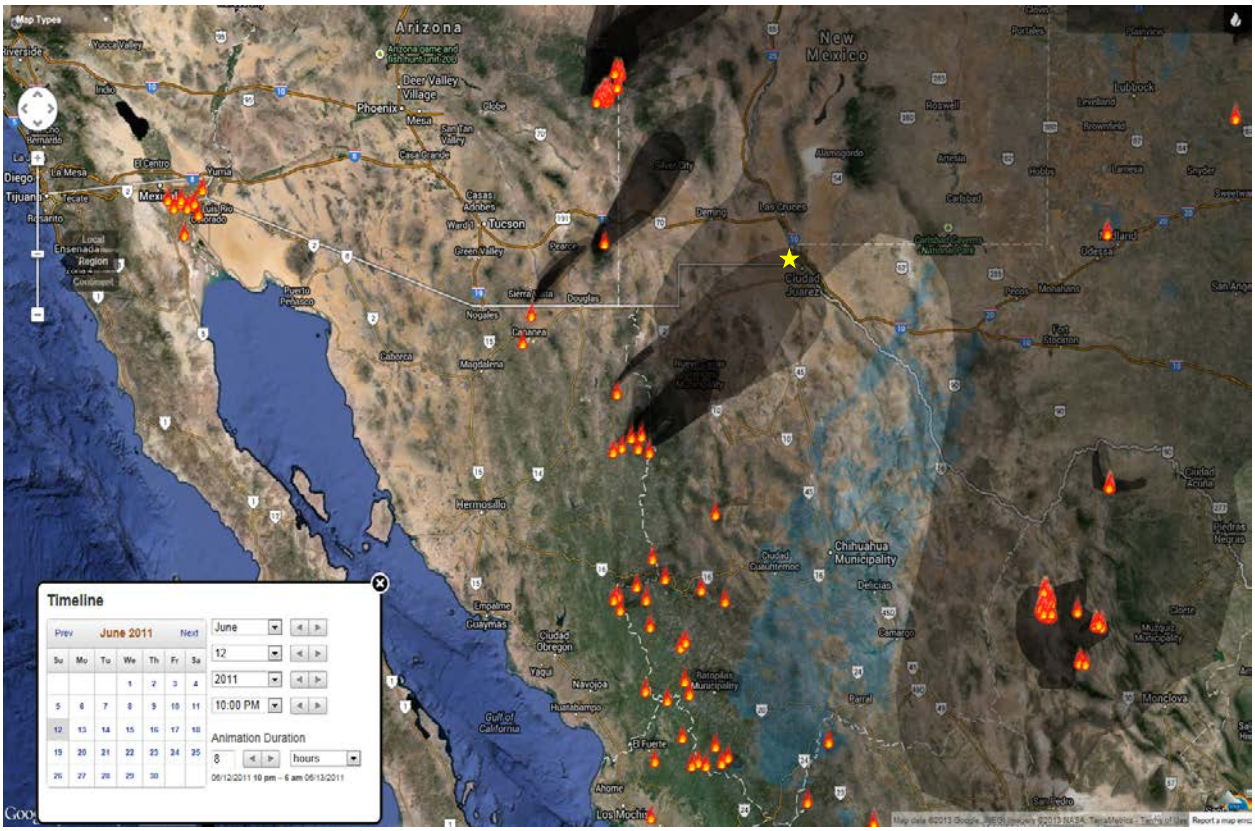

Figure 30-23. Satellite-detected active fires June 12, 2011 at 2200 hr MDT

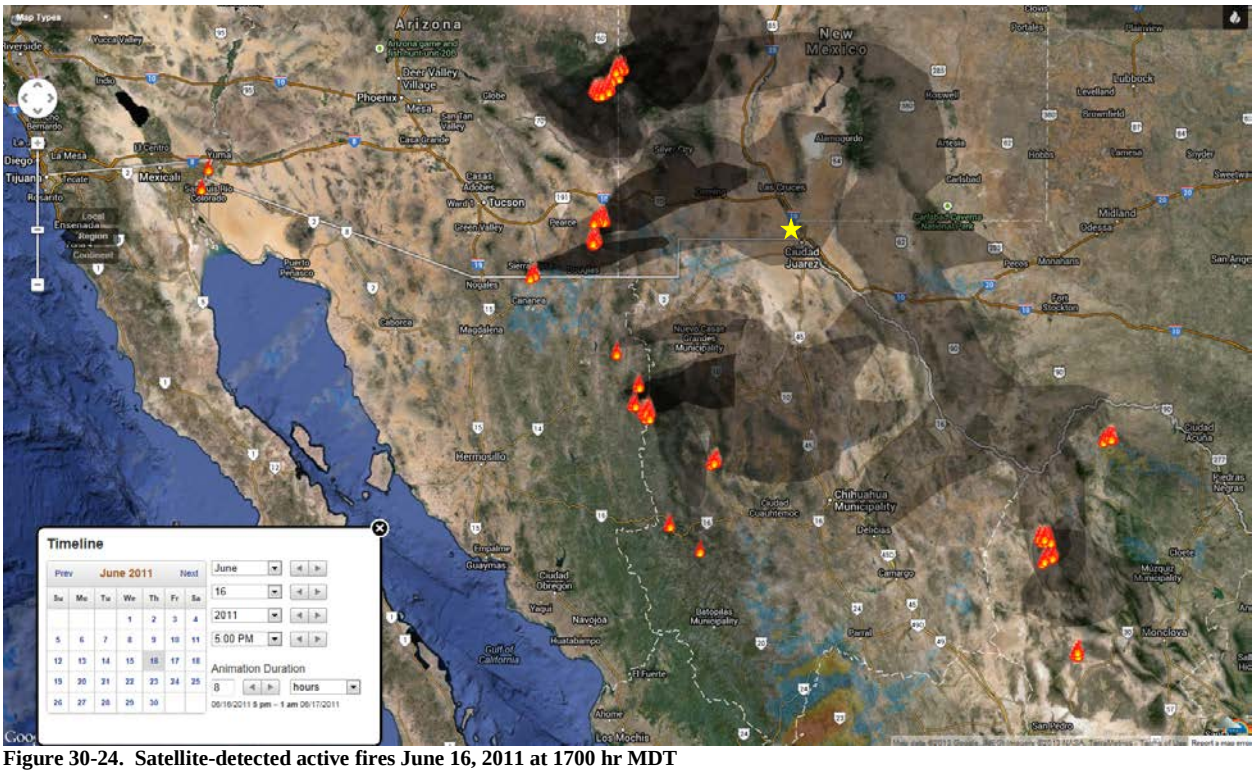

Figure 30-24. Satellite-detected active fires June 16, 2011 at 1700 hr MDT

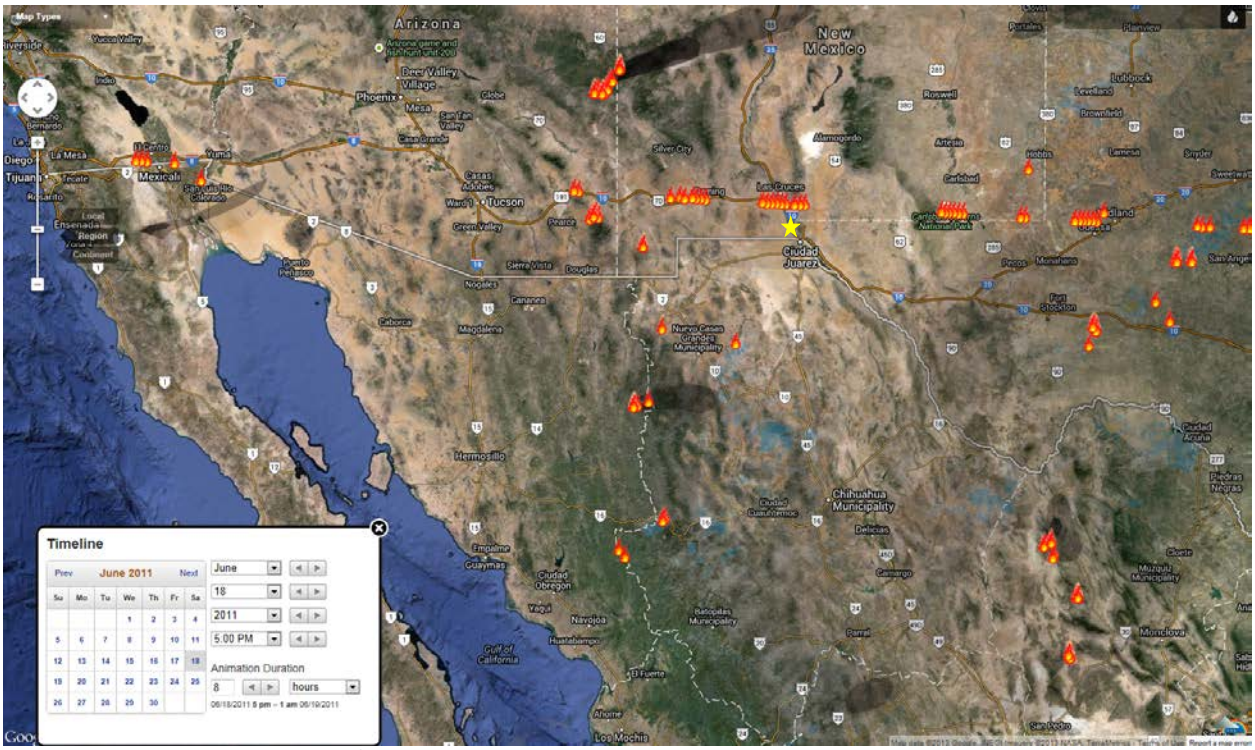

Figure 30-25. Satellite-detected active fires June 18, 2011 at 1700 hr MDT

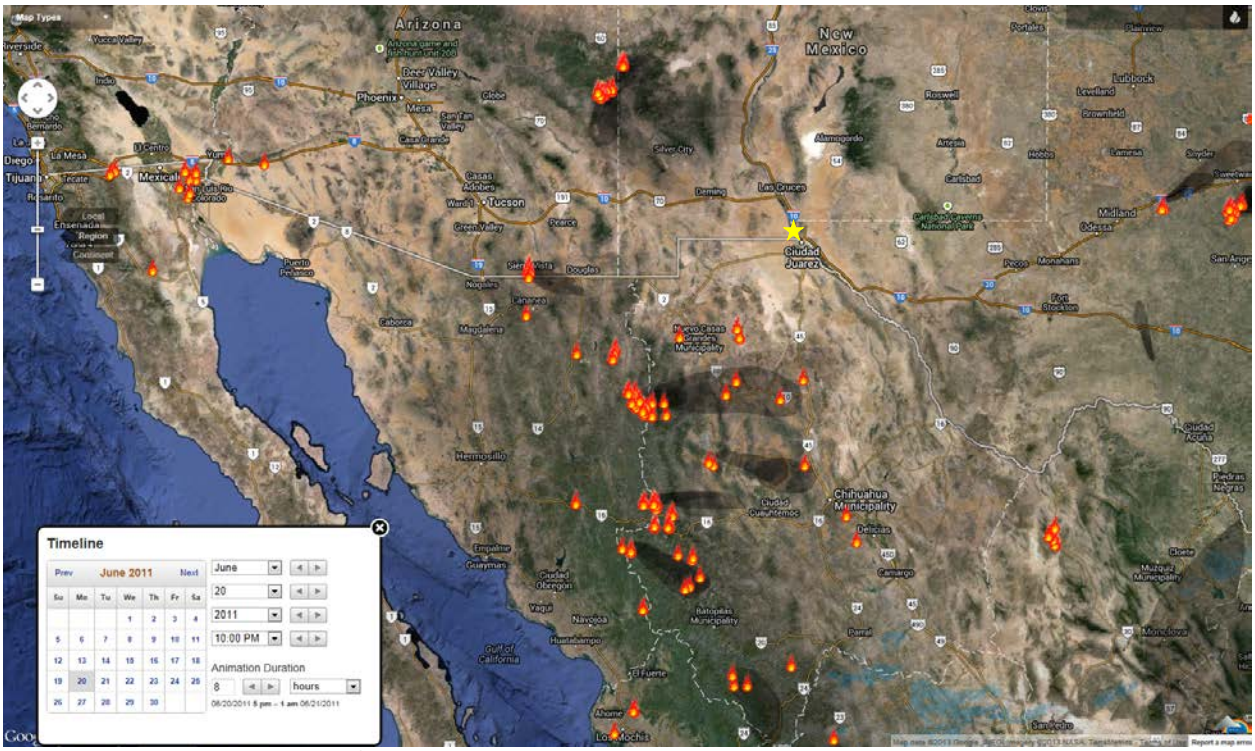

Figure 30-26. Satellite-detected active fires June 20, 2011 at 2200 hr MDT

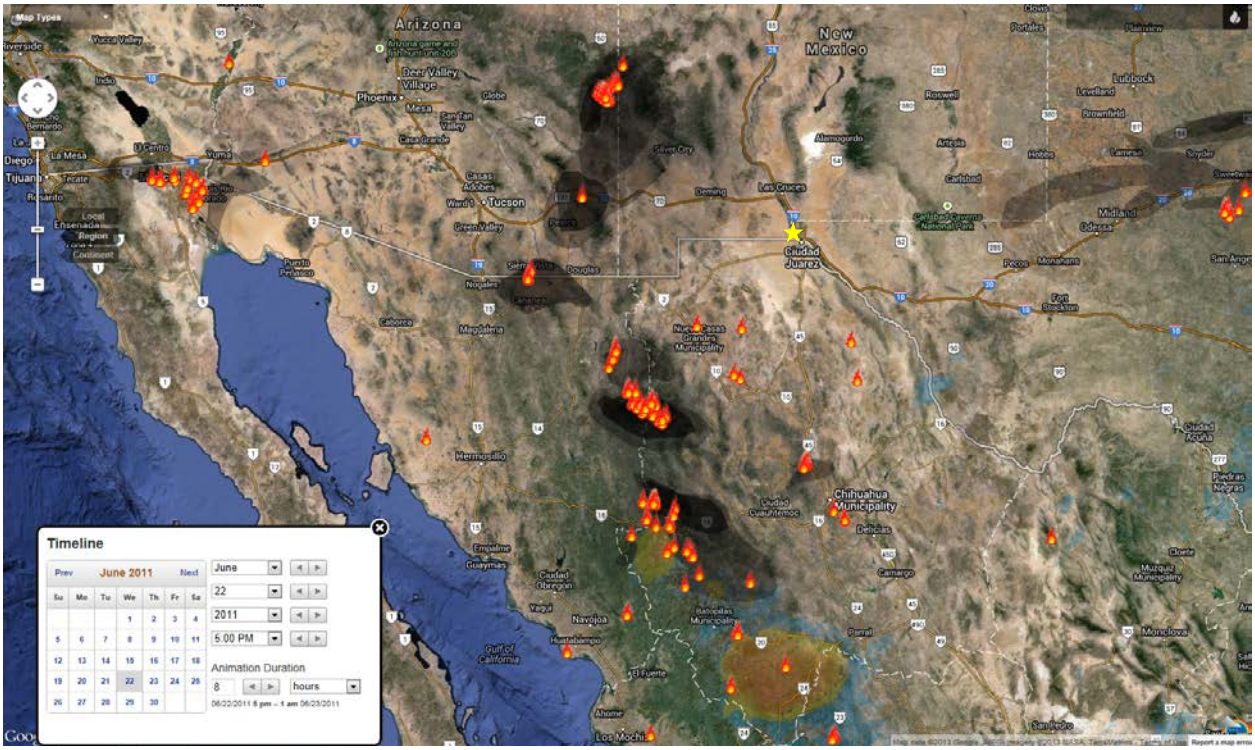

Figure 30-27. Satellite-detected active fires June 22, 2011 at 1700 hr MDT

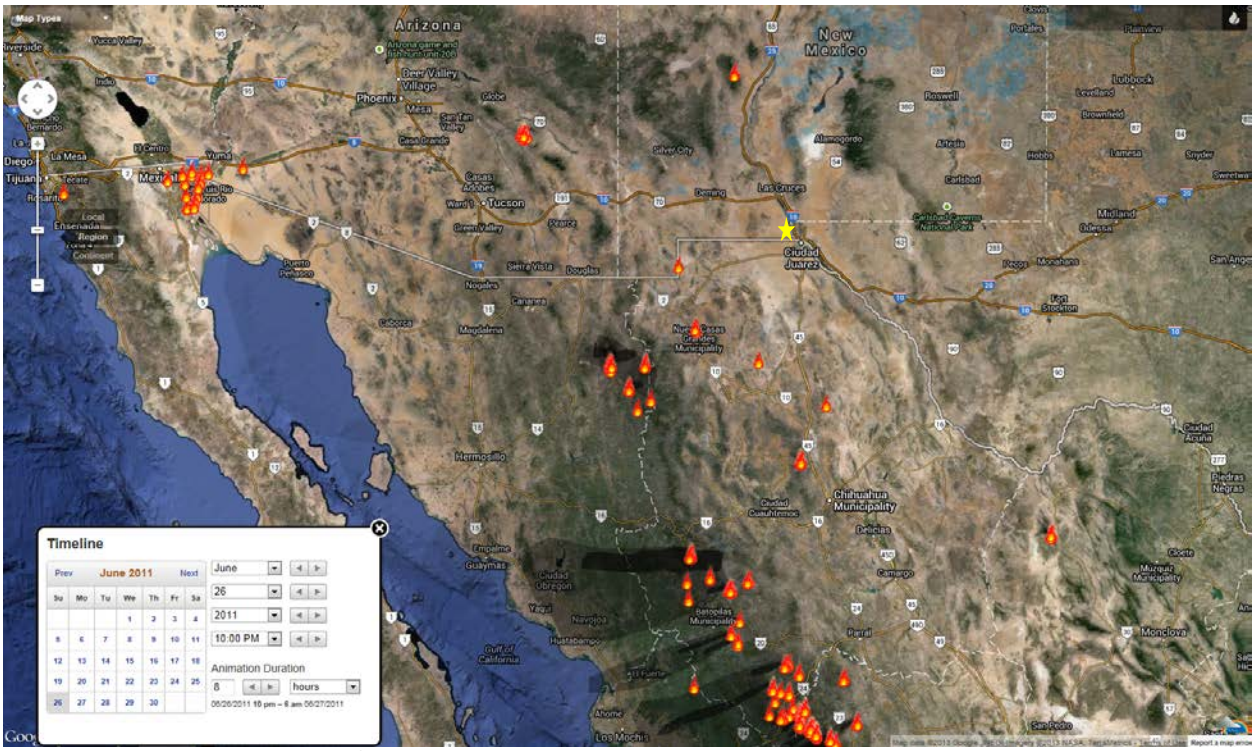

Figure 30-28. Satellite-detected active fires June 26, 2011 at 2200 hr MDT

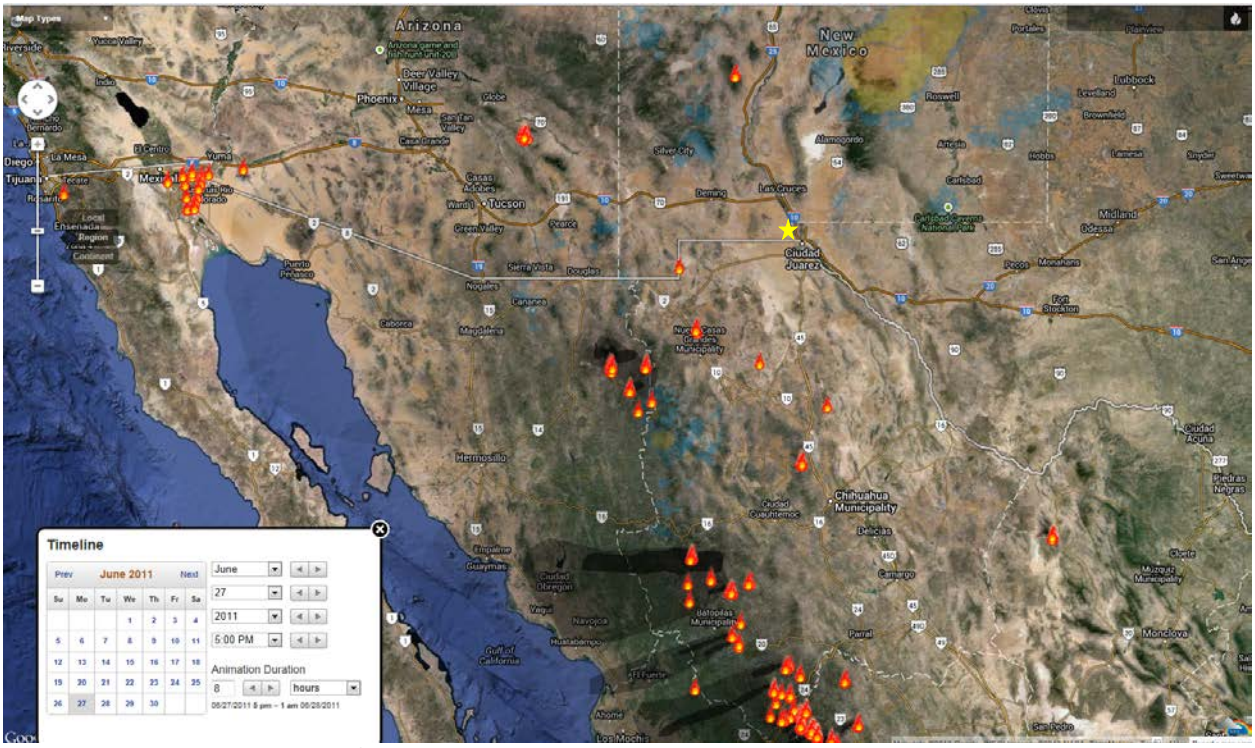

Figure 30-29. Satellite-detected active fires June 27, 2011 at 1700 hr MDT

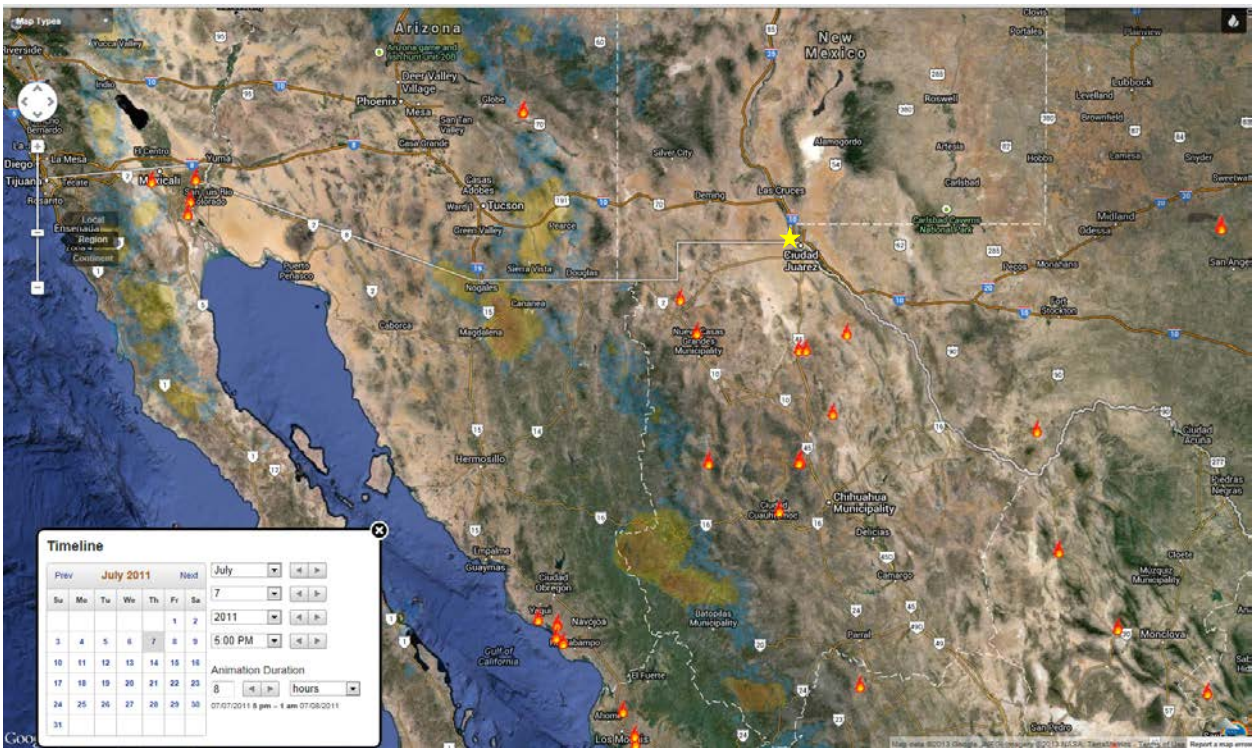

Figure 30-30. Satellite-detected active fires July 7, 2011 at 1700 hr MDT

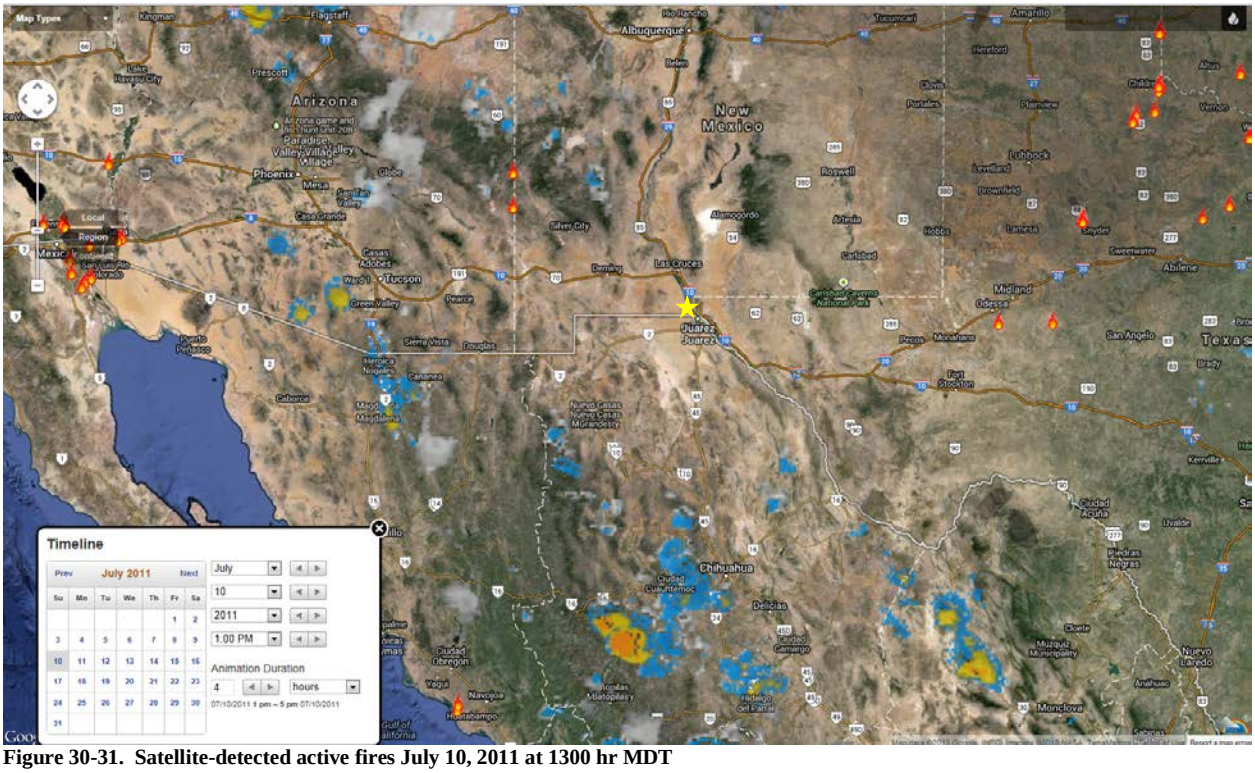

Figure 30-31. Satellite-detected active fires July 10, 2011 at 1300 hr MDT

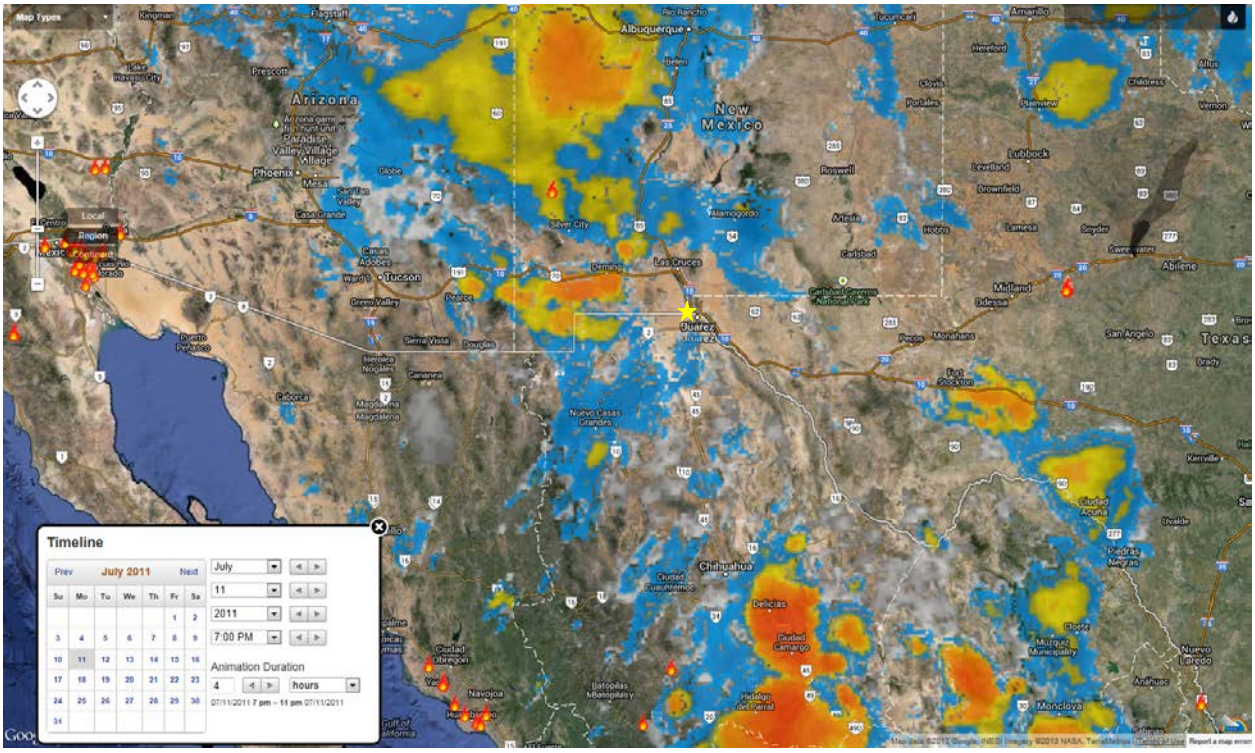

Figure 30-32. Satellite-detected active fires July 11, 2011 at 1900 hr MDT

As can be seen from the images above, smoke was added to the atmosphere beginning in April and building in intensity through June, then decreasing again in July. By mid-July, smoke was no longer a significant factor for New Mexico's air quality as indicated by more normalized concentrations at the SPCY $PM_{2.5}$ Partisol monitor.

As the events unfolded, winds blew from various directions throughout the border region, carrying smoke from myriad fires into the Sunland Park area. The presence of smoke-producing wildfires, little to no point sources in the area, and the high $PM_{2.5}$ concentrations support the assertion that these were exceptional events, specifically natural events caused by wildfire smoke.

30.2 Is Not Reasonably Controllable or Preventable

30.1.1 Suspected Source Areas and Categories Contributing to the Event

Sources of smoke contributing to these exceedances include wildfires from eastern Arizona, southwestern New Mexico, and northern Mexico. The largest and most likely sources of smoke are from the Horseshoe 2 fire in southeastern Arizona and the various fires in northern Mexico, although some contribution may also have been made by the various fires in New Mexico, depending on the wind directions and speeds on each given date.

The sources of smoke were widespread, often covering large portions of northern Mexico and sometimes covering more than half of the U.S. 48 contiguous states, as Figures 30-33 to 30-64 show. This series of figures uses HYSPLIT smoke dispersion modeling superimposed over Google Earth satellite imaging and was retrieved through NOAA's Air Resources Laboratory

smoke verification website. The red pin icon indicates the location of the SPCY $PM_{2.5}$ Partisol monitor. Each image shown is a prediction of smoke concentrations at 1200 hours MDT. These models use the previous day's AOD data as a starting point, along with weather data to predict the smoke dispersion on an hourly basis. The highest concentrations of smoke expected are shown in red, followed by orange, then yellow, then green. These models predict dispersion from active fires and do not take into account smoke already in the atmosphere from previous days. Smoke impact from already-entrained smoke would be added to the impacts shown here. Further, actual weather conditions may differ from predicted conditions at the time the model was initiated so actual smoke concentrations may vary from those predicted. Of note is the large amount of smoke already in the atmosphere by April 5, building through May and June, and then tapering off by mid-July.

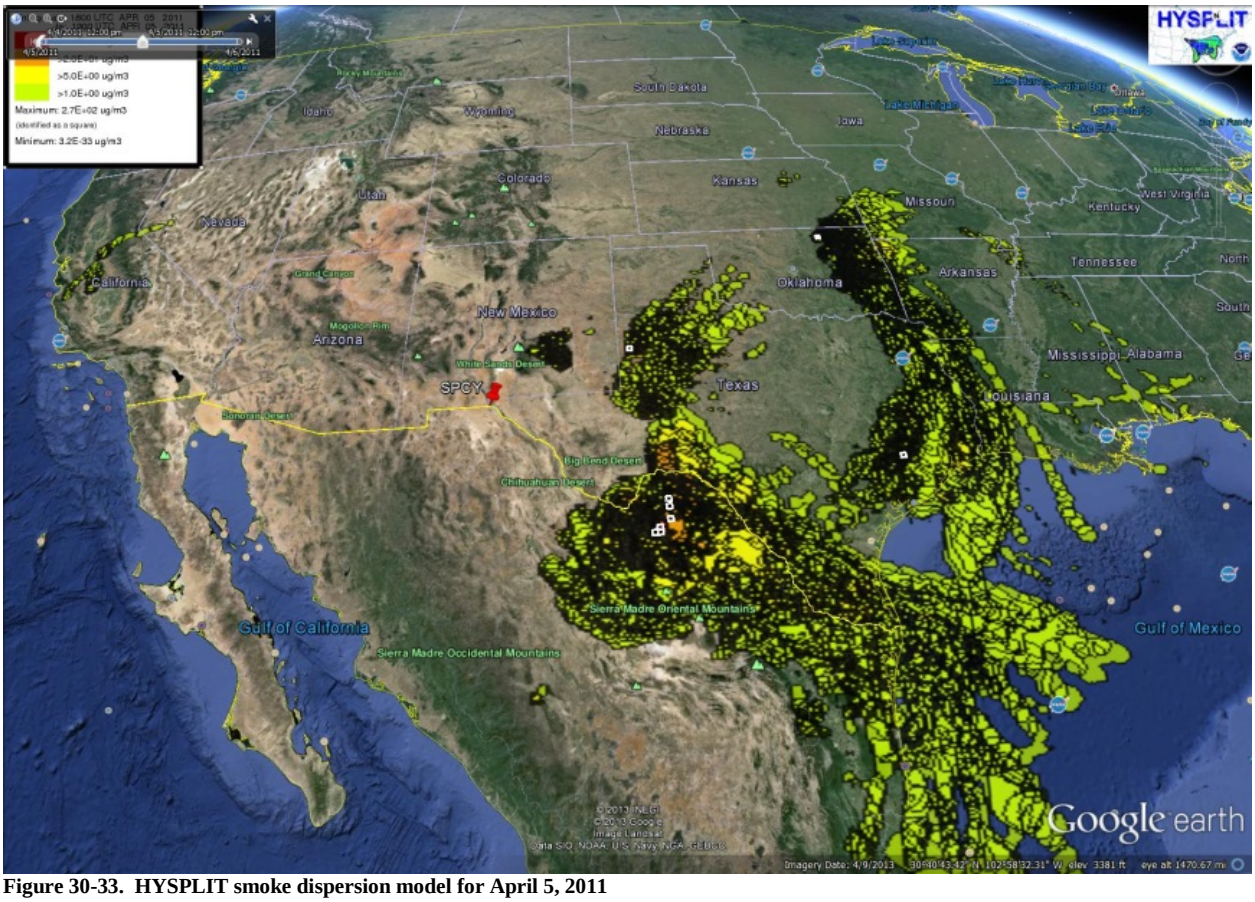

Figure 30-33. HYSPLIT smoke dispersion model for April 5, 2011

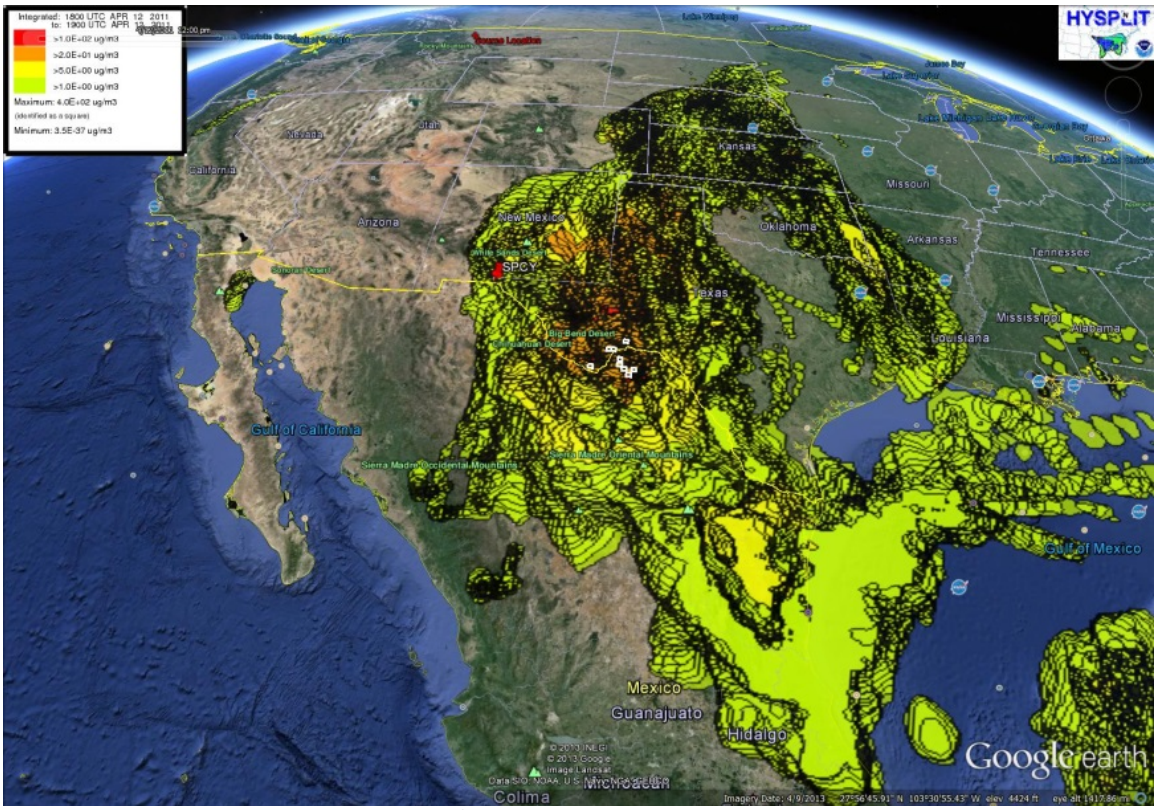

Figure 30-34. HYSPLIT smoke dispersion model for April 12, 2011

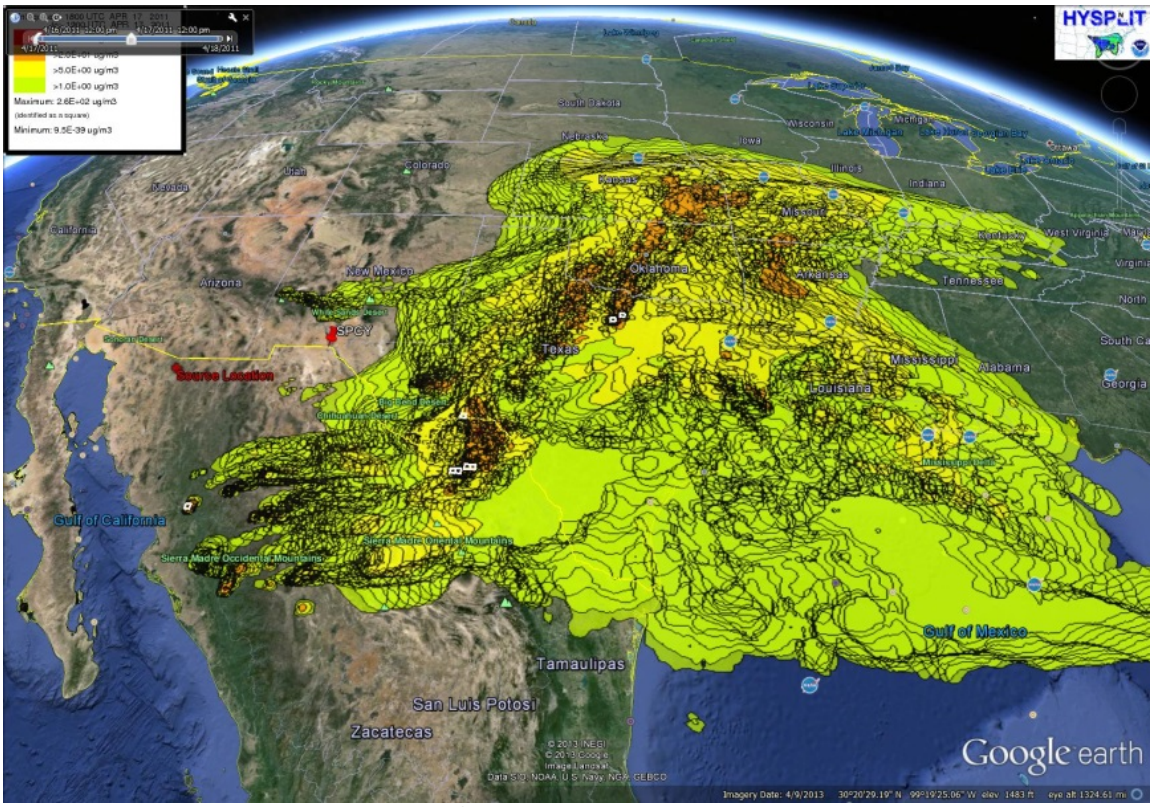

Figure 30-35. HYSPLIT smoke dispersion model for April 17, 2011

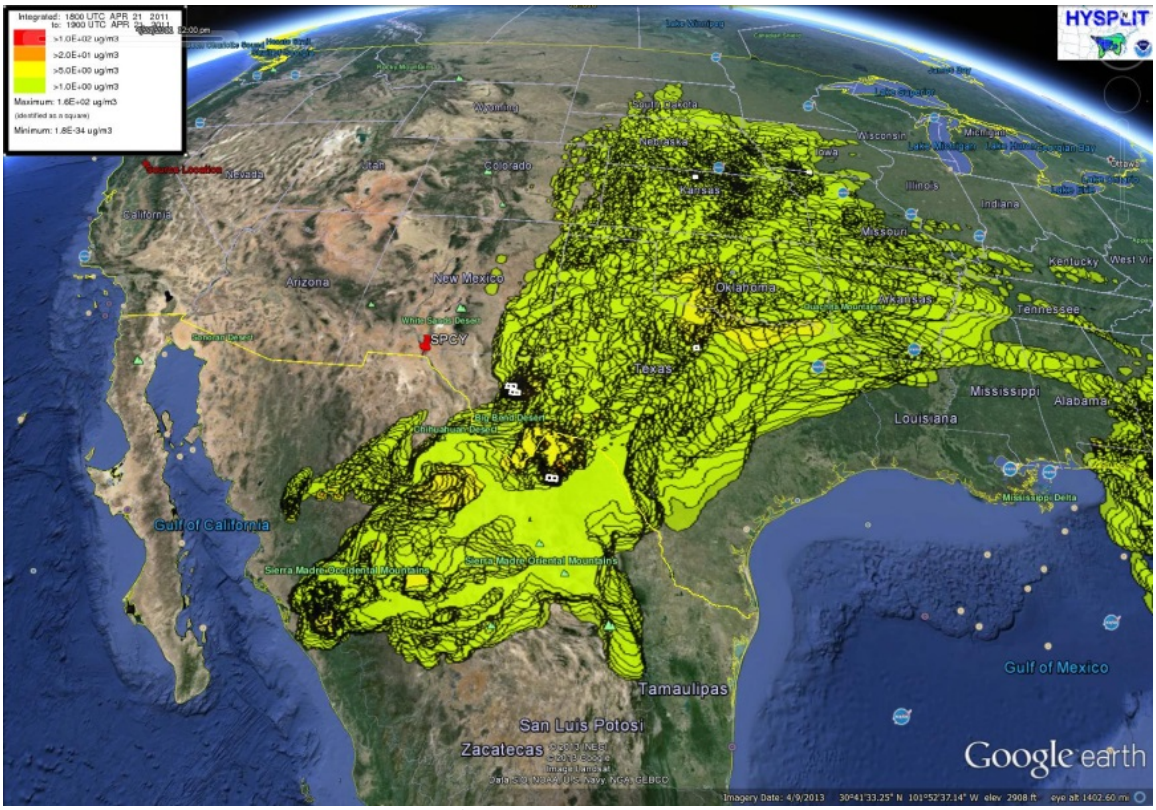

Figure 30-36. HYSPLIT smoke dispersion model for April 21, 2011

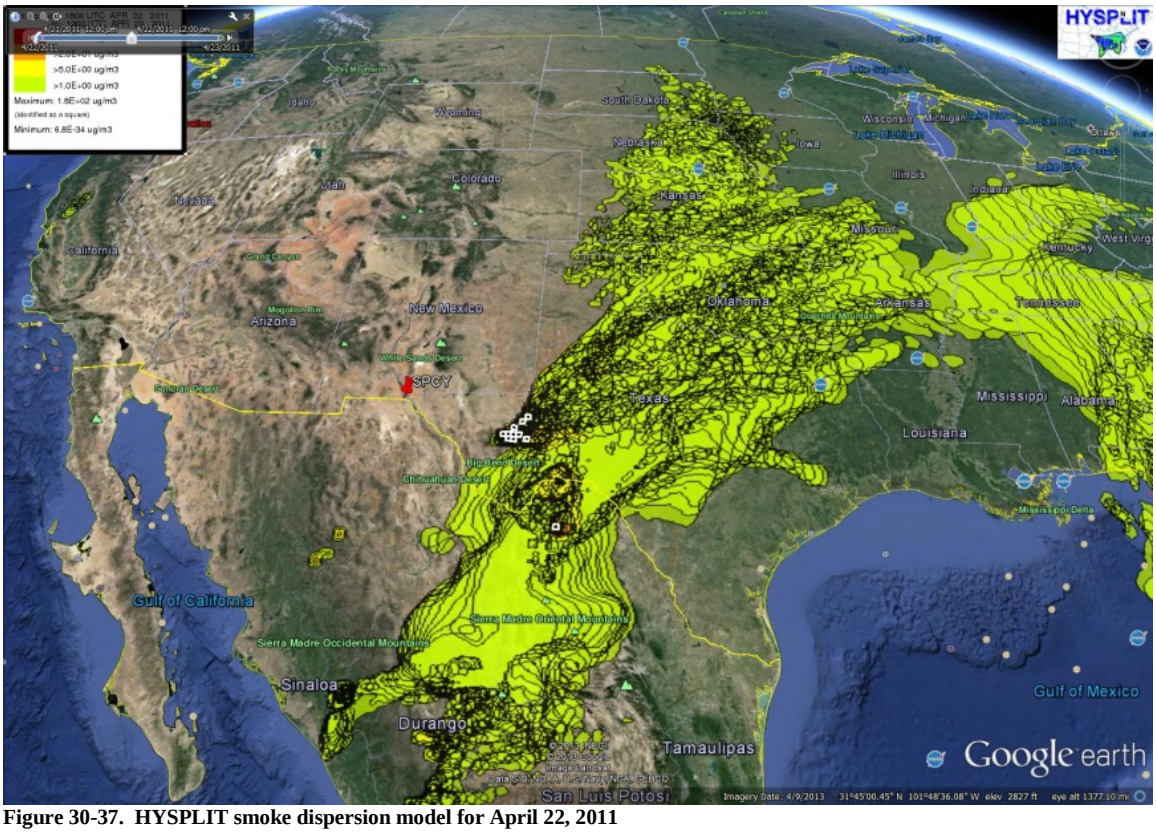

Figure 30-37. HYSPLIT smoke dispersion model for April 22, 2011

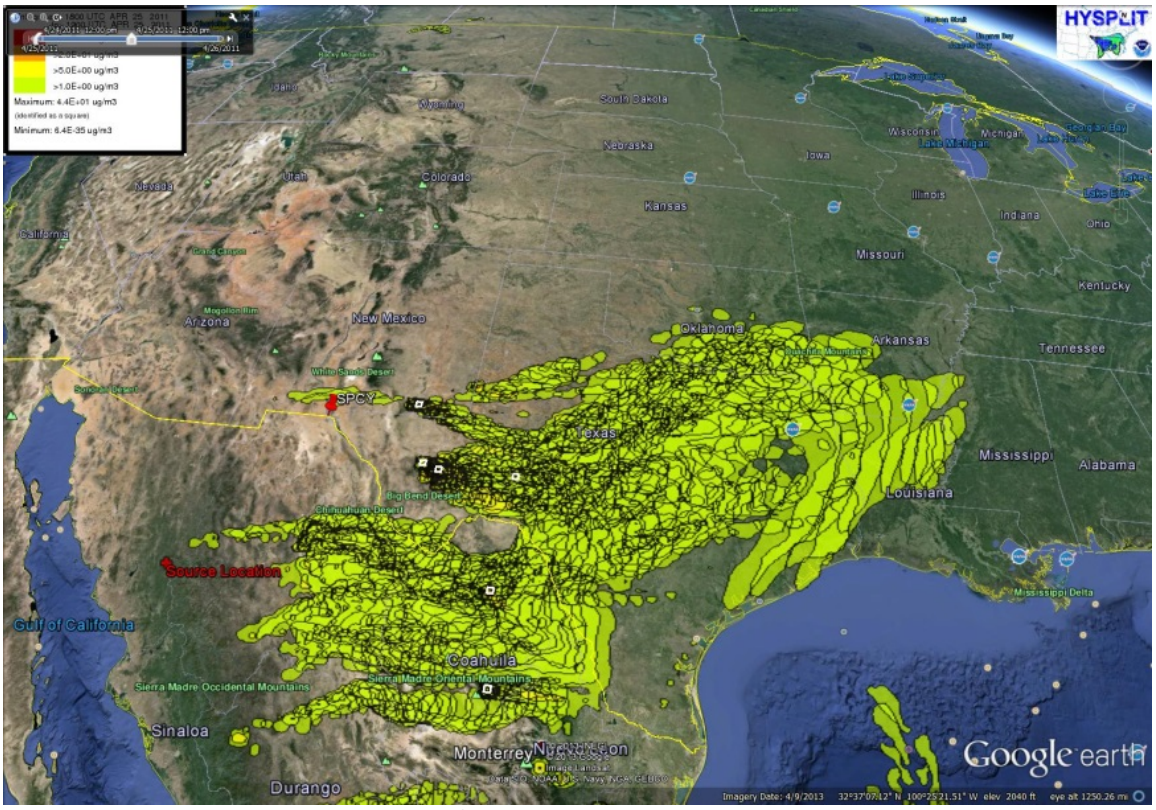

Figure 30-38. HYSPLIT smoke dispersion model for April 25, 2011

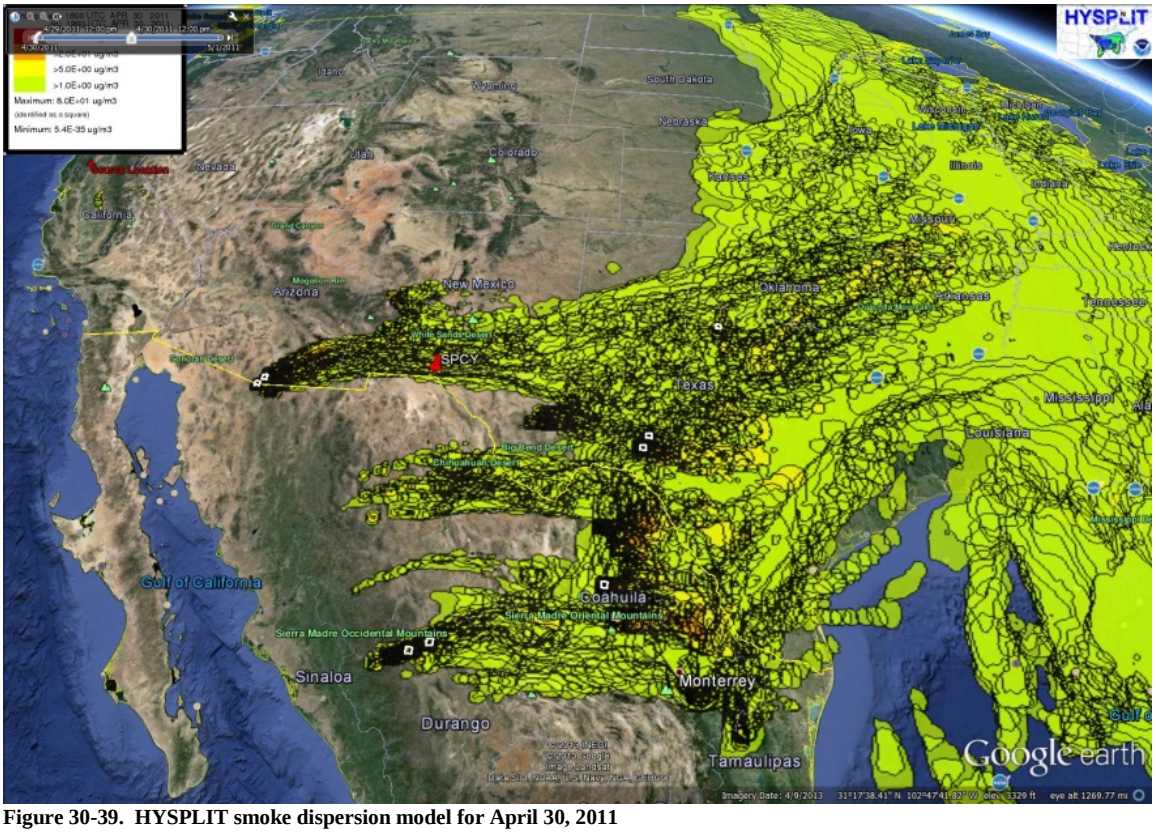

Figure 30-39. HYSPLIT smoke dispersion model for April 30, 2011

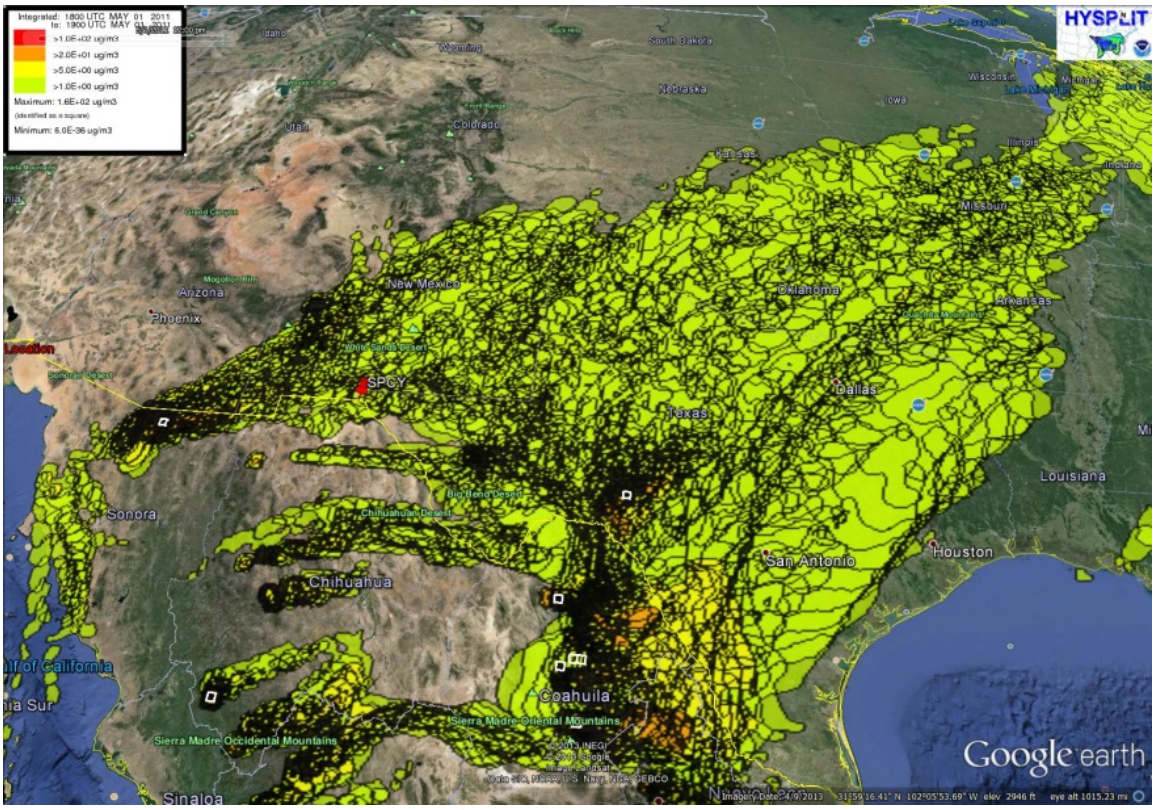

Figure 30-40. HYSPLIT smoke dispersion model for May 1, 2011

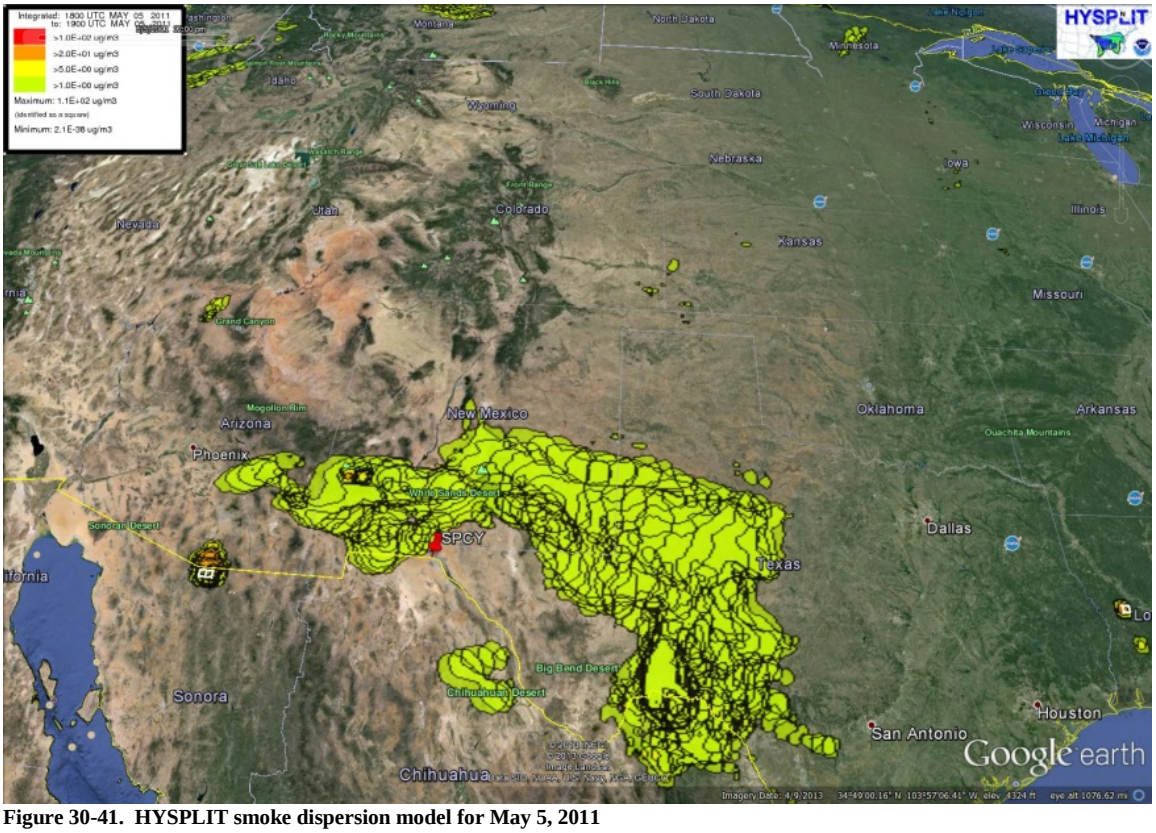

Figure 30-41. HYSPLIT smoke dispersion model for May 5, 2011

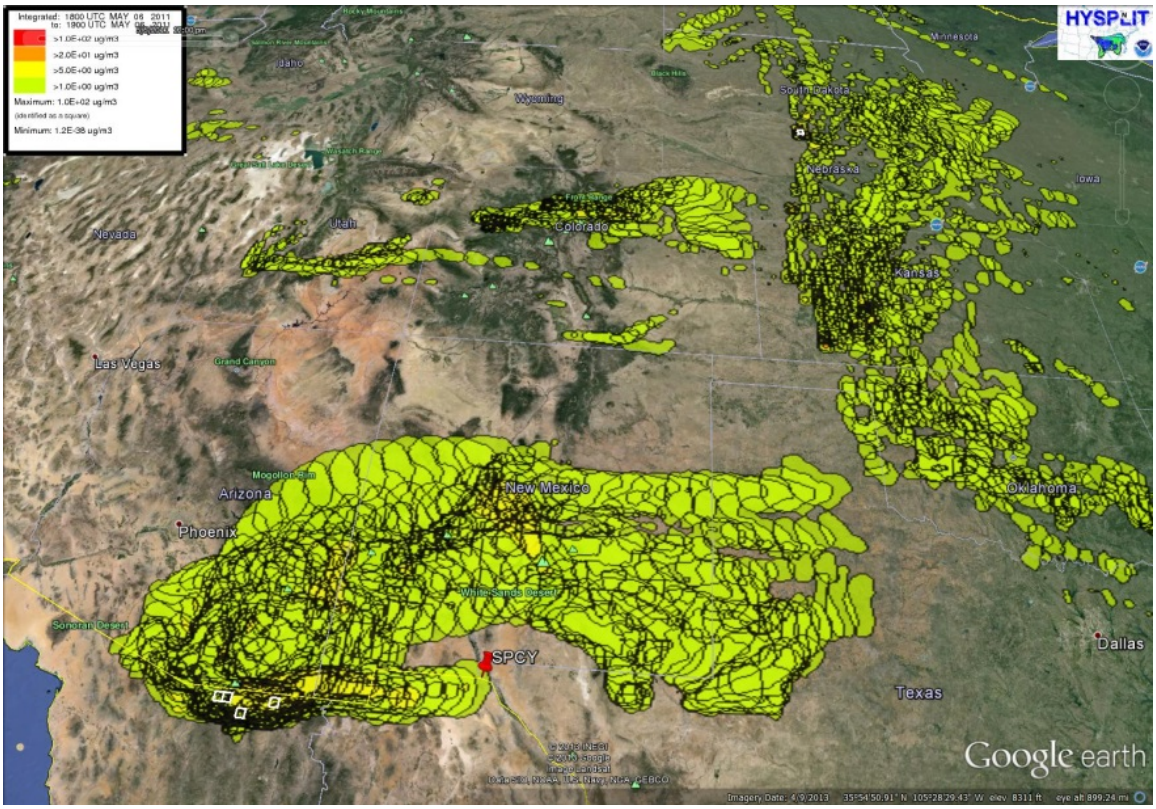

Figure 30-42. HYSPLIT smoke dispersion model for May 6, 2011

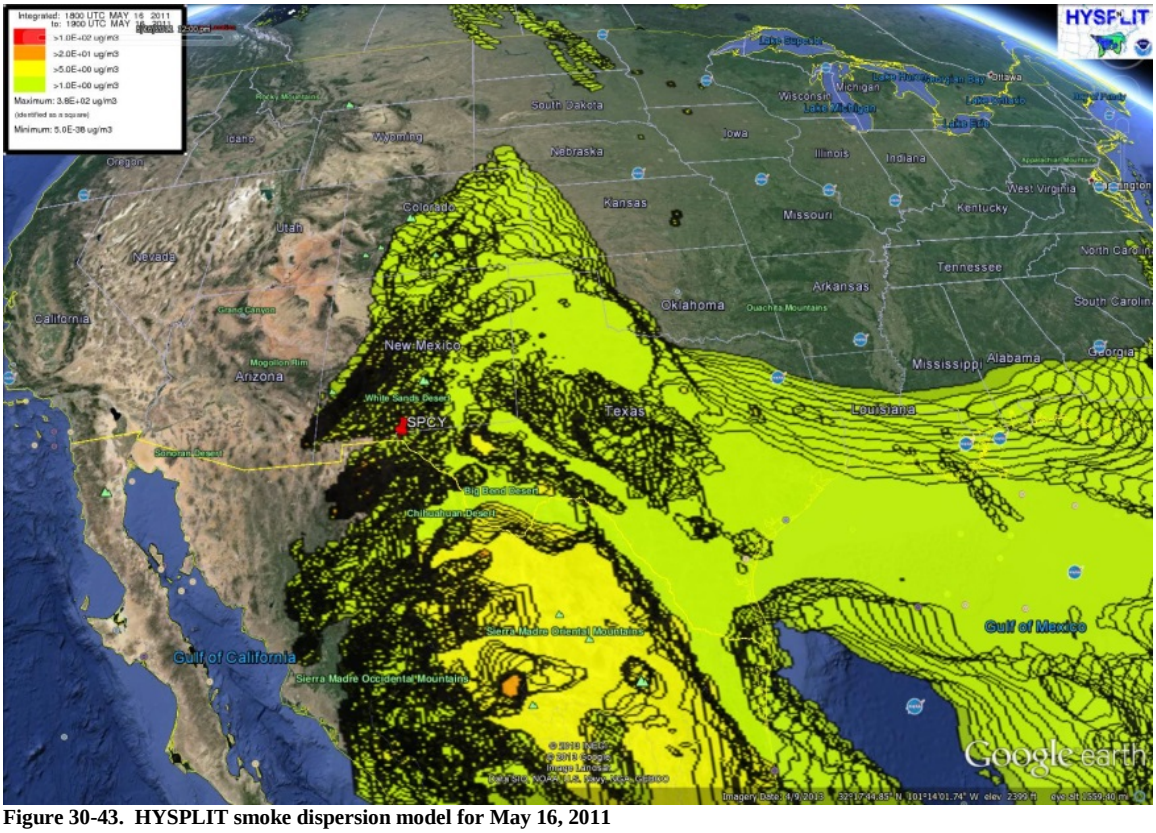

Figure 30-43. HYSPLIT smoke dispersion model for May 16, 2011

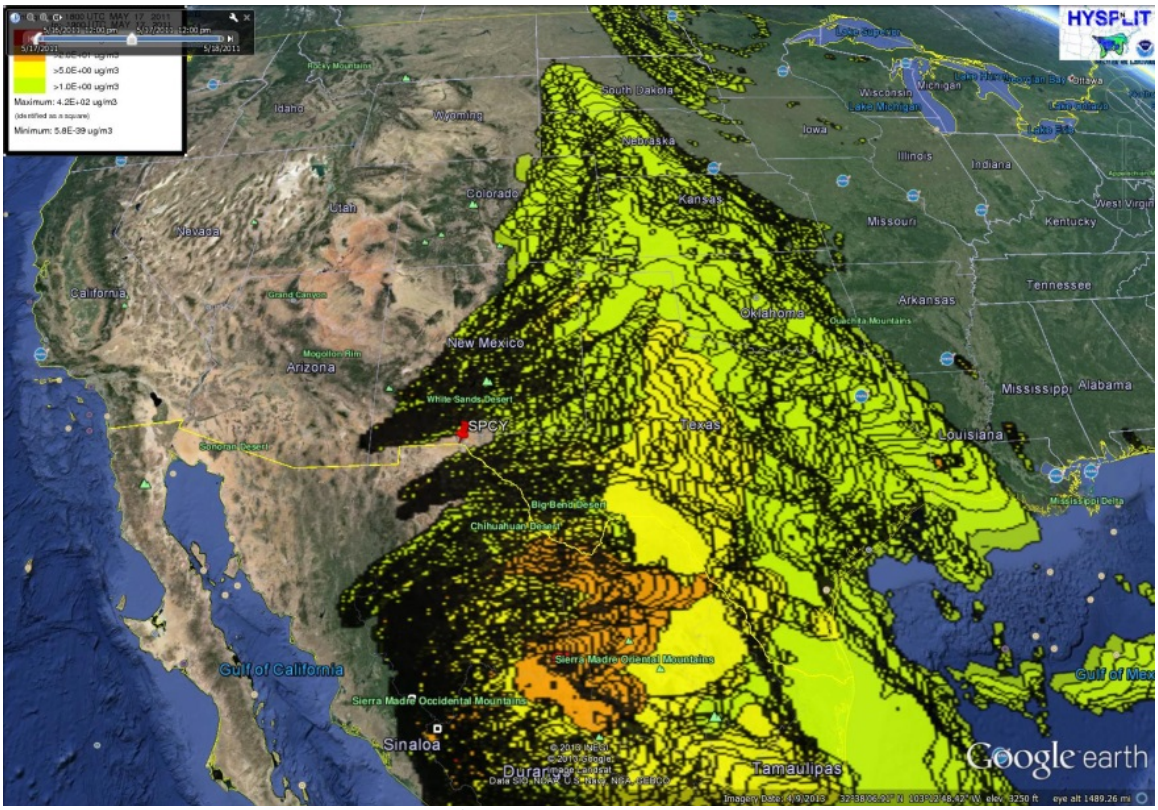

Figure 30-44. HYSPLIT smoke dispersion model for May 17, 2011

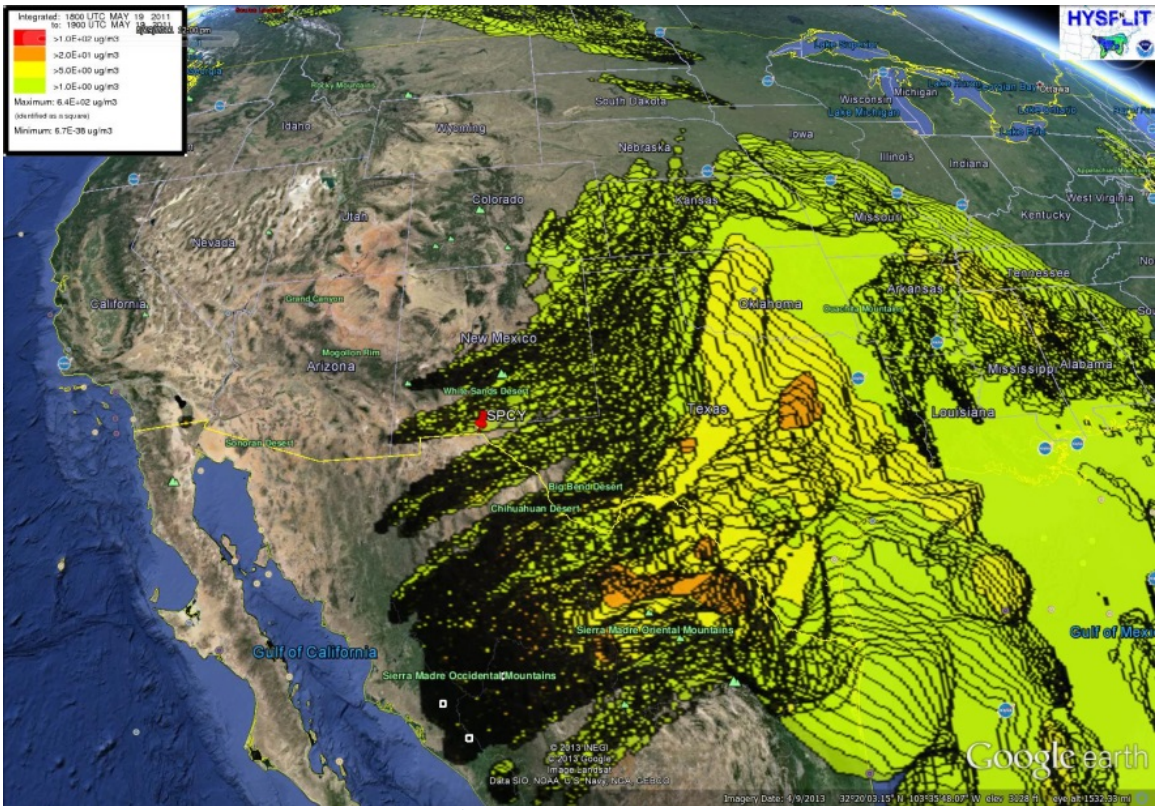

Figure 30-45. HYSPLIT smoke dispersion model for May 19, 2011

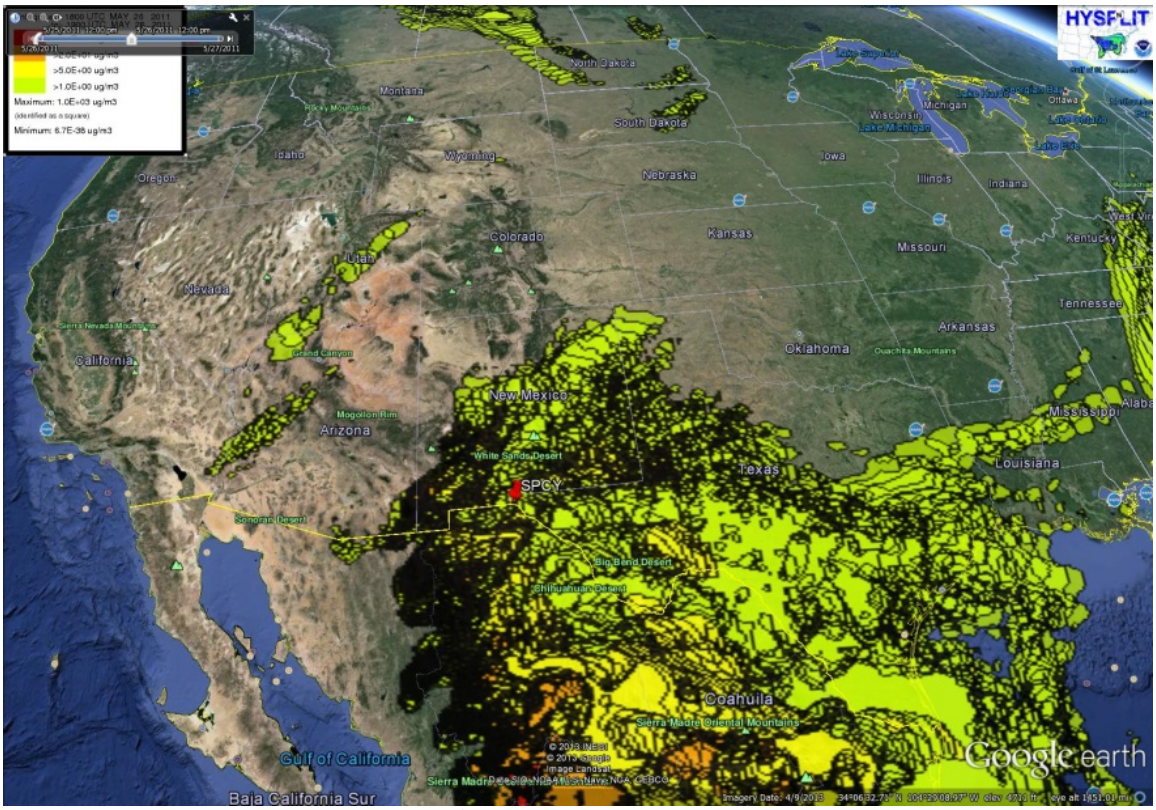

Figure 30-46. HYSPLIT smoke dispersion model for May 26, 2011

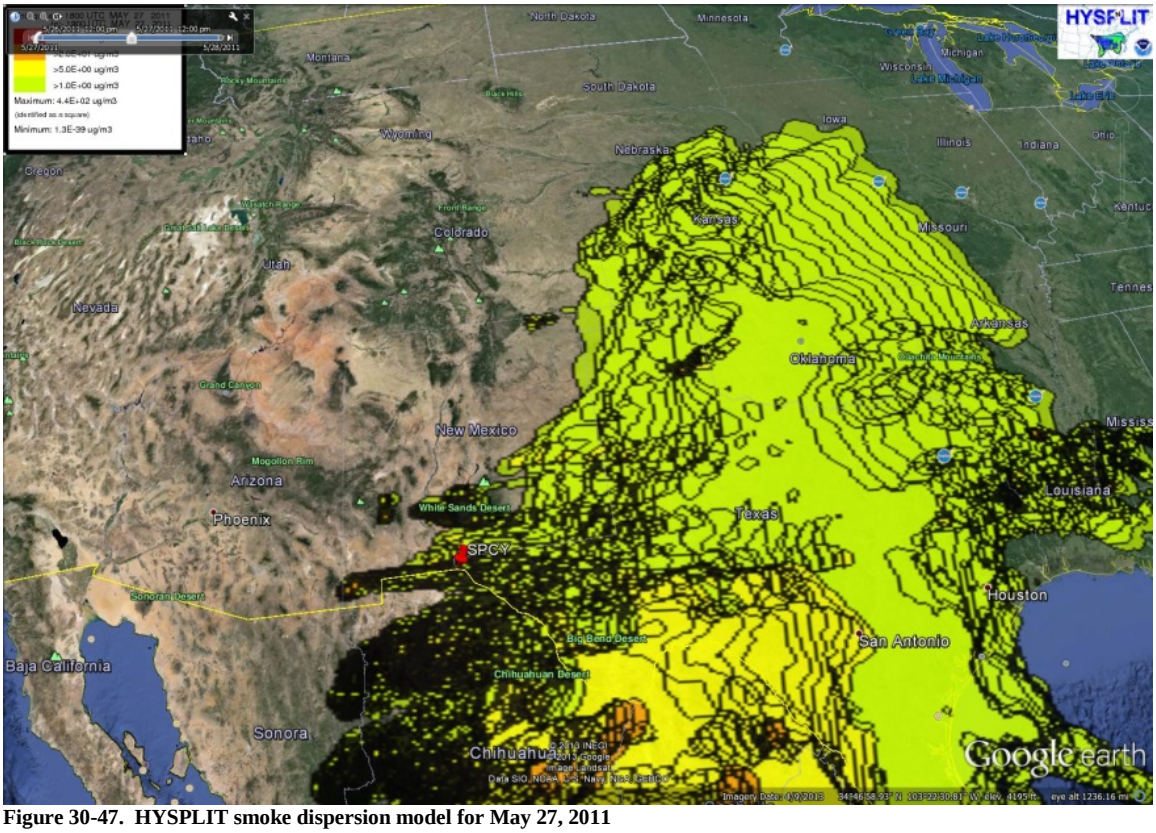

Figure 30-47. HYSPLIT smoke dispersion model for May 27, 2011

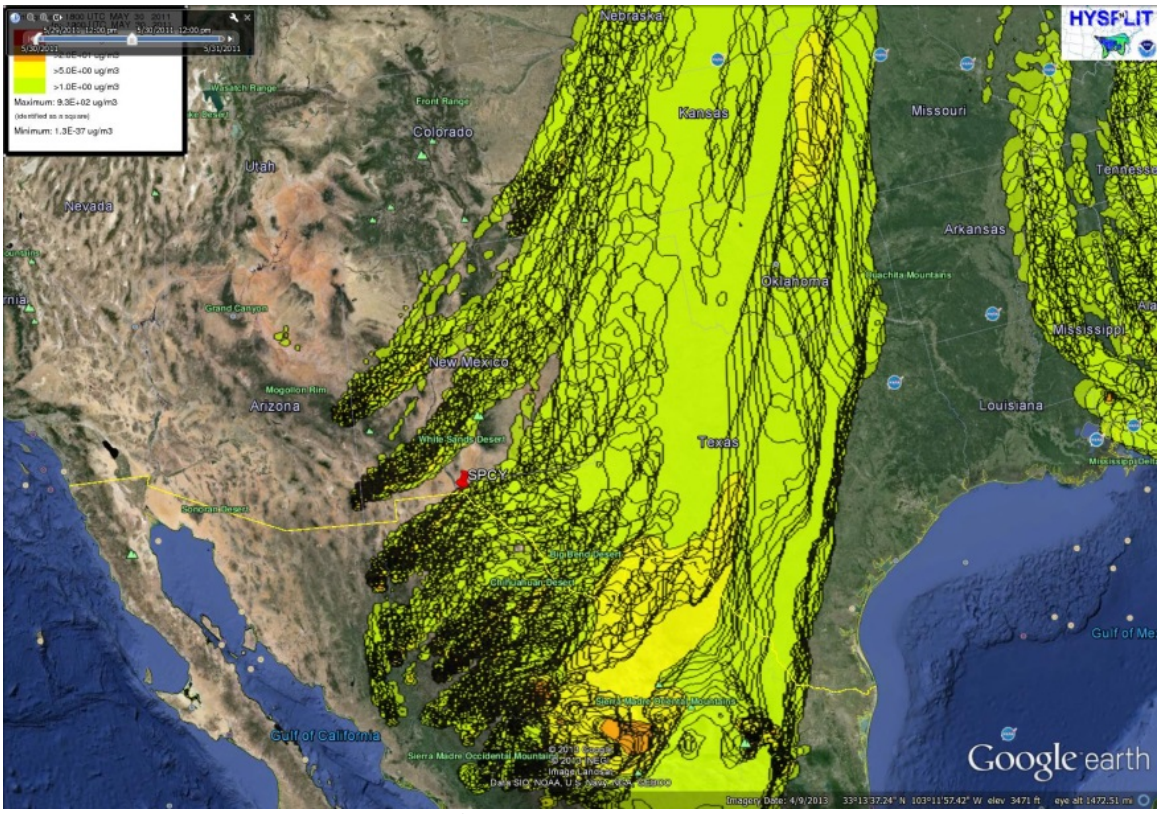

Figure 30-48. HYSPLIT smoke dispersion model for May 30, 2011

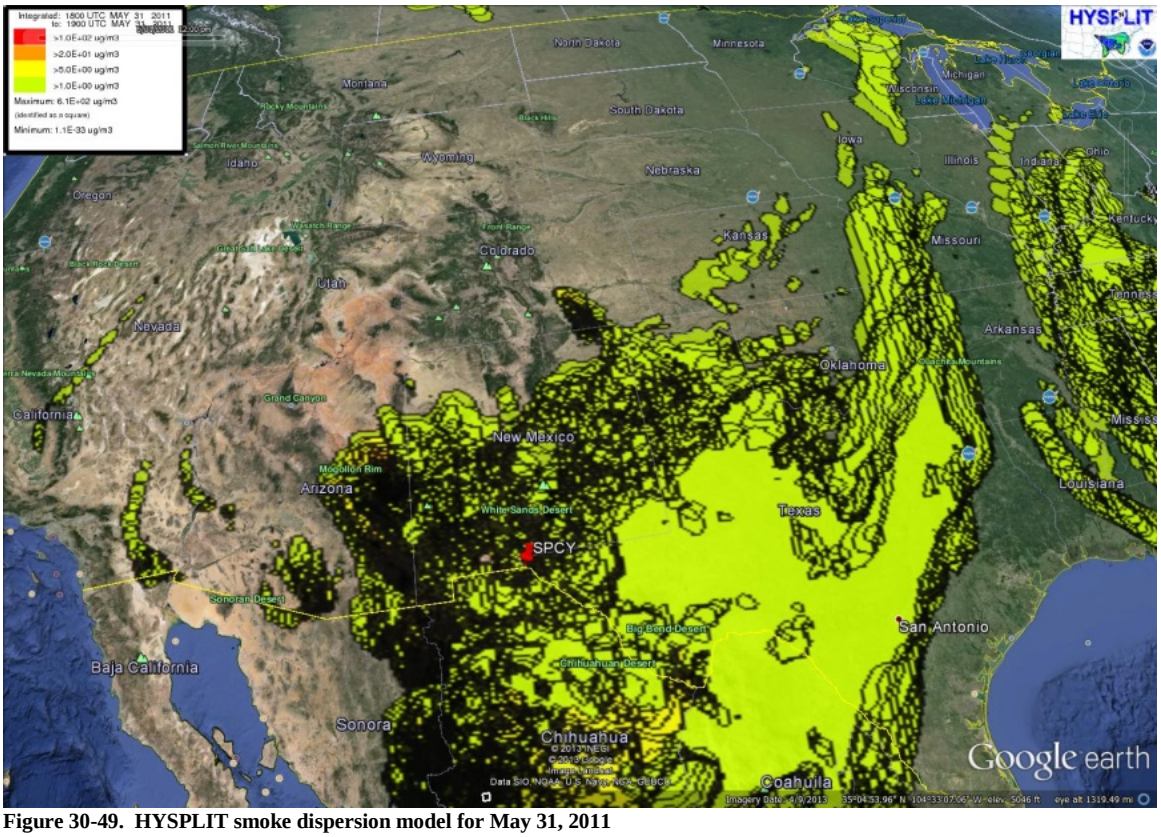

Figure 30-49. HYSPLIT smoke dispersion model for May 31, 2011

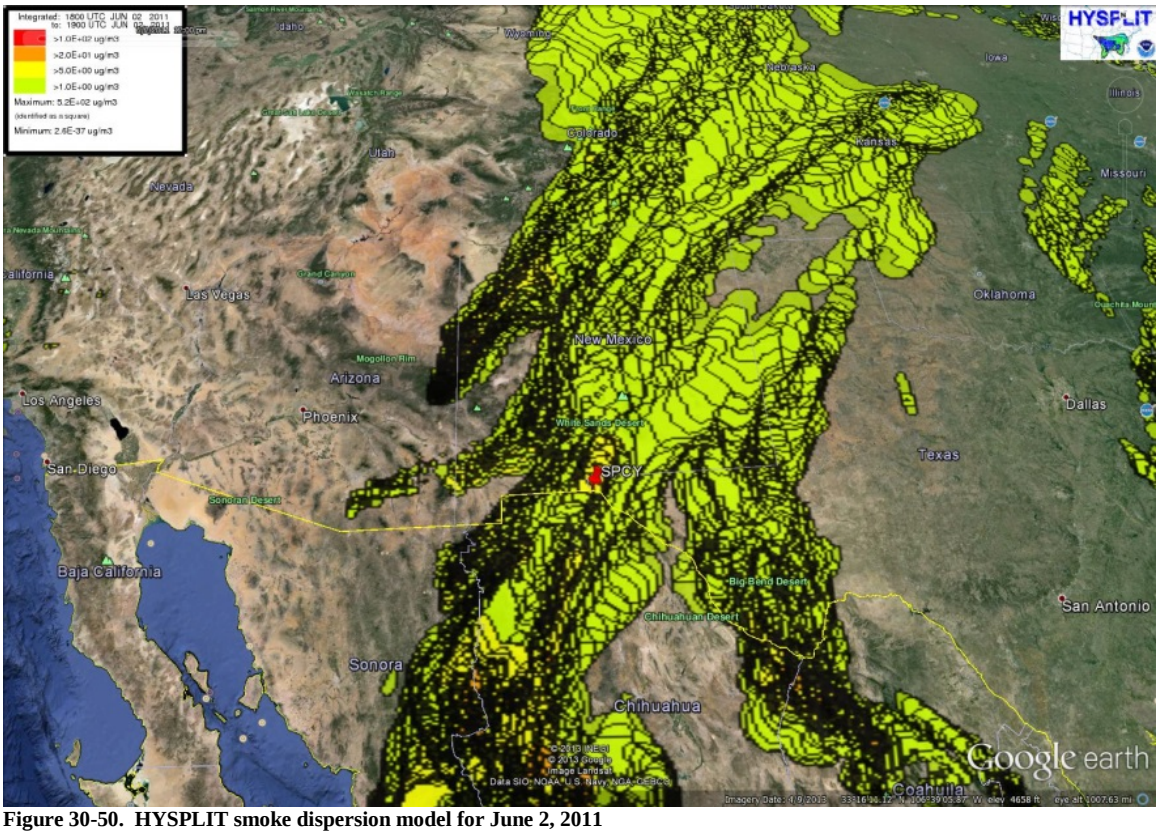

Figure 30-50. HYSPLIT smoke dispersion model for June 2, 2011

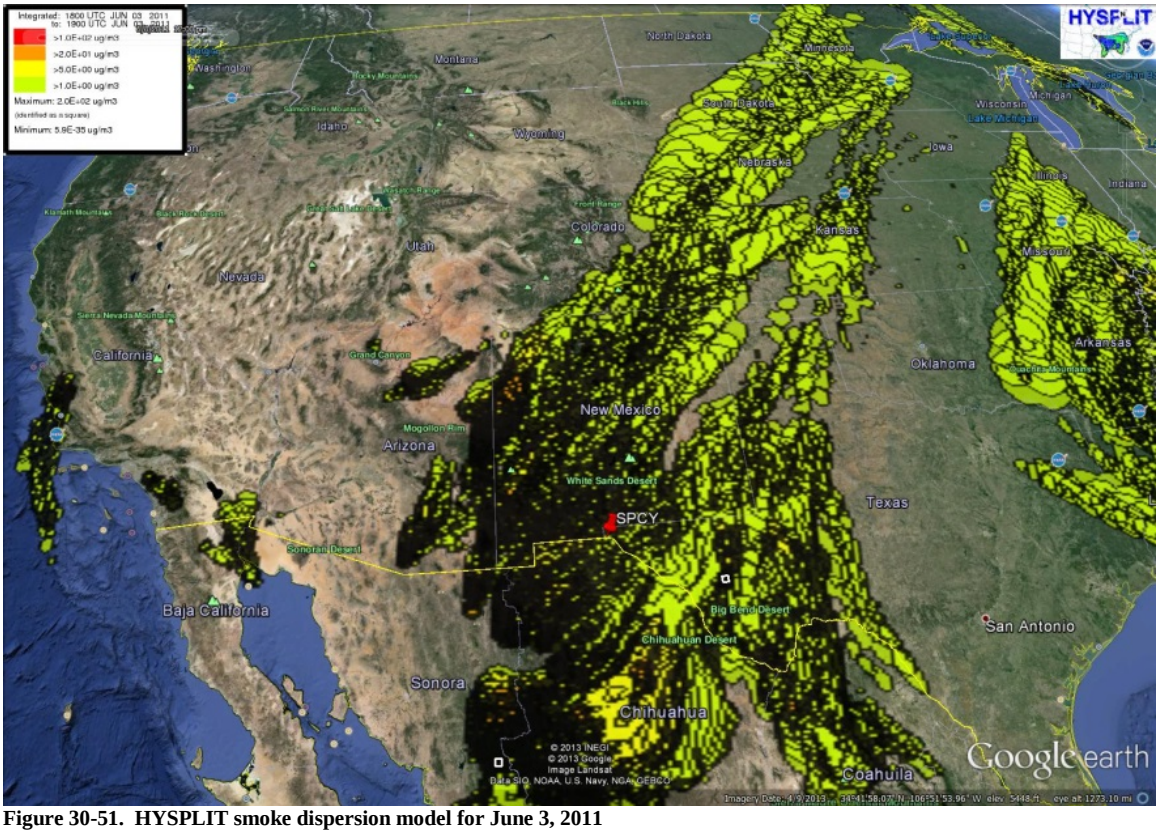

Figure 30-51. HYSPLIT smoke dispersion model for June 3, 2011

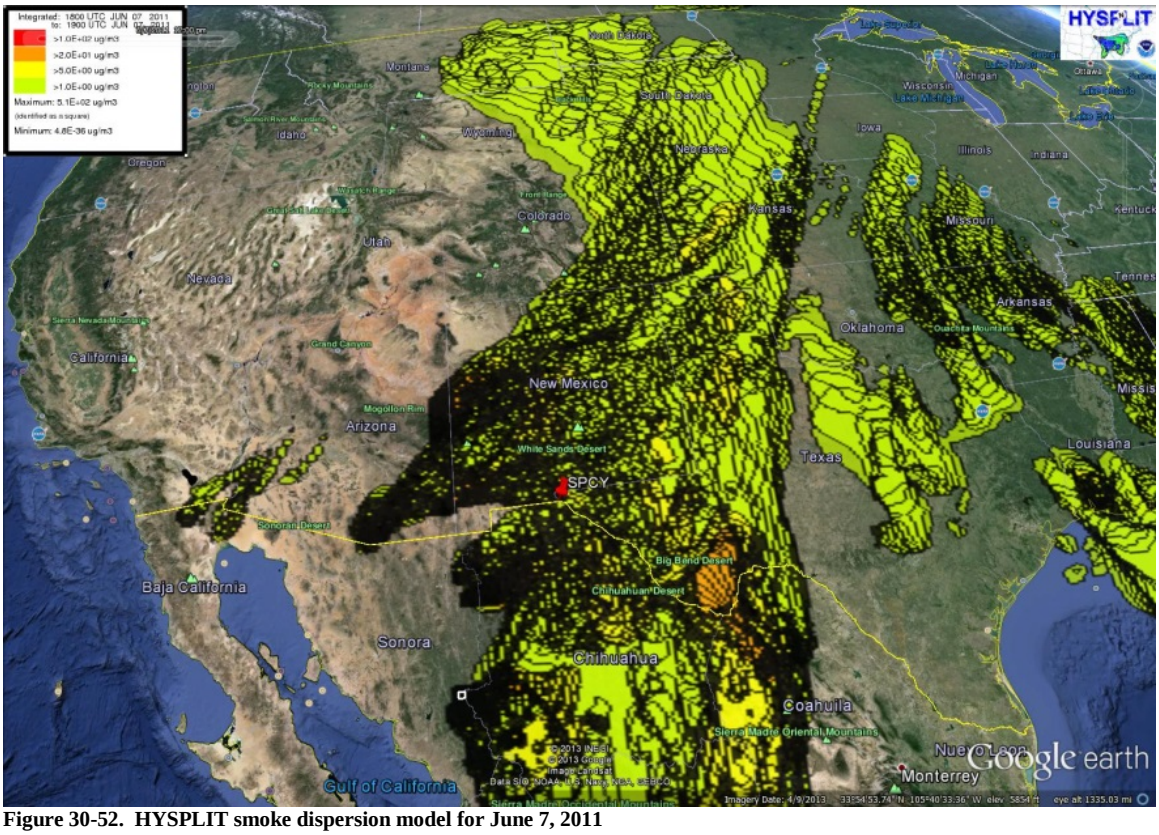

Figure 30-52. HYSPLIT smoke dispersion model for June 7, 2011

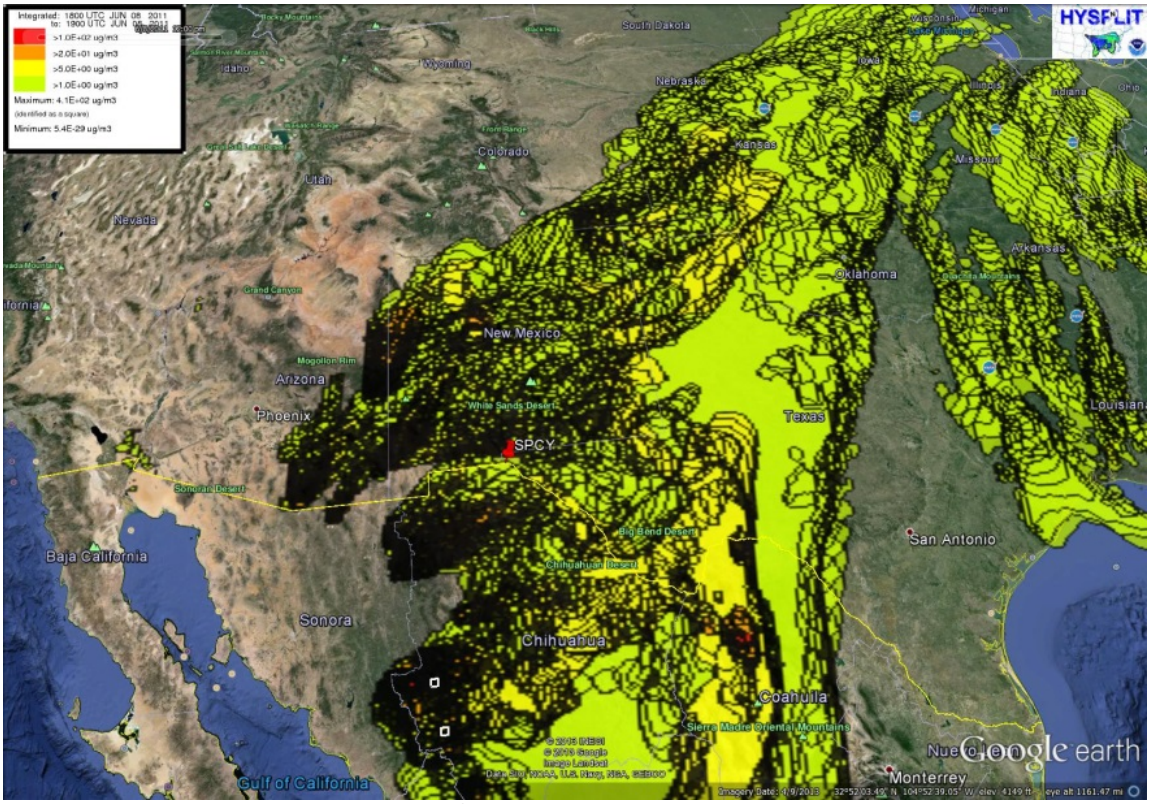

Figure 30-53. HYSPLIT smoke dispersion model for June 8, 2011

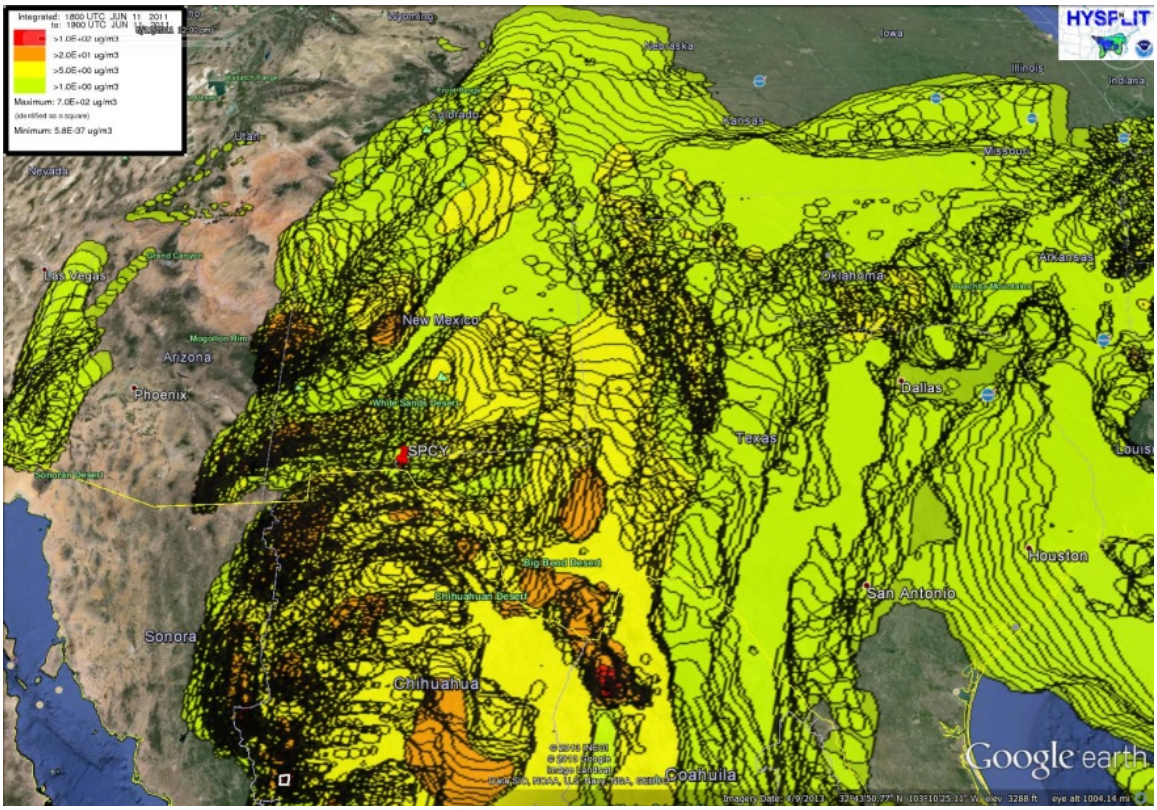

Figure 30-54. HYSPLIT smoke dispersion model for June 11, 2011

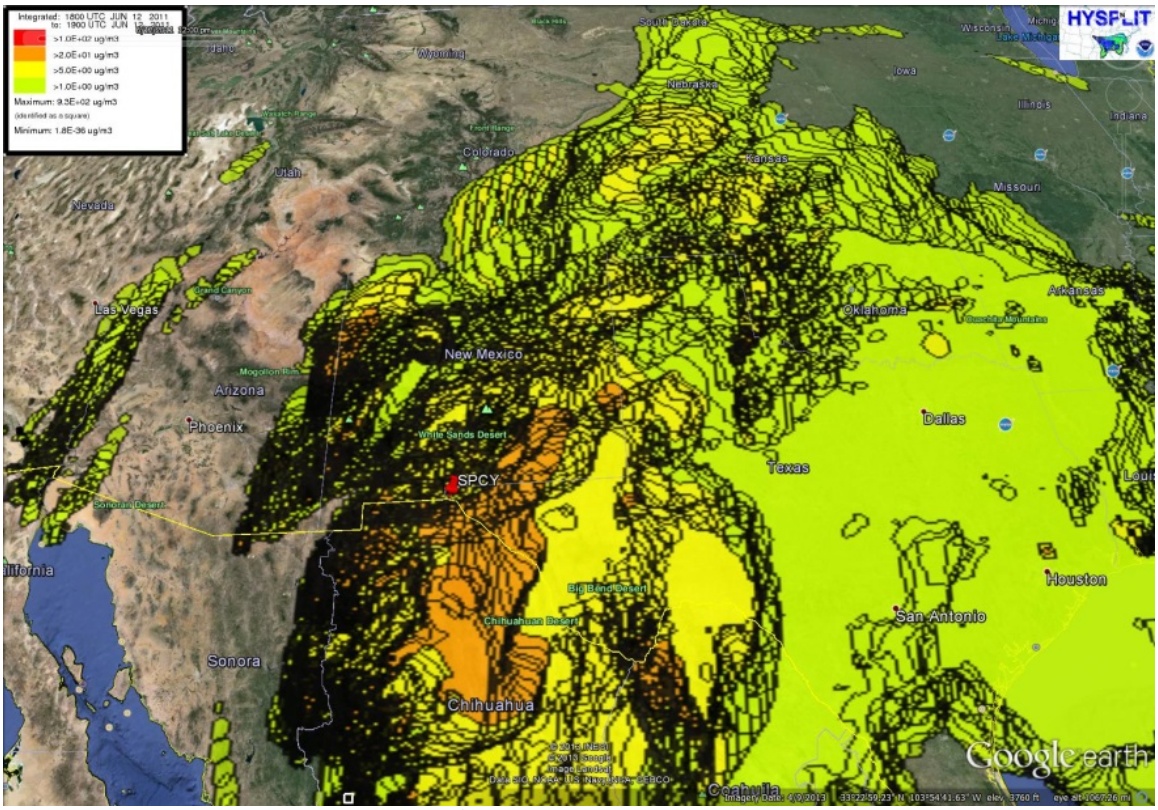

Figure 30-55. HYSPLIT smoke dispersion model for June 12, 2011

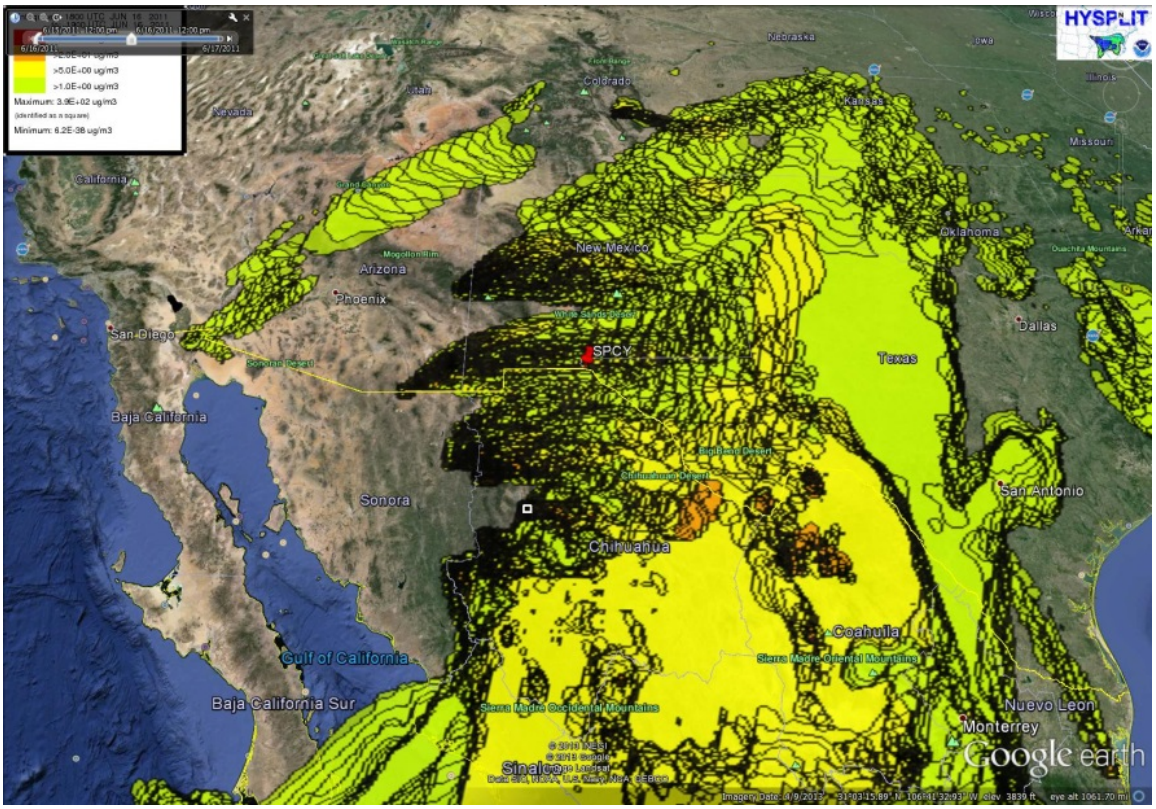

Figure 30-56. HYSPLIT smoke dispersion model for June 16, 2011

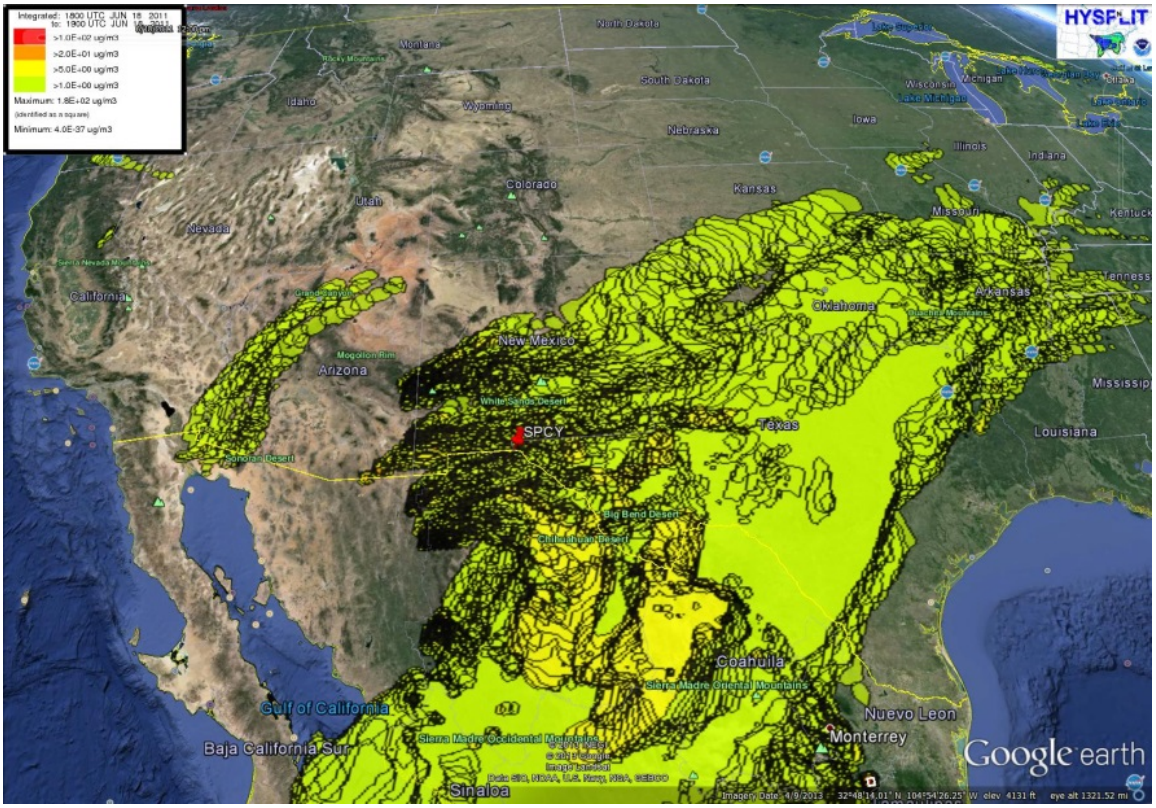

Figure 30-57. HYSPLIT smoke dispersion model for June 18, 2011

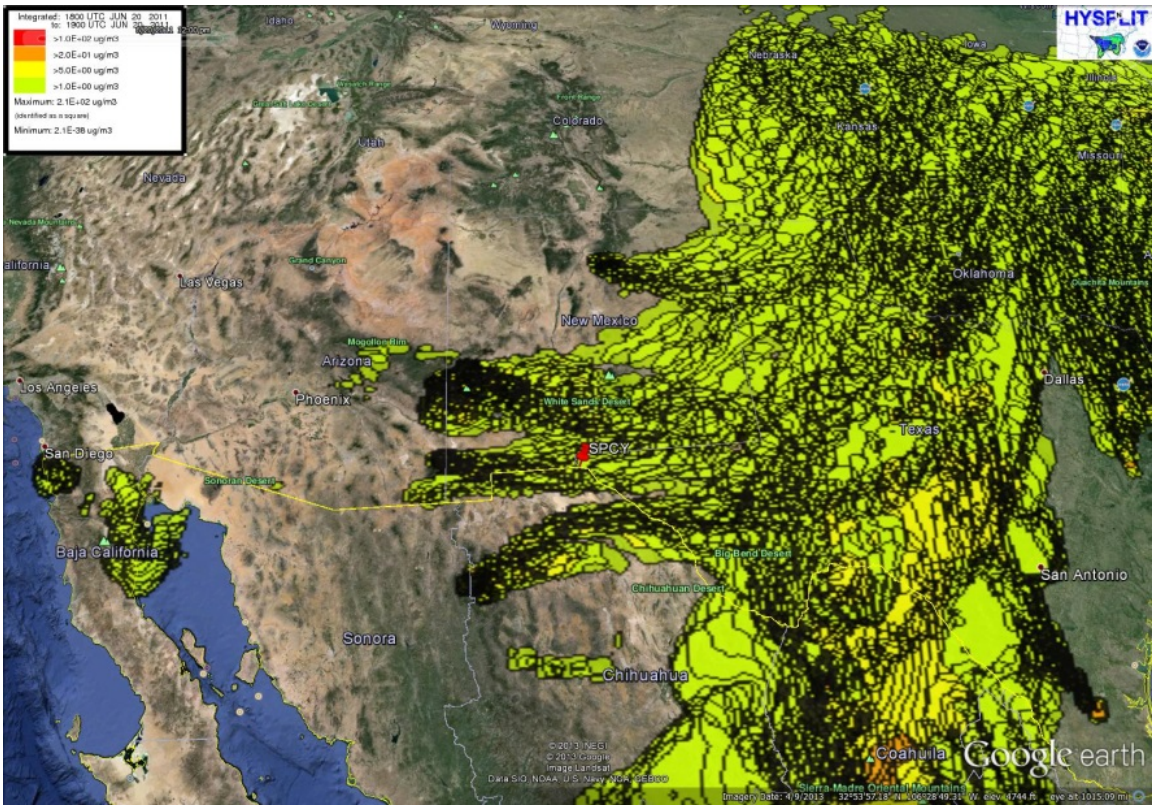

Figure 30-58. HYSPLIT smoke dispersion model for June 20, 2011

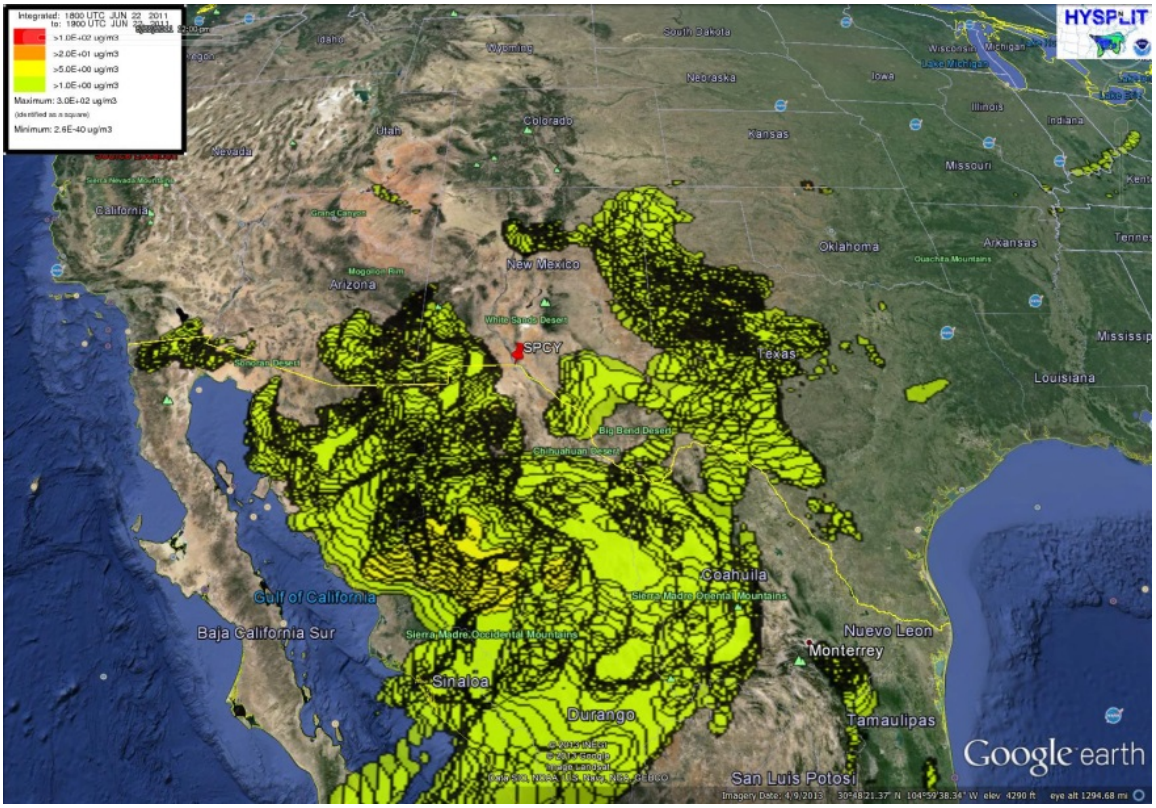

Figure 30-59. HYSPLIT smoke dispersion model for June 22, 2011

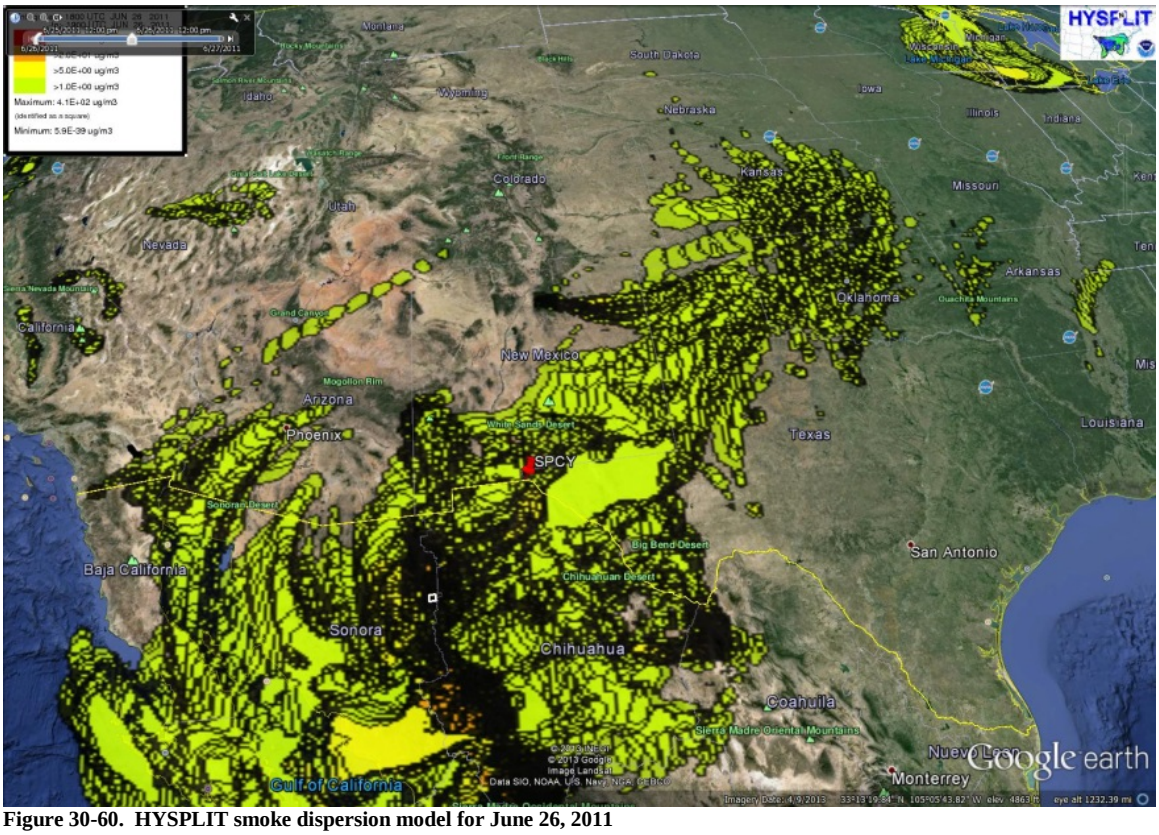

Figure 30-60. HYSPLIT smoke dispersion model for June 26, 2011

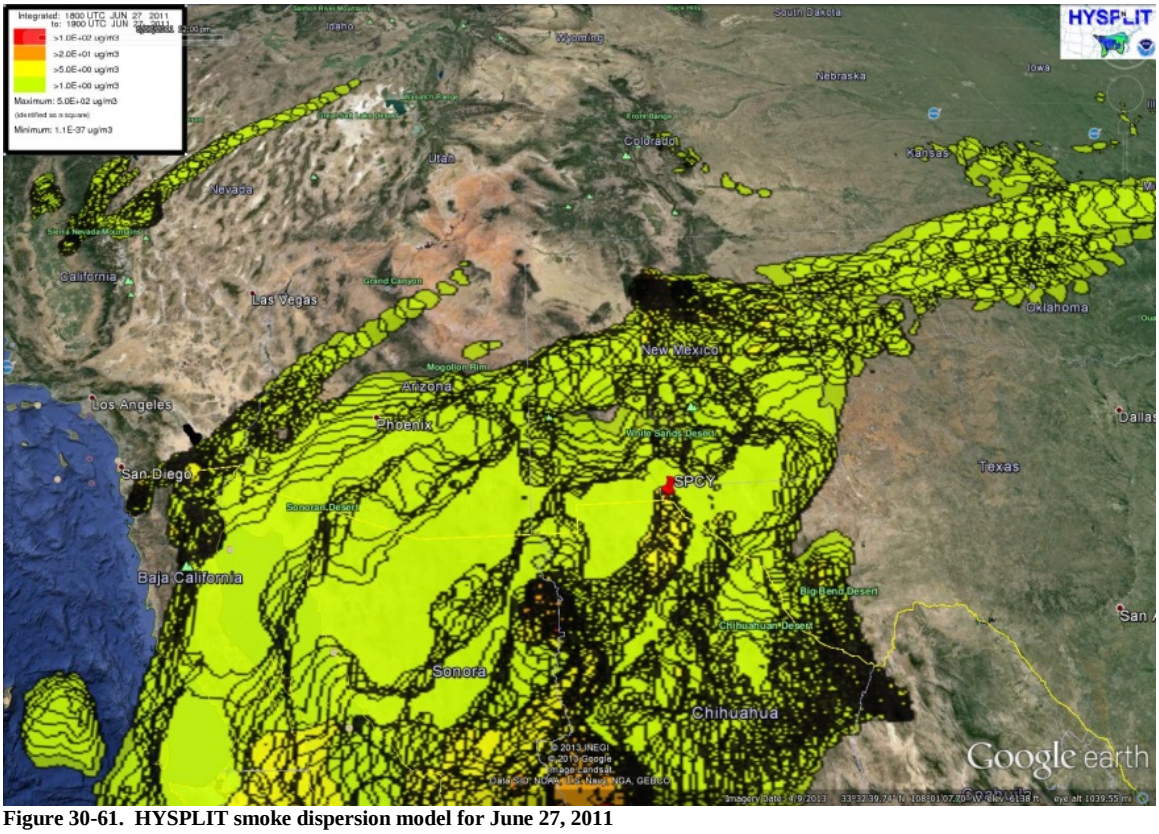

Figure 30-61. HYSPLIT smoke dispersion model for June 27, 2011

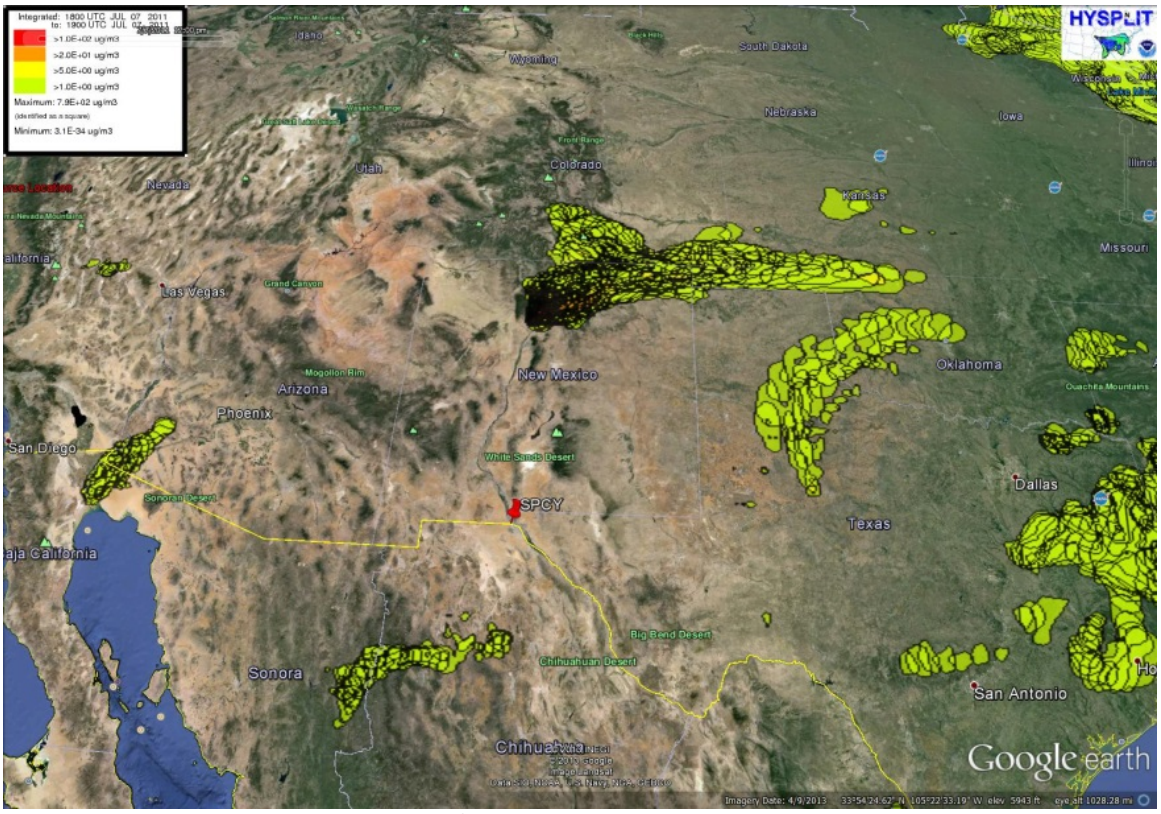

Figure 30-62. HYSPLIT smoke dispersion model for July 7, 2011

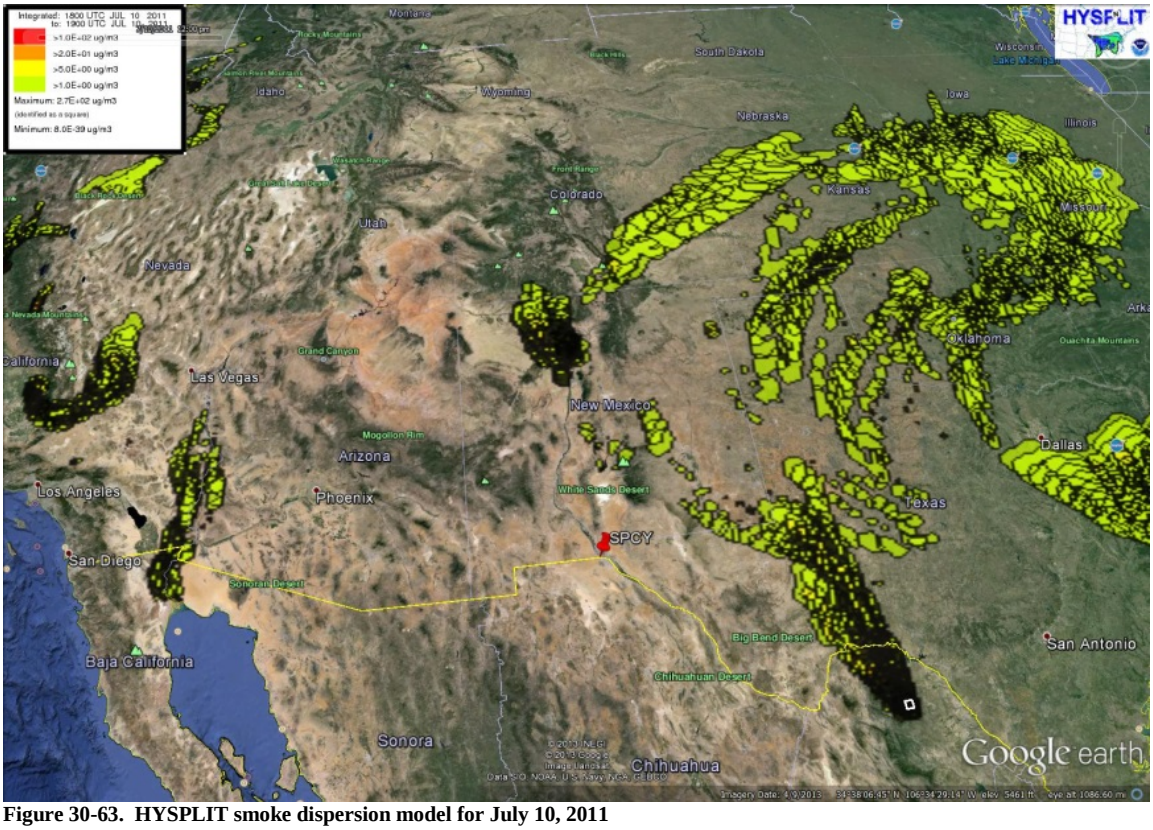

Figure 30-63. HYSPLIT smoke dispersion model for July 10, 2011

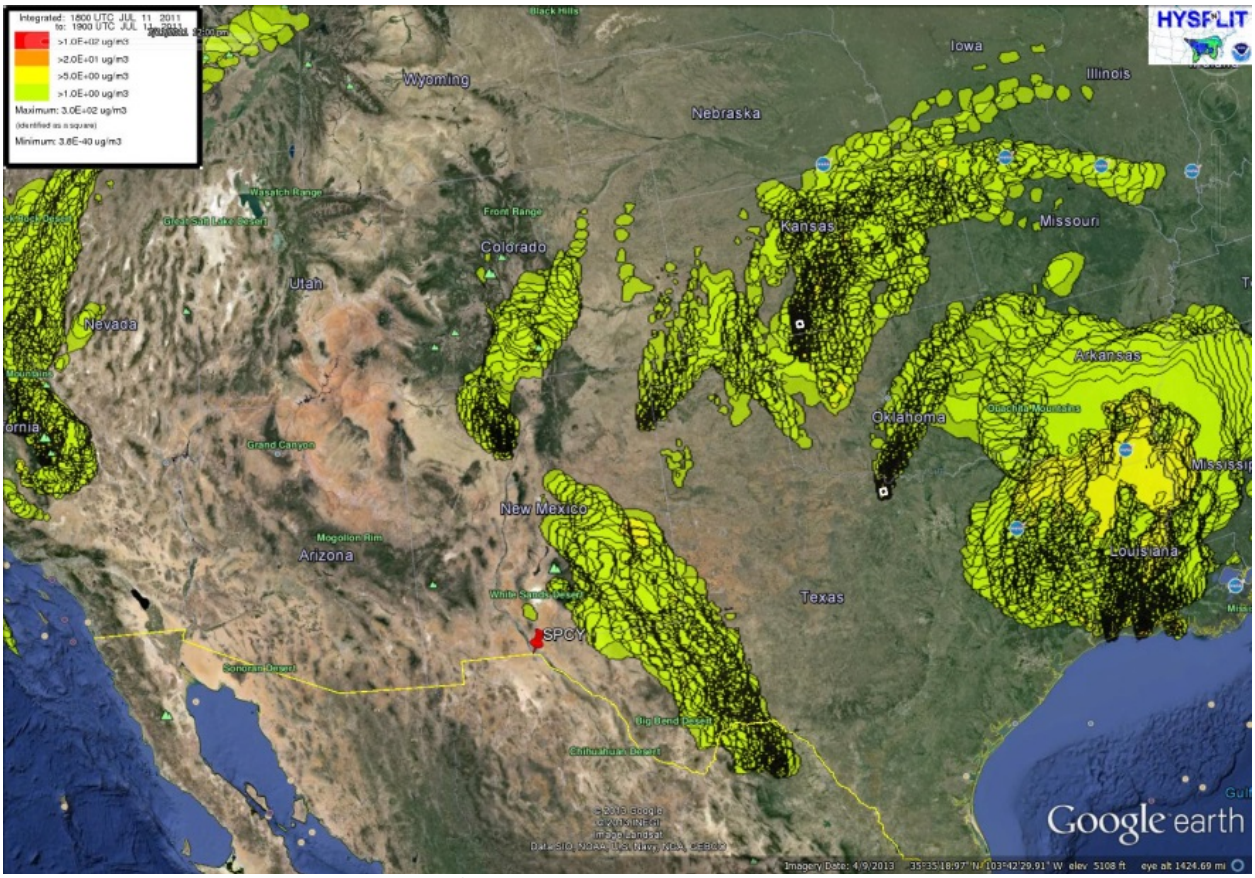

Figure 30-64. HYSPLIT smoke dispersion model for July 11, 2011

30.1.2 Recurrence Frequency

The forests, rangelands and grasslands of New Mexico are fire-adapted ecosystems where long absence of fire has led to hazardous fuel and unhealthy forest conditions. Similar conditions exist in Arizona and northern Mexico. Most fires occur during the spring and early summer when conditions are commonly dry and windy. The frequency and intensity of wildfires, including the frequency of catastrophic fires, has been exacerbated by ongoing drought conditions. Between April 5, 2011 and July 12, 2011, southern New Mexico advanced from a drought intensity of extreme to a drought intensity of exceptional. (See Figure 30-65) Southeastern Arizona saw a similar, although less drastic drought intensity increase during this period as well. (See Figure 30-66) Conditions of high fire risk persisted in general across most of the western half of the North American Continent.

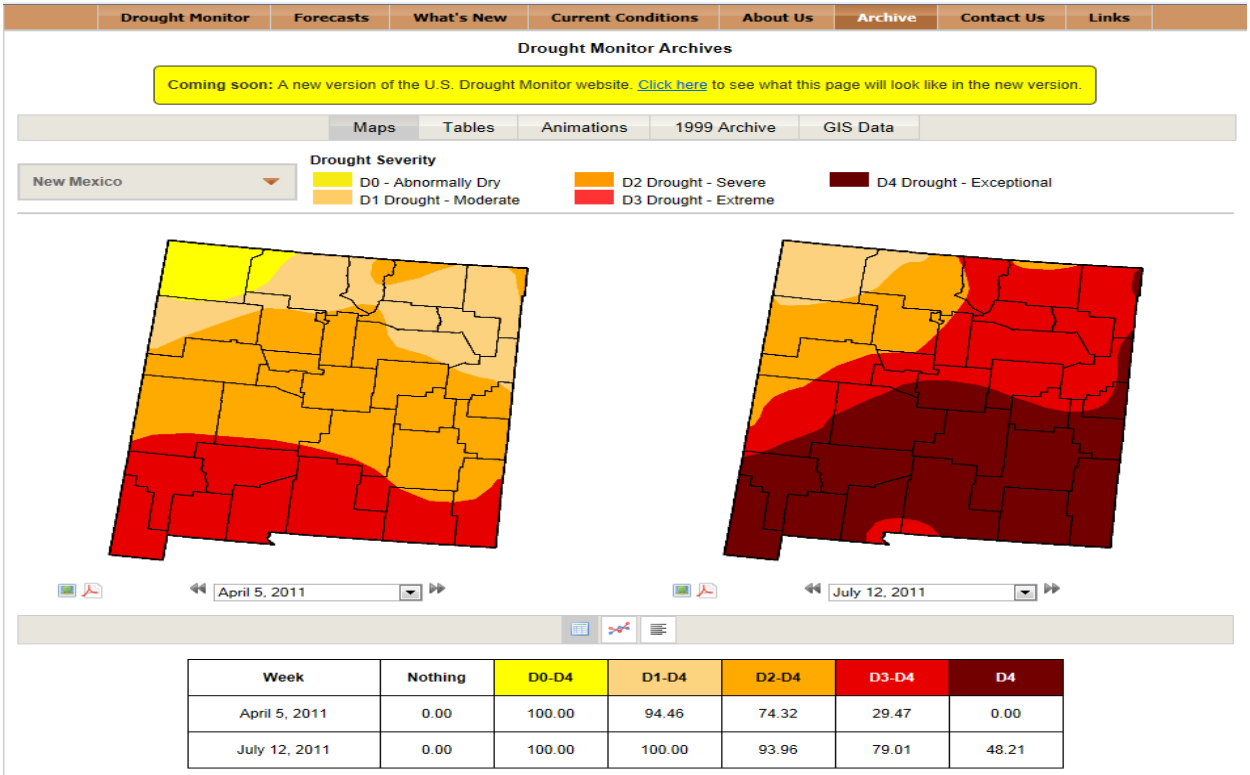

Week	Nothing	D0-D4	D1-D4	D2-D4	D3-D4	D4
April 5, 2011	0.00	100.00	94.46	74.32	29.47	0.00
July 12, 2011	0.00	100.00	100.00	93.96	79.01	48.21

Figure 30-65. U.S. Drought Monitor Archives image showing the movement of New Mexico's drought intensity from April 5, 2011 to July 12, 2011.

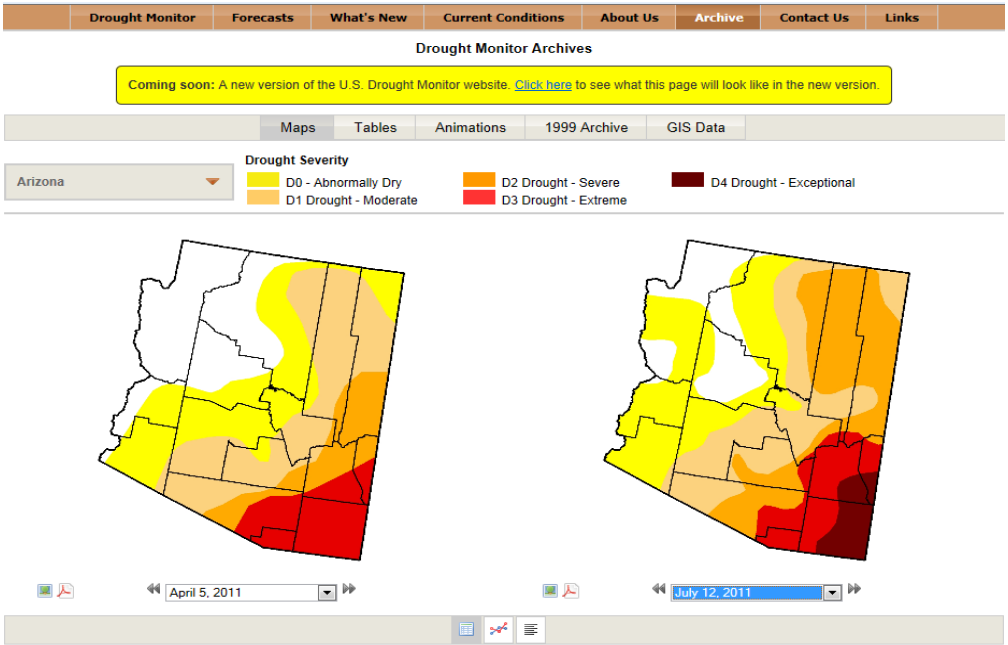

Week	Nothing	D0-D4	D1-D4	D2-D4	D3-D4	D4
April 5, 2011	25.66	74.34	49.27	22.05	11.84	0.00
July 12, 2011	12.78	87.22	60.35	38.20	15.02	4.83

Figure 30-66. U.S. Drought Monitor Archives image showing the movement of Arizona's drought intensity from April 5, 2011 to July 12, 2011.

Drought conditions are predicted to intensify and temperatures are predicted to increase. If fires are located in remote and rugged terrain, the ability to contain fires is dramatically reduced. While the recurrence frequency for exceptional events resulting from smoke cannot be estimated, such events will continue to recur and may increase.

30.1.3 Controls Analysis

In the United States, various agencies are responsible for land management, including the management of forests. These agencies include the Bureau of Land Management, U.S. Forest Service, State Forest agencies, and State Land Offices. Lands where fires may occur also include private land. As such, the individual managers make decisions on forest thinning for the purpose of wildfire prevention. Agencies or private land owners may use controlled burns to manage grasslands, forests and agricultural residue.

Further, when public lands are in extremely dry conditions, managers may close them to public use in order to minimize the risk of human-induced fires. However, no control strategy is 100% effective and further, lightning strikes are completely uncontrollable. Lightning-induced wildfires account for widely varying percentages of total acreage burned. For 2011, lighting-induced fires accounted for only 20.66% of total acreage burned in the southwest. Data are not available for Mexico fires.

30.3 Historical Fluctuations Analysis

A historical record of the number and burned acreage of wildfires in Arizona, New Mexico and western Texas (Figure 30-67) has been documented by the Southwest Coordination Center. There is significant variability in the number of fires, the general trend is toward fewer fires. Significant variability also exists in the number of acres burned. It should be noted, however, the dramatic increase in acreage burned for 2011. These historical data suggest that, even though fewer fires may start, extreme drought conditions – especially when coupled with an exceptionally windy fire season – will promote conditions conducive to extensive wildfire burning.

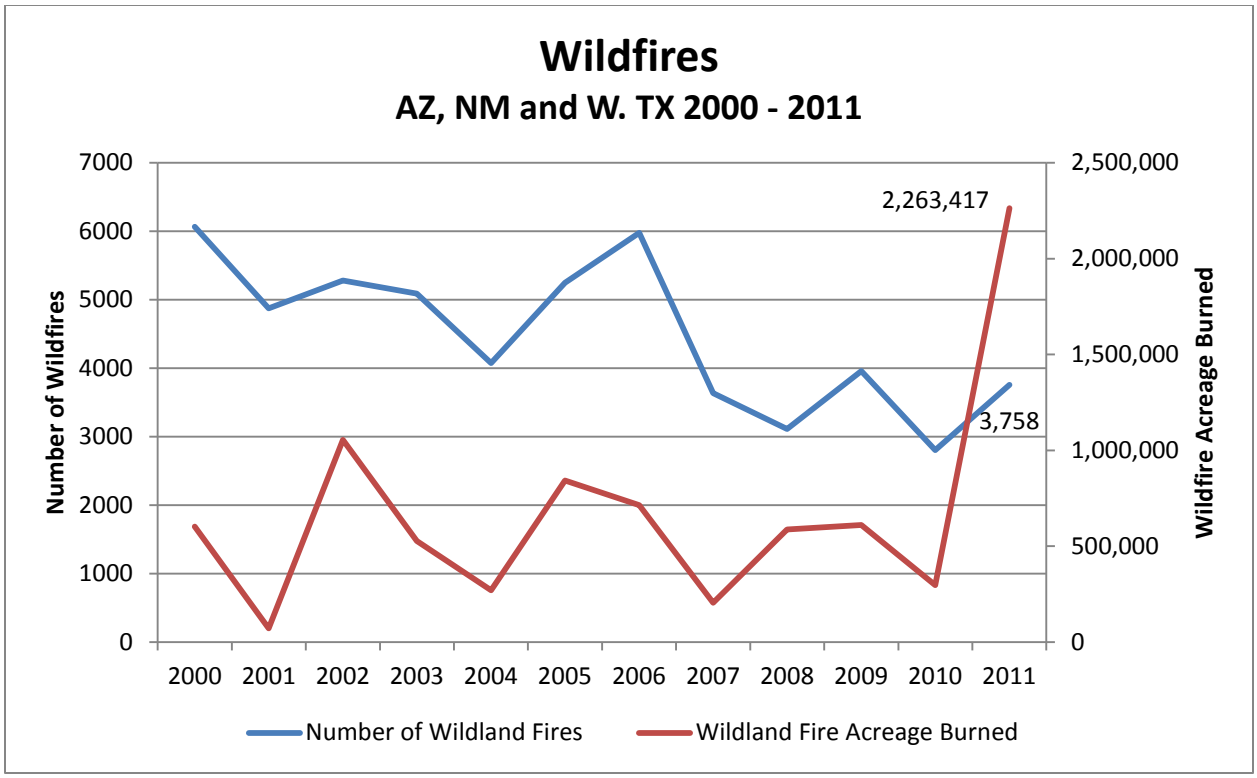

Figure 30-67. Historical record from the Southwest Coordination Center showing the number and acreage burned of wildfires in Arizona, New Mexico and western Texas for the years 2000 through 2011. Data are not available for Mexico.

30.4 Clear Causal Relationship

A very active fire season caused excessive amounts of smoke to be entrained in the atmosphere beginning in April and continuing through July

For each of the dates listed in Table 30-1, a Naval Research Laboratory's Navy Aerosol Analysis and Prediction System (NAAPS) product is available in 6-hour increments. This product breaks down the aerosols, using the AOD data, fire locations, weather data, and microchemistry and physics, into sulfates, dust and smoke and projects these onto a map. The following images show, from the NAAPS Archive, that for each of these dates, smoke was present and affected the SPCY $PM_{2.5}$ Partisol monitor. (Figures 30-68 to 30-99) While only one image is shown for each date, most dates have several available confirming images. As these images are actual analyses, they prove that smoke was a factor for each date.

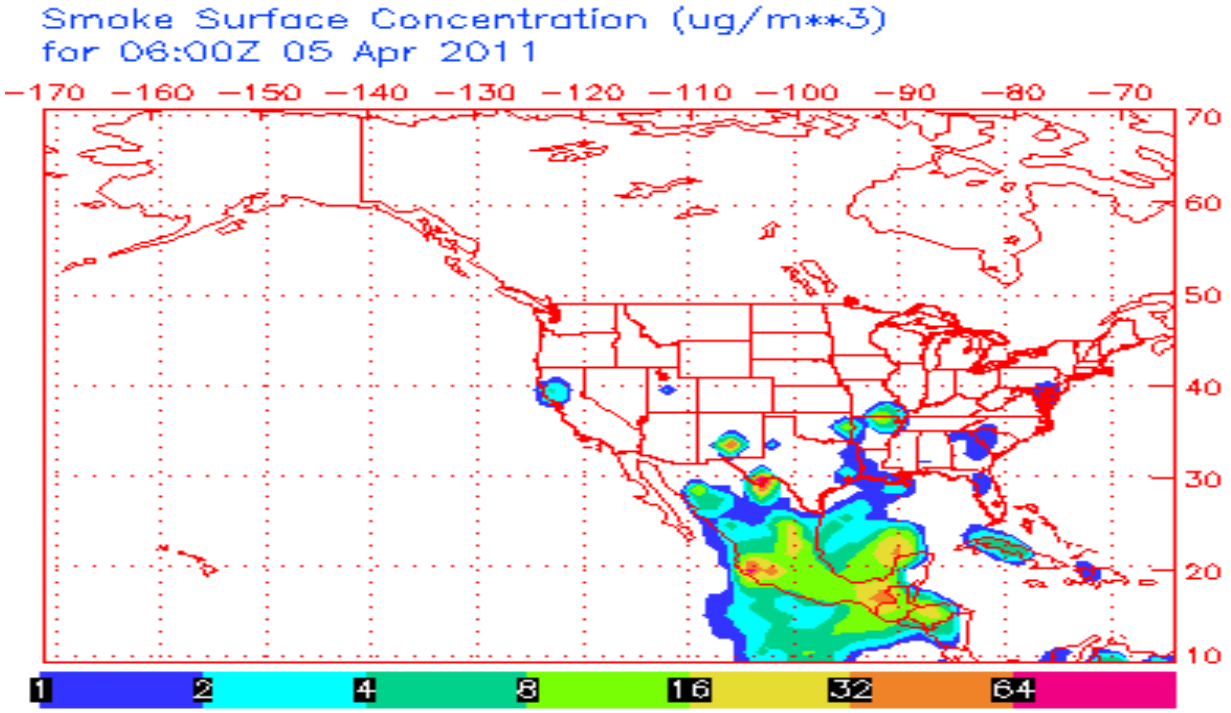

Figure 30-68. NAAPS Smoke Surface Concentration for April 5, 2011 at 0000 hr MDT. Smoke was also detected at SPCY at 0600 hr, inferring that it was present for at least 6 hours.

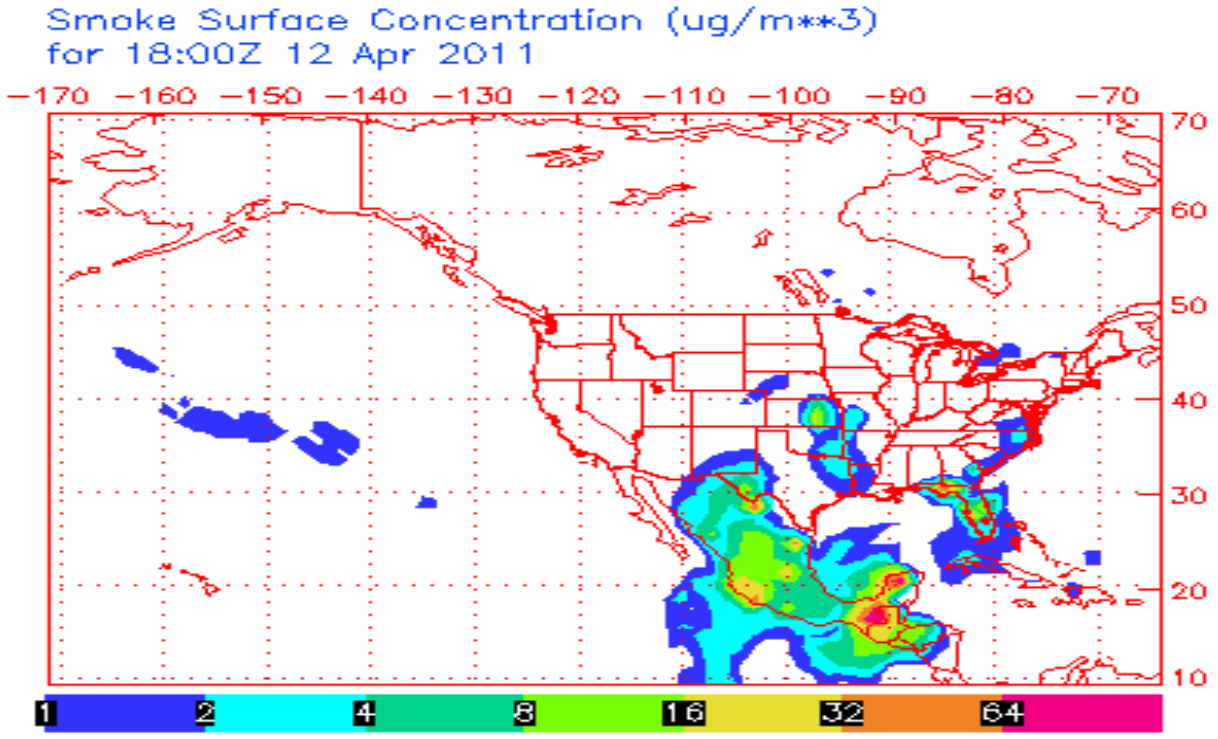

Figure 30-69. NAAPS Smoke Surface Concentration (in micrograms per cubic meter) for April 12, 2011 at 1200 hr MDT. Smoke was also detected at 1800 hr, inferring that smoke was present for at least 6 hours.

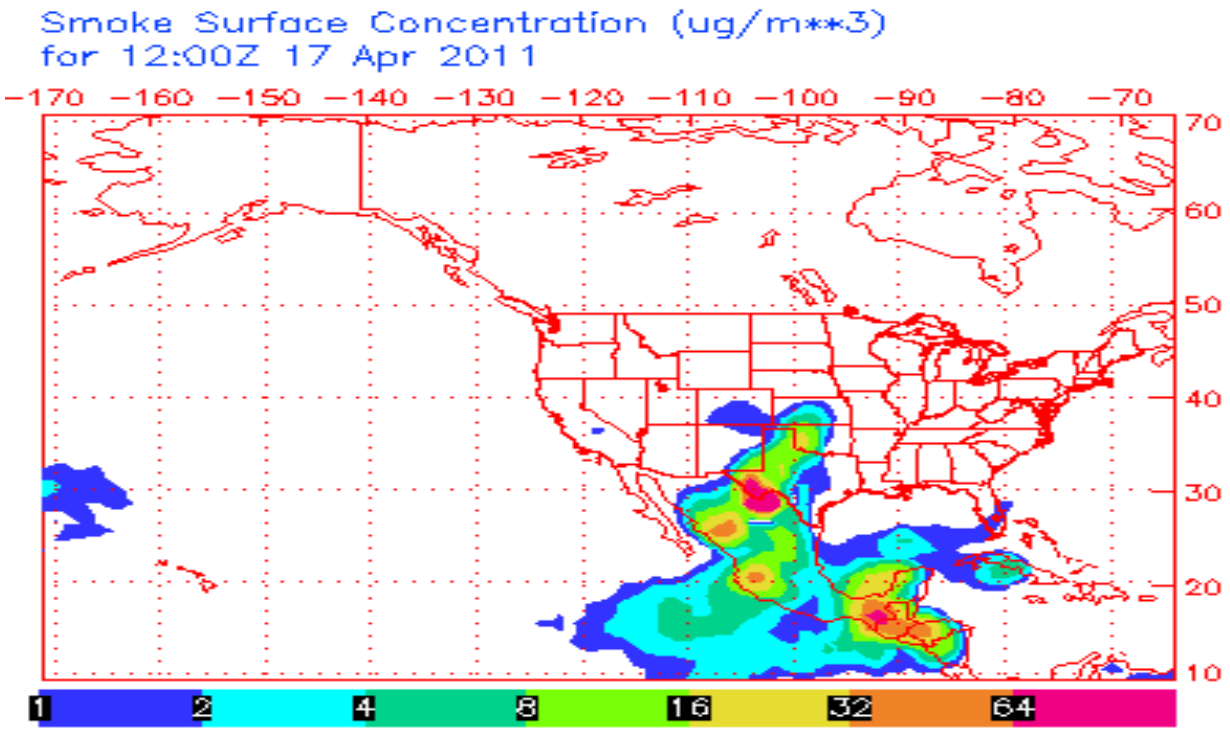

Figure 30-70. NAAPS Smoke Surface Concentration (in micrograms per cubic meter) for April 17, 2011 at 0600 hr MDT.

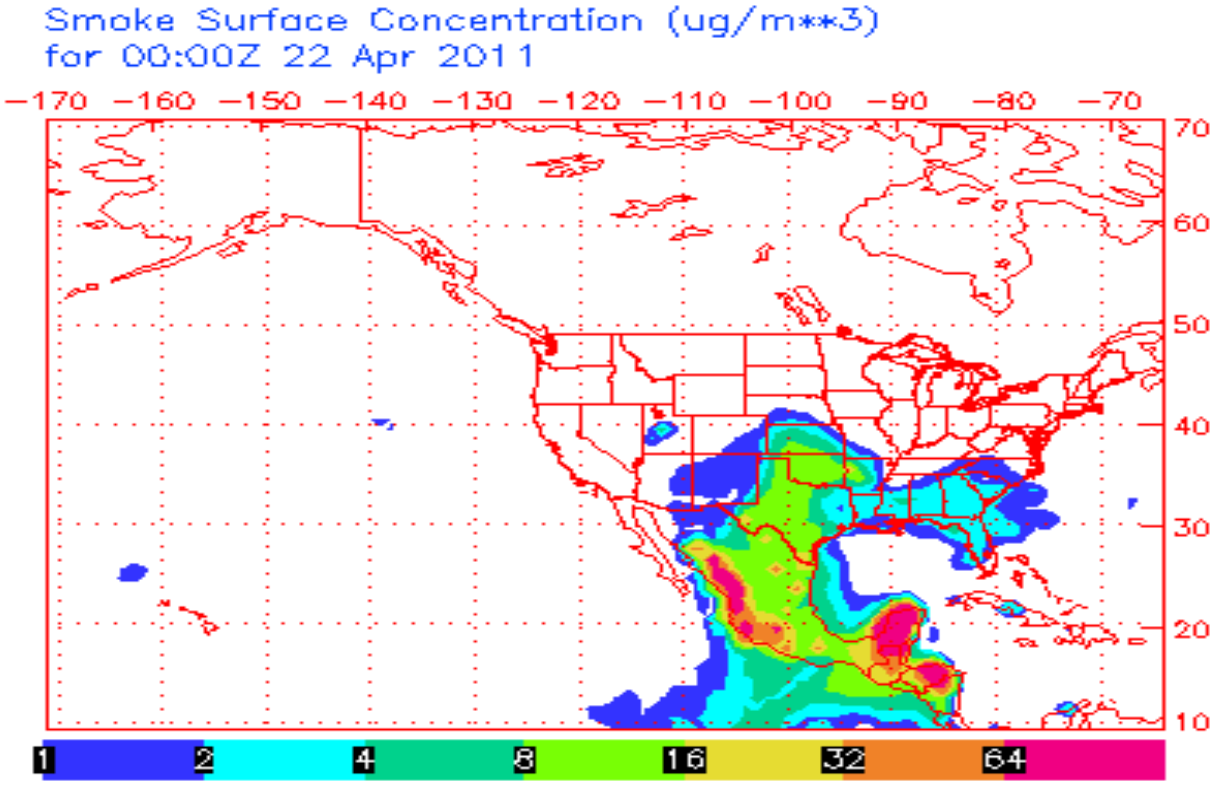

Figure 30-71. NAAPS Smoke Surface Concentration (in micrograms per cubic meter) for April 21, 2011 at 1800 hr MDT

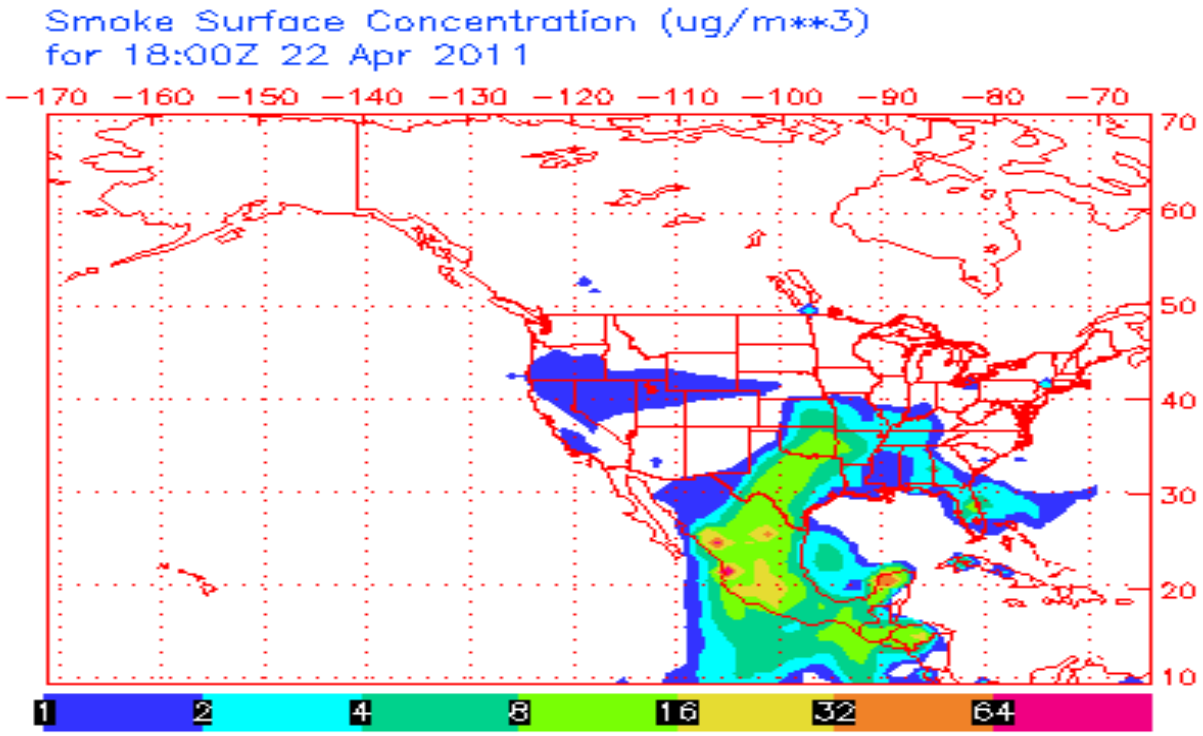

Figure 30-72. NAAPS Smoke Surface Concentration (in micrograms per cubic meter) for April 22, 2011 at 1200 hr MDT. Smoke was also detected at 1800 hr, inferring that smoke was present for at least 6 hours.

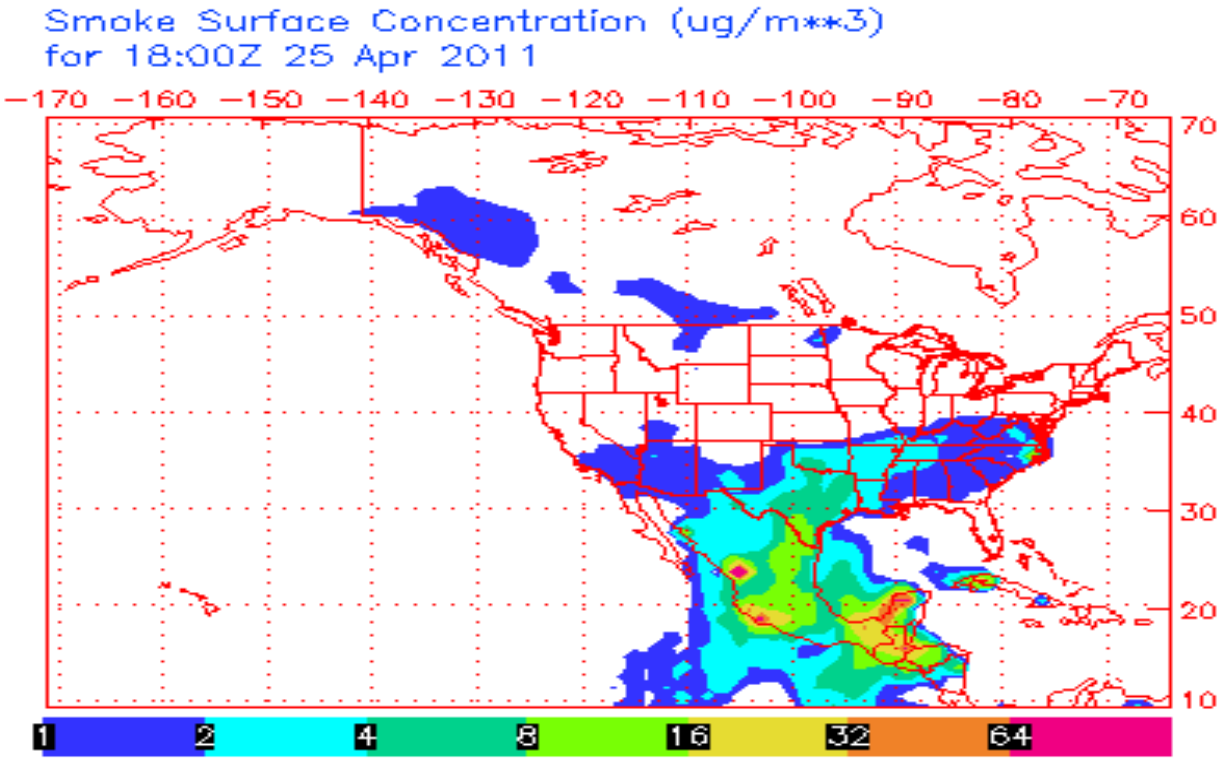

Figure 30-73. NAAPS Smoke Surface Concentration (in micrograms per cubic meter) for April 25, 2011 at 1200 hr MDT. Smoke was also detected at 0000 hr, 0600 hr, 1800 hr and 2400 hr, inferring that smoke was present for the full 24 hours.

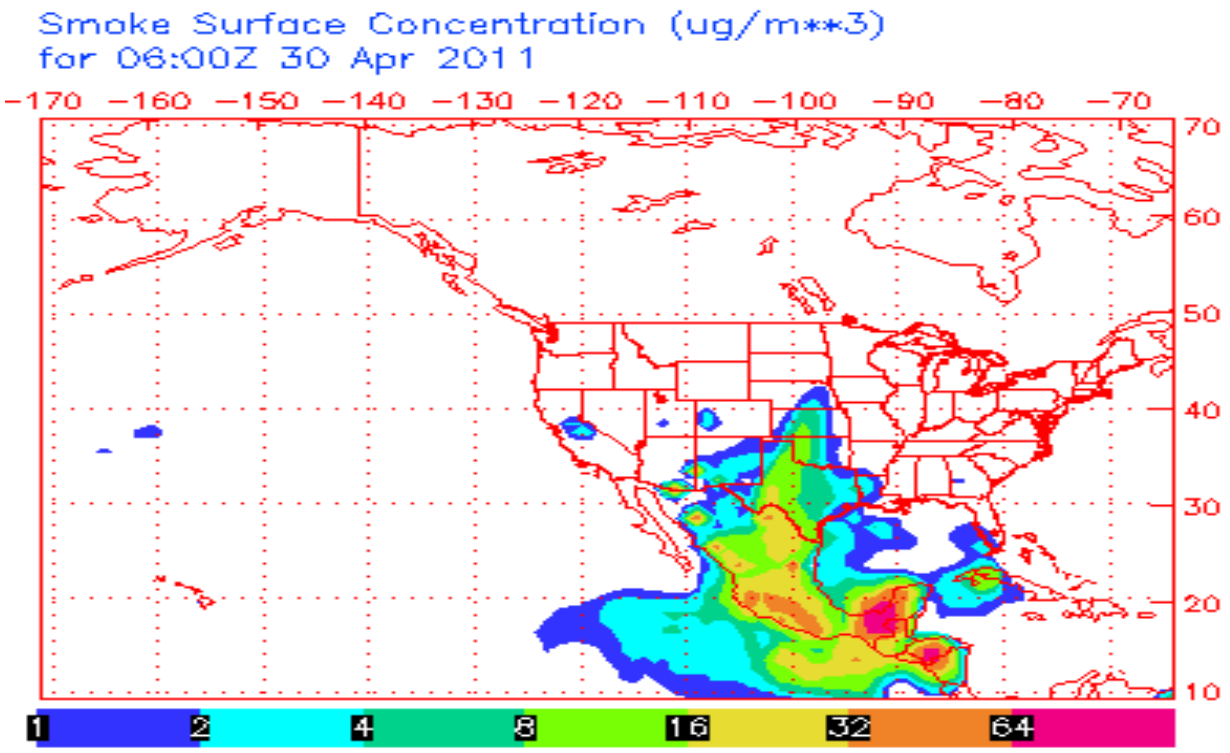

Figure 30-74. NAAPS Smoke Surface Concentration (in micrograms per cubic meter) for April 30, 2011 at 0000 hr MDT. Smoke was also detected at 0600 hr, 1200 hr, 1800 hr and 2400 hr, inferring that smoke was present for the full 24 hours.

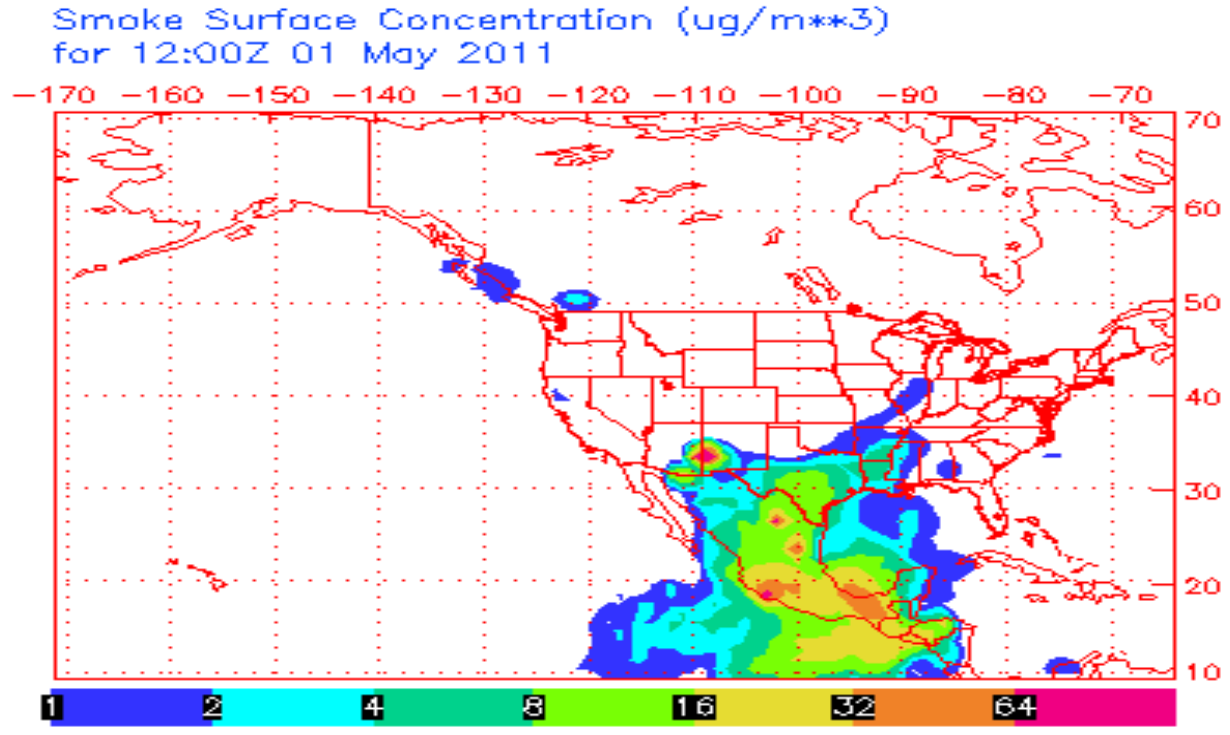

Figure 30-75. NAAPS Smoke Surface Concentration (in micrograms per cubic meter) for May 1, 2011 at 0600 hr MDT. Smoke was also detected at 0000 hr, 1200 hr, 1800 hr and 2400 hr, inferring that smoke was present for the full 24 hours.

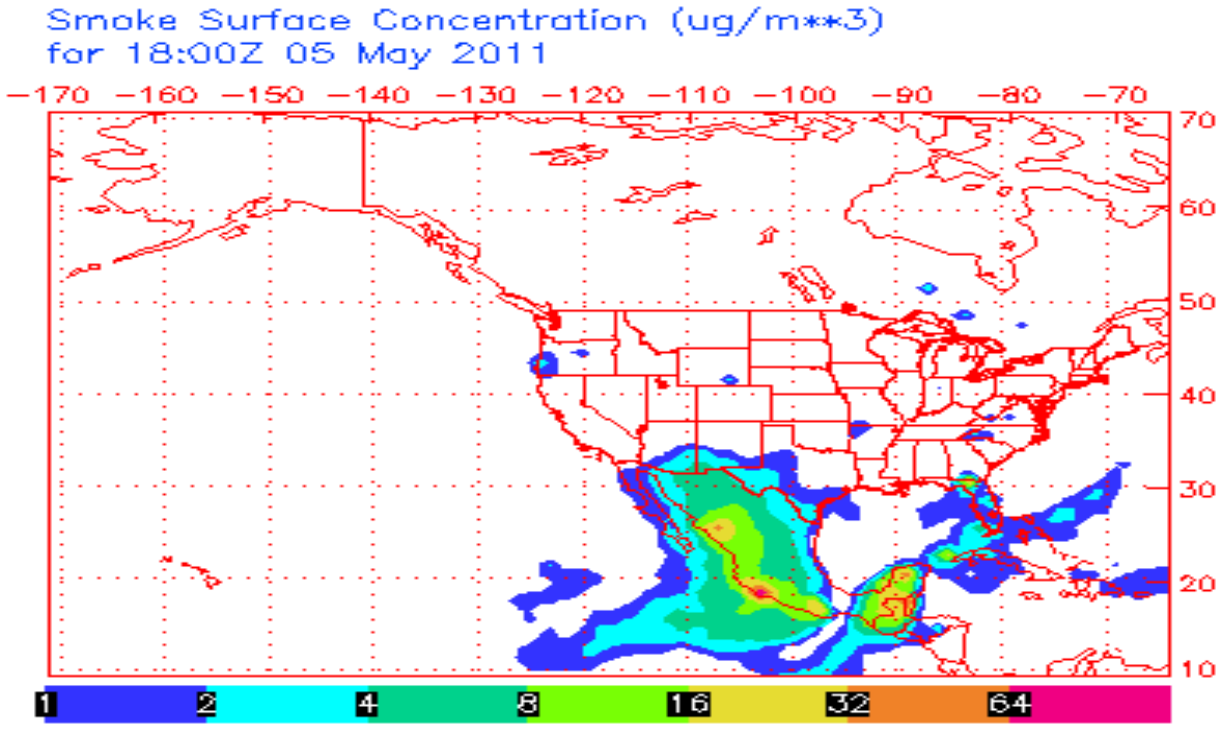

Figure 30-76. NAAPS Smoke Surface Concentration (in micrograms per cubic meter) for May 5, 2011 at 1200 hr MDT. Smoke was also detected at 0000 hr, 0600 hr, 1800 hr and again at 2400 hr, inferring that smoke was present for the full 24 hours.

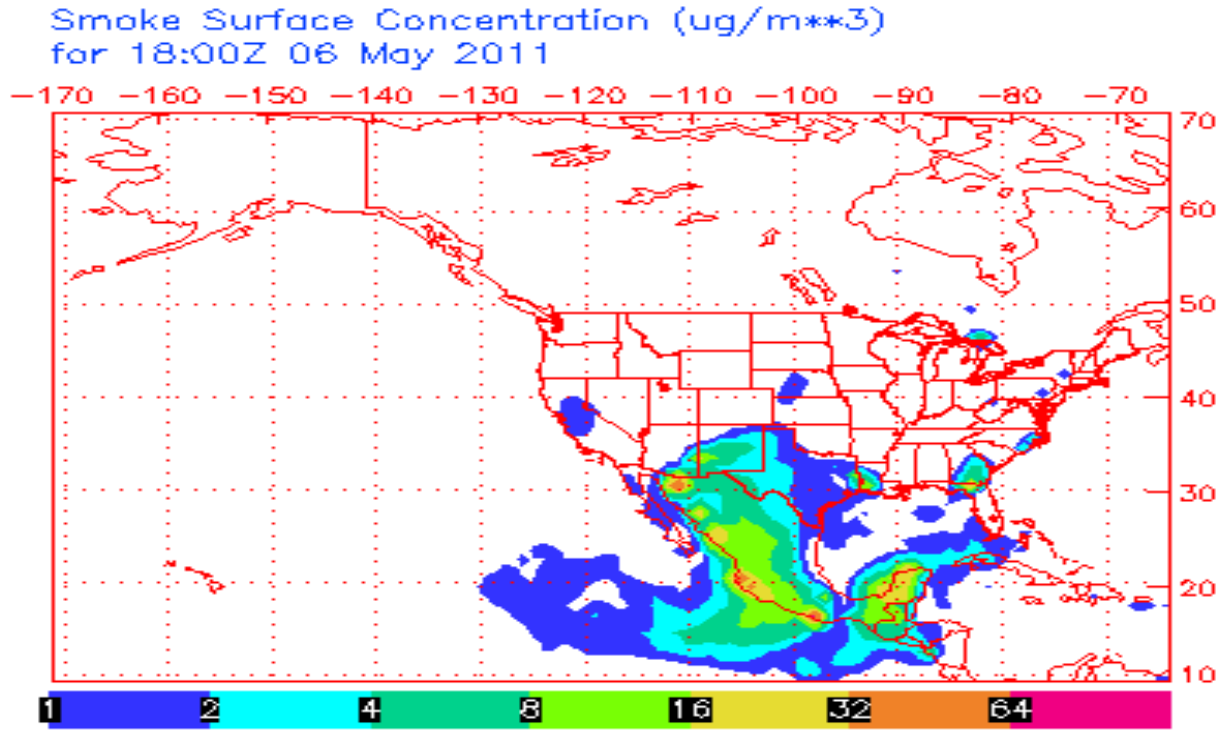

Figure 30-77. NAAPS Smoke Surface Concentration (in micrograms per cubic meter) for May 6, 2011 at 1200 hr MDT. Smoke was also detected at 0000 hr, 0600 hr, 1800 hr and 2400 hr, inferring that smoke was present for all 24 hours.

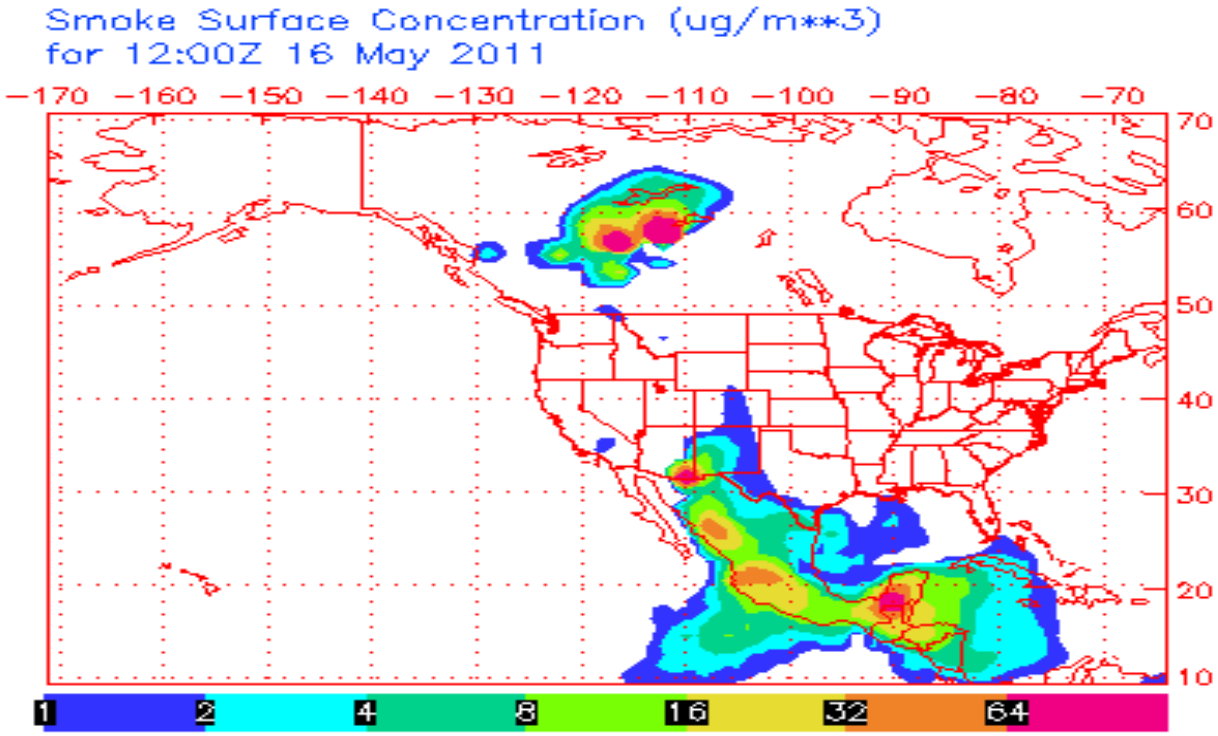

Figure 30-78. NAAPS Smoke Surface Concentration (in micrograms per cubic meter) for May 16, 2011 at 0600 hr MDT. Smoke was also detected at 0000 hr, 1200 hr, 1800 hr and 2400 hr, inferring that smoke was present all 24 hours.

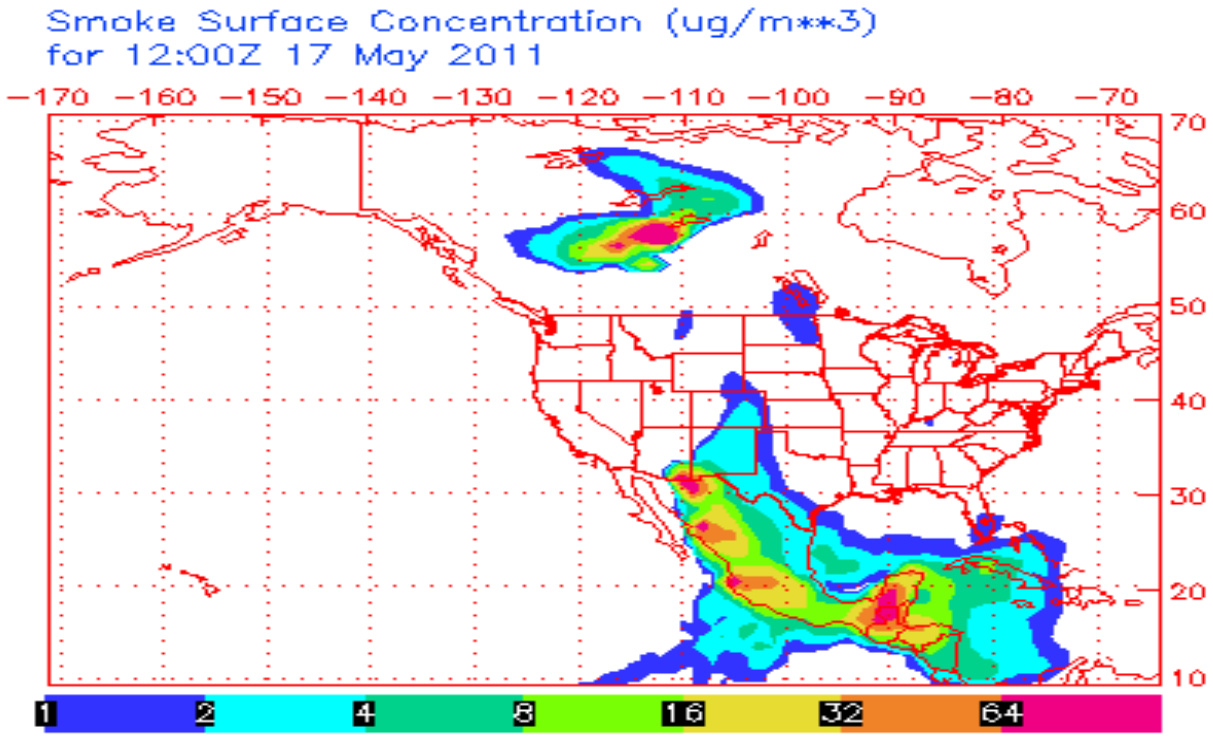

Figure 30-79. NAAPS Smoke Surface Concentration (in micrograms per cubic meter) for May 17, 2011 at 0600 hr MDT. Smoke was also detected at 0000 hr, 1200 hr, 1800 hr and 2400 hr, inferring that smoke was present for all 24 hours.

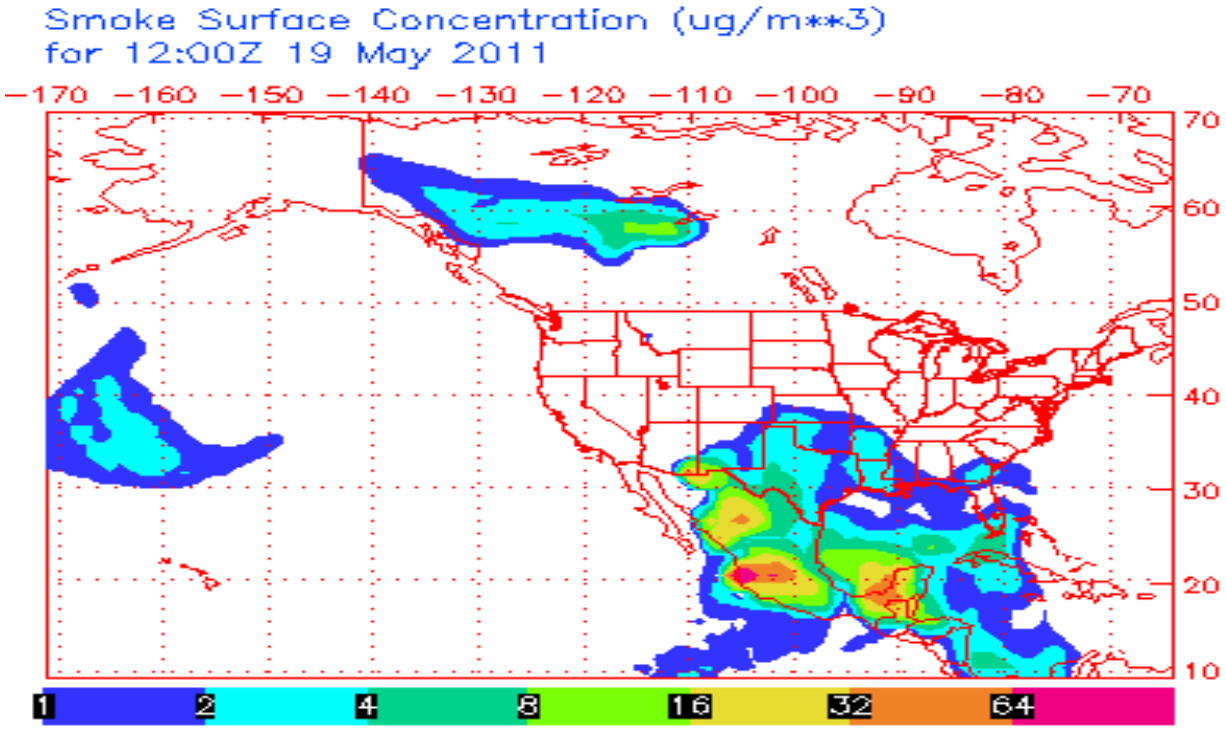

Figure 30-80. NAAPS Smoke Surface Concentration (in micrograms per cubic meter) for May 19, 2011 at 0600 hr MDT. Smoke was also detected at 0000 hr and 1200 hr, inferring that smoke was present for at least 12 hours.

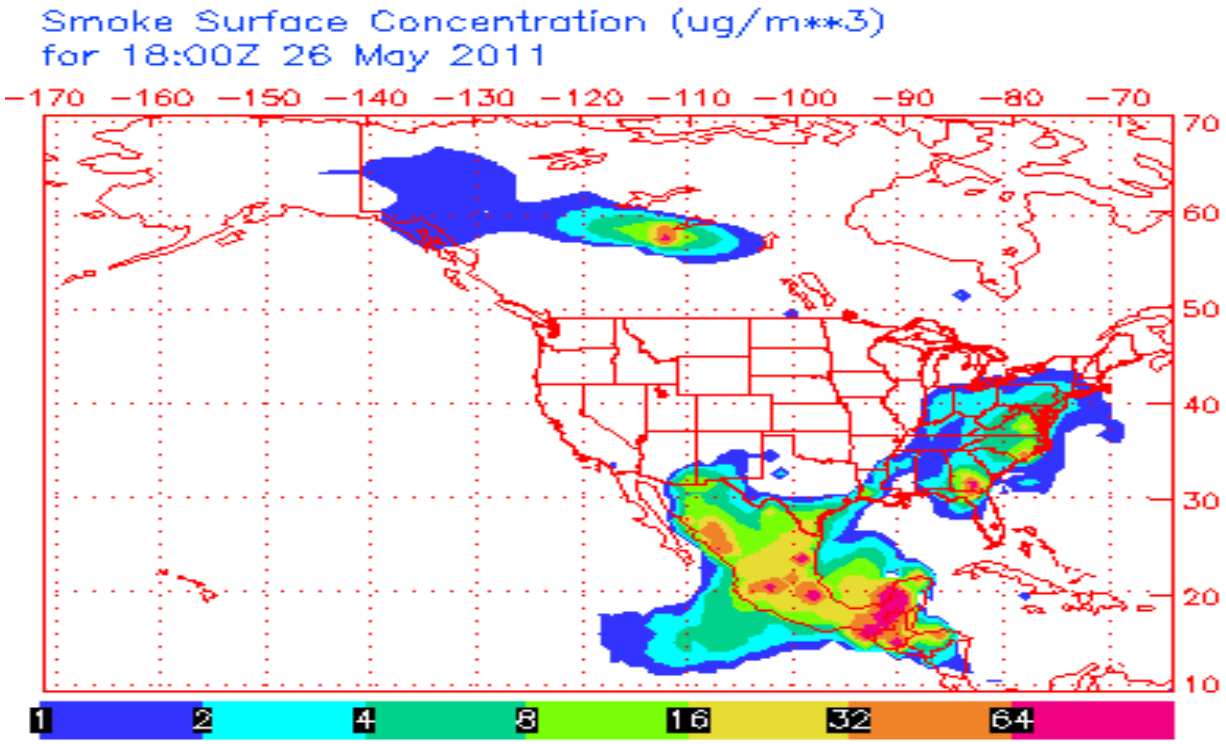

Figure 30-81. NAAPS Smoke Surface Concentration (in micrograms per cubic meter) for May 26, 2011 at 1200 hr MDT. Smoke was also detected at 0000 hr, 0600 hr, 1800 hr and 2400 hr, inferring that smoke was present for the full 24 hours.

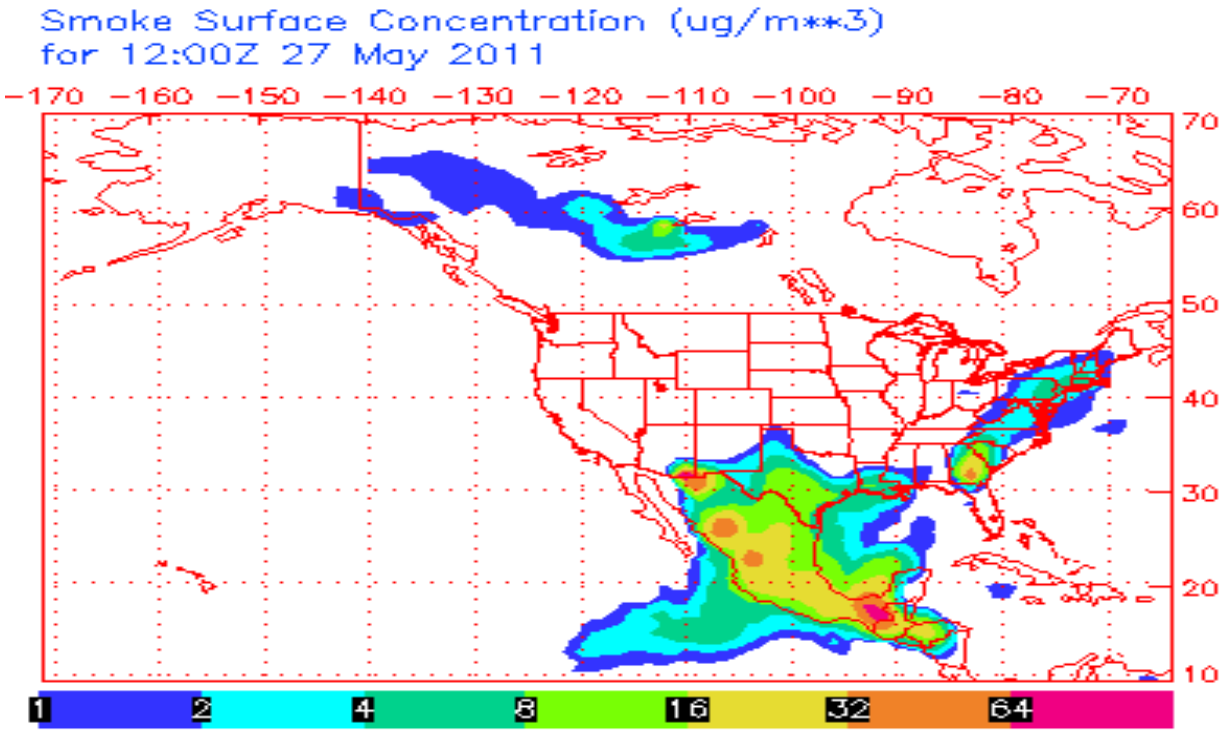

Figure 30-82. NAAPS Smoke Surface Concentration (in micrograms per cubic meter) for May 27, 2011 at 0600 hr MDT. Smoke was also detected at 0000 hr, 1200 hr, 1800 hr and 2400 hr, inferring that smoke was present for the full 24 hours.

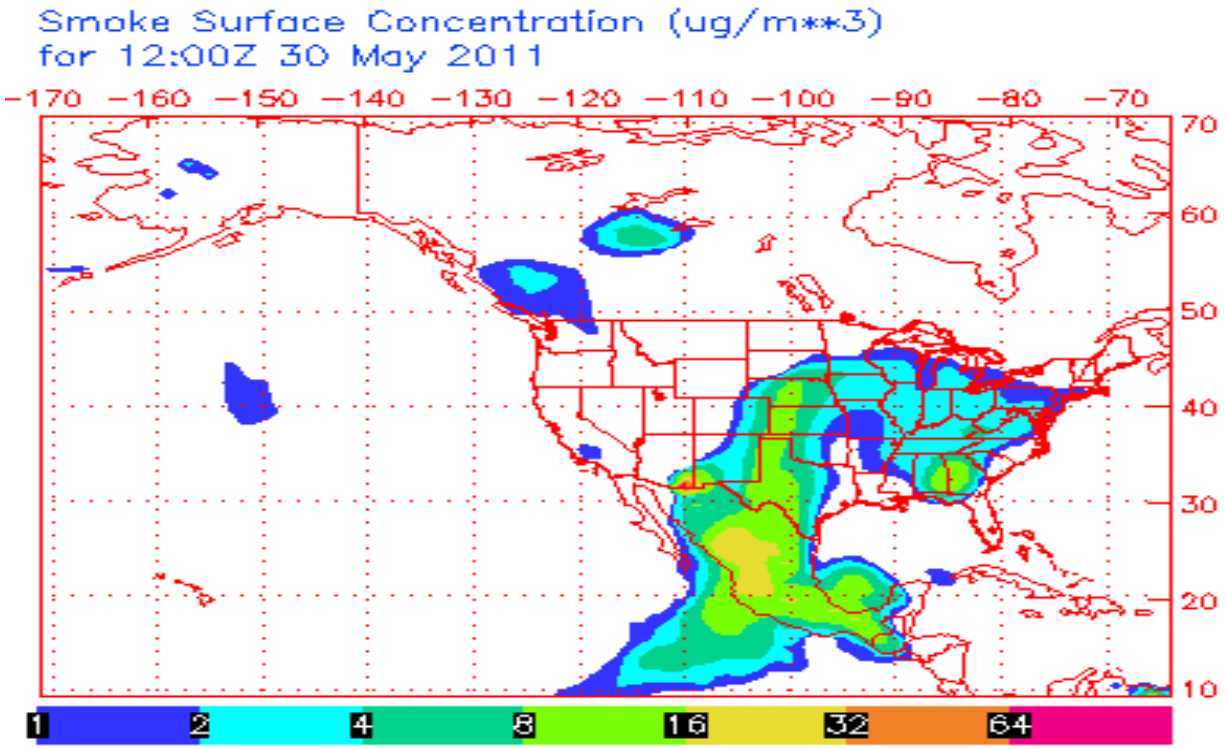

Figure 30-83. NAAPS Smoke Surface Concentration (in micrograms per cubic meter) for May 30, 2011 at 0600 hr. Smoke was also detected at 0000 hr, 1200 hr, 1800 hr and 2400 hr, inferring that smoke was present for the full 24 hours.

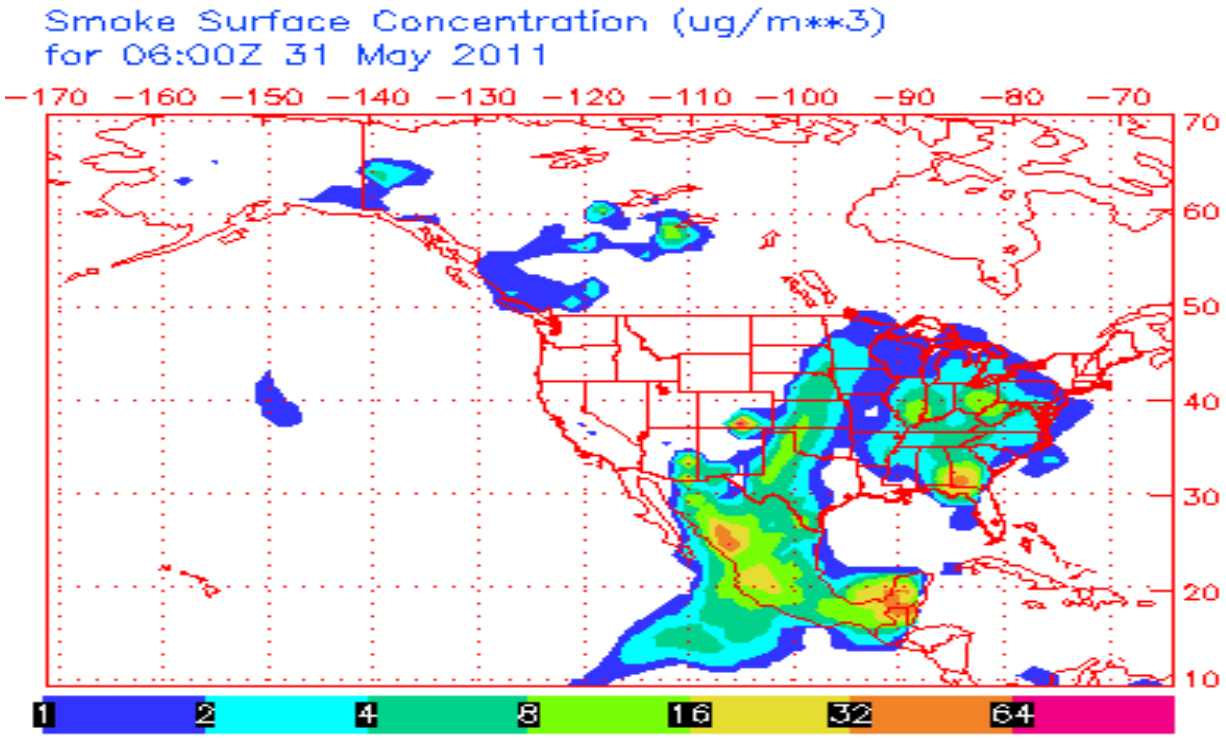

Figure 30-84. NAAPS Smoke Surface Concentration (in micrograms per cubic meter) for May 31, 2011 at 0000 hr MDT. Smoke was also detected at 0600 hr, 1200 hr, 1800 hr and 2400 hr, inferring that smoke was present for the full 24 hours.

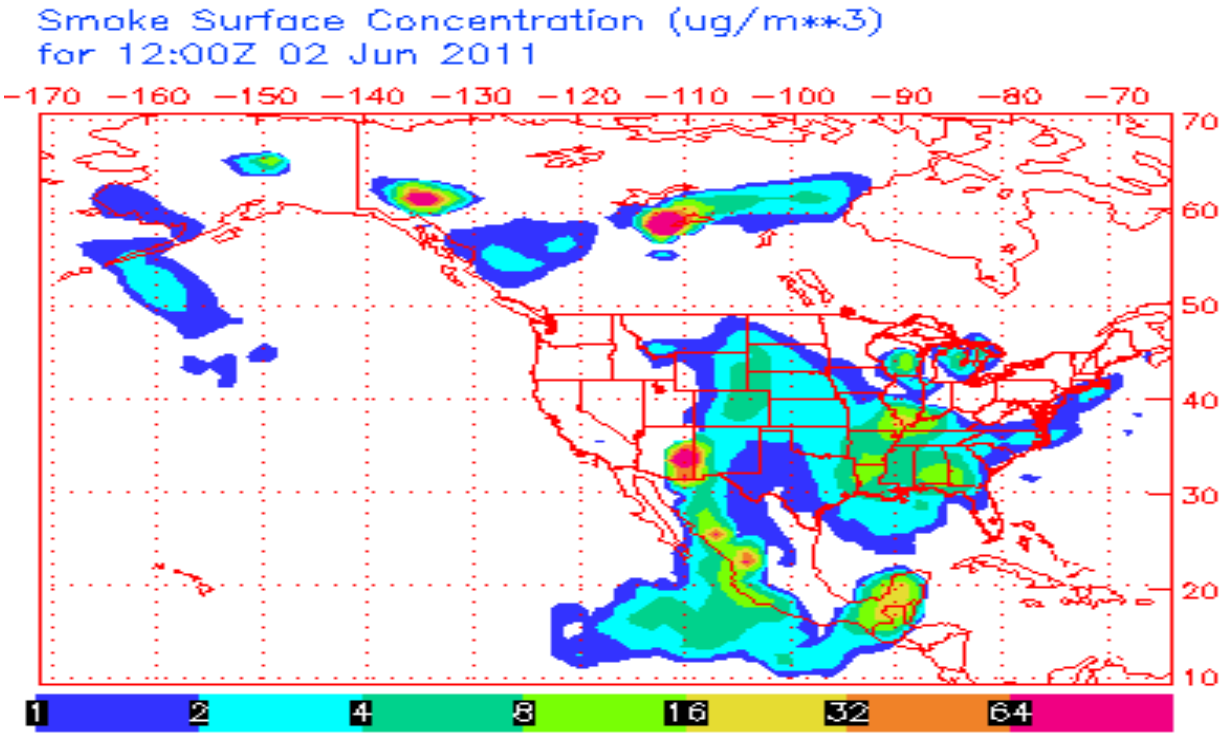

Figure 30-85. NAAPS Smoke Surface Concentration (in micrograms per cubic meter) for June 2, 2011 at 0600 hr. Smoke was also detected at 0000 hr, 1200 hr, 1800 hr and 2400 hr, inferring that smoke was present for the full 24 hours.

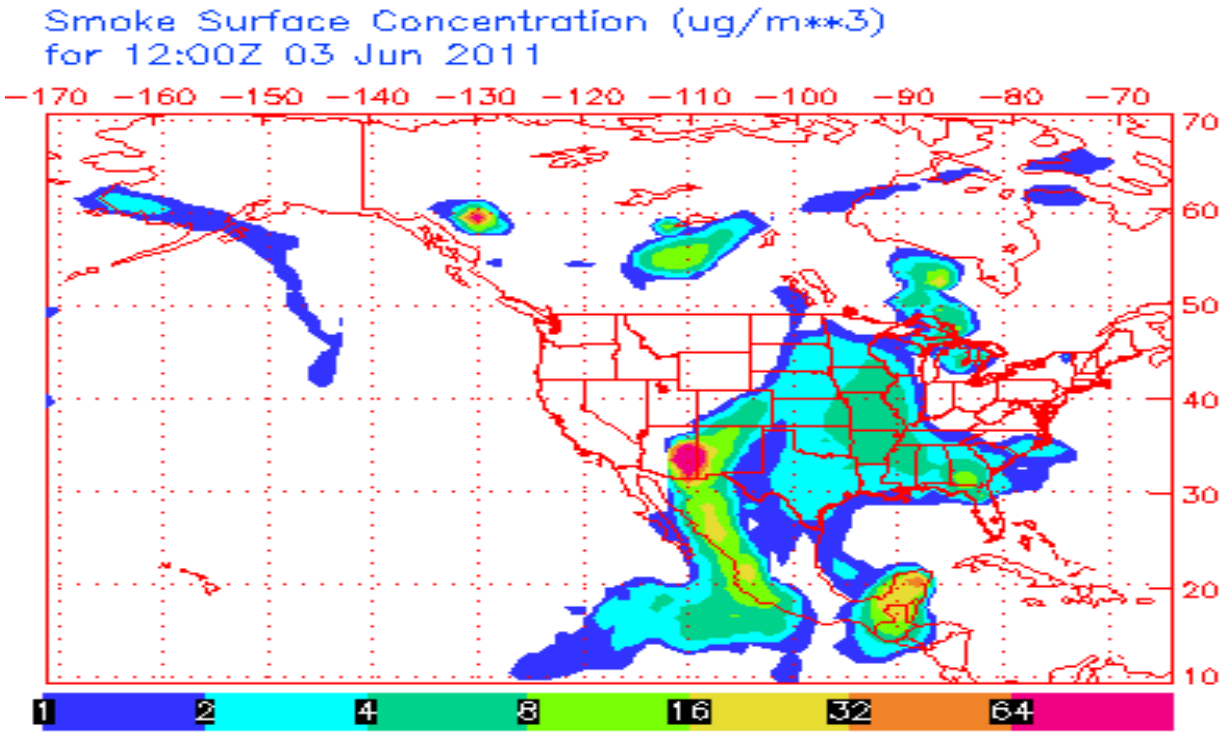

Figure 30-86. NAAPS Smoke Surface Concentration (in micrograms per cubic meter) for June 3, 2011 at 0600 hr MDT. Smoke was also detected at 0000 hr, 1200 hr, 1800 hr and 2400 hr, inferring that smoke was present for the full 24 hours.

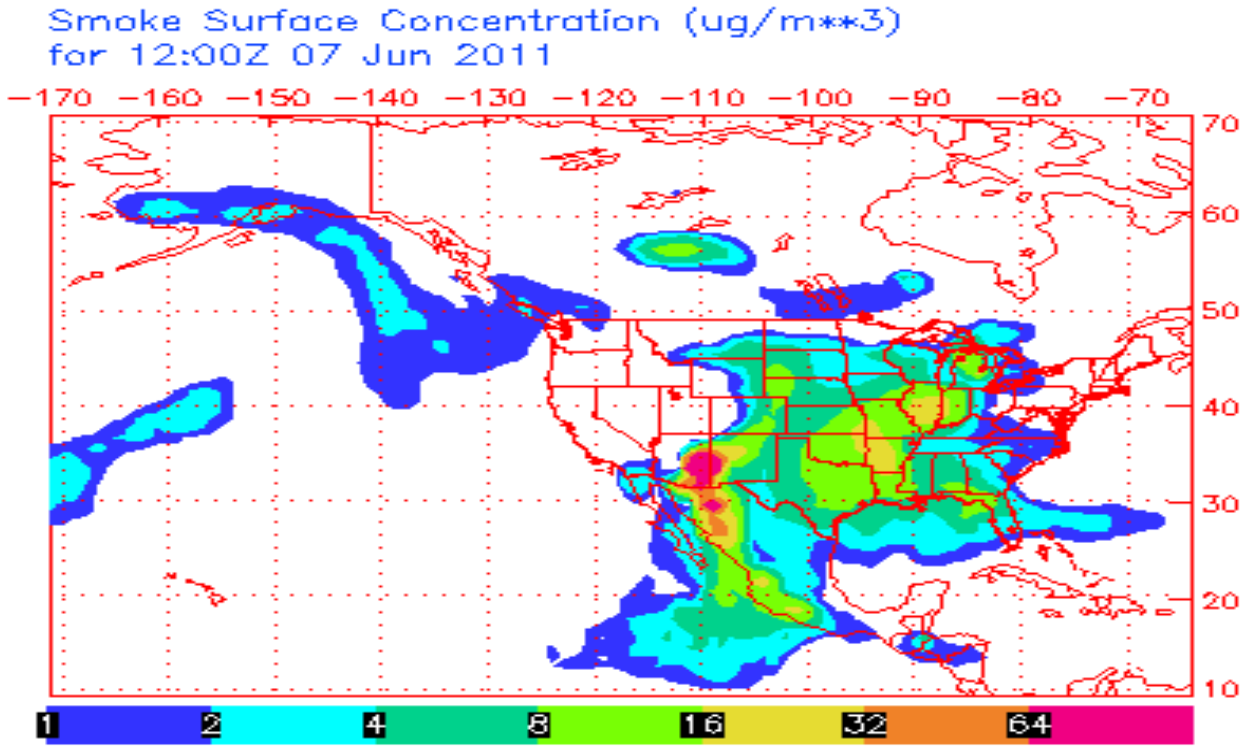

Figure 30-87. NAAPS Smoke Surface Concentration (in micrograms per cubic meter) for June 7, 2011 at 0600 hr MDT. Smoke was also detected at 0000 hr, 1200 hr, 1800 hr and 2400 hr, inferring that smoke was present for the full 24 hours.

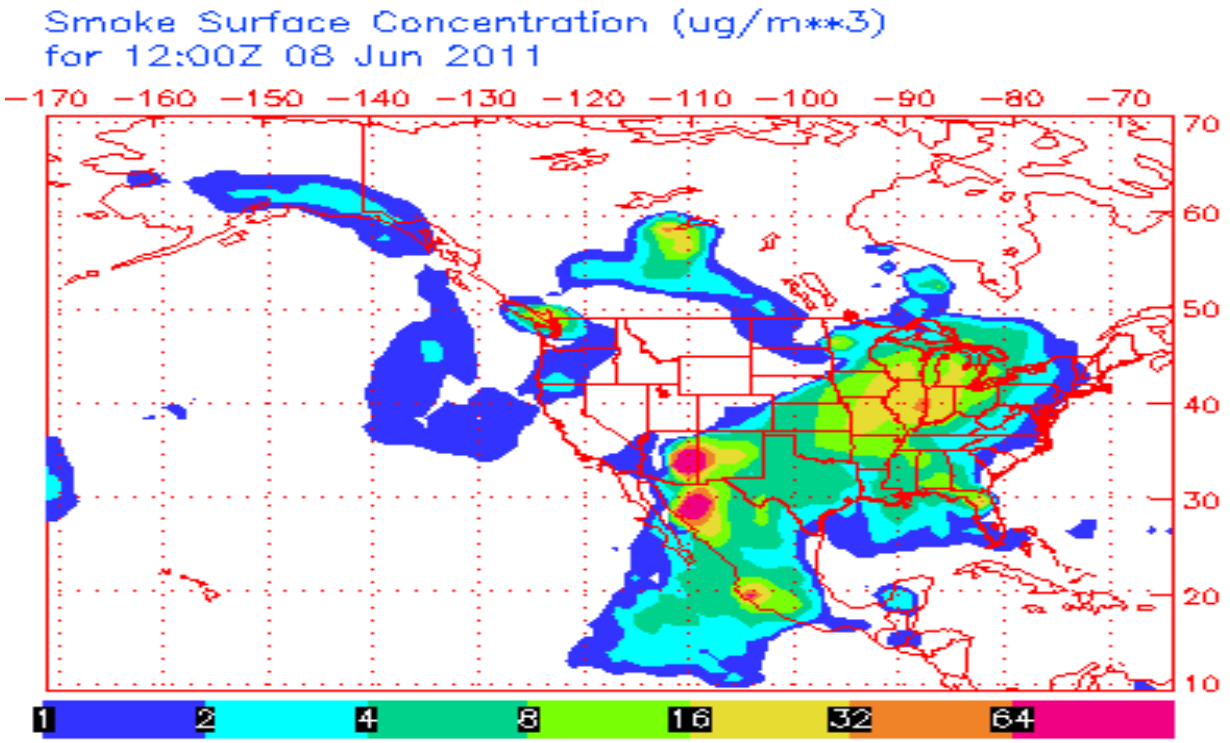

Figure 30-88. NAAPS Smoke Surface Concentration (in micrograms per cubic meter) for June 8, 2011 at 0600 hr MDT. Smoke was also detected at 0000 hr, 1200 hr, 1800 hr and 2400 hr, inferring that smoke was present for the full 24 hours.

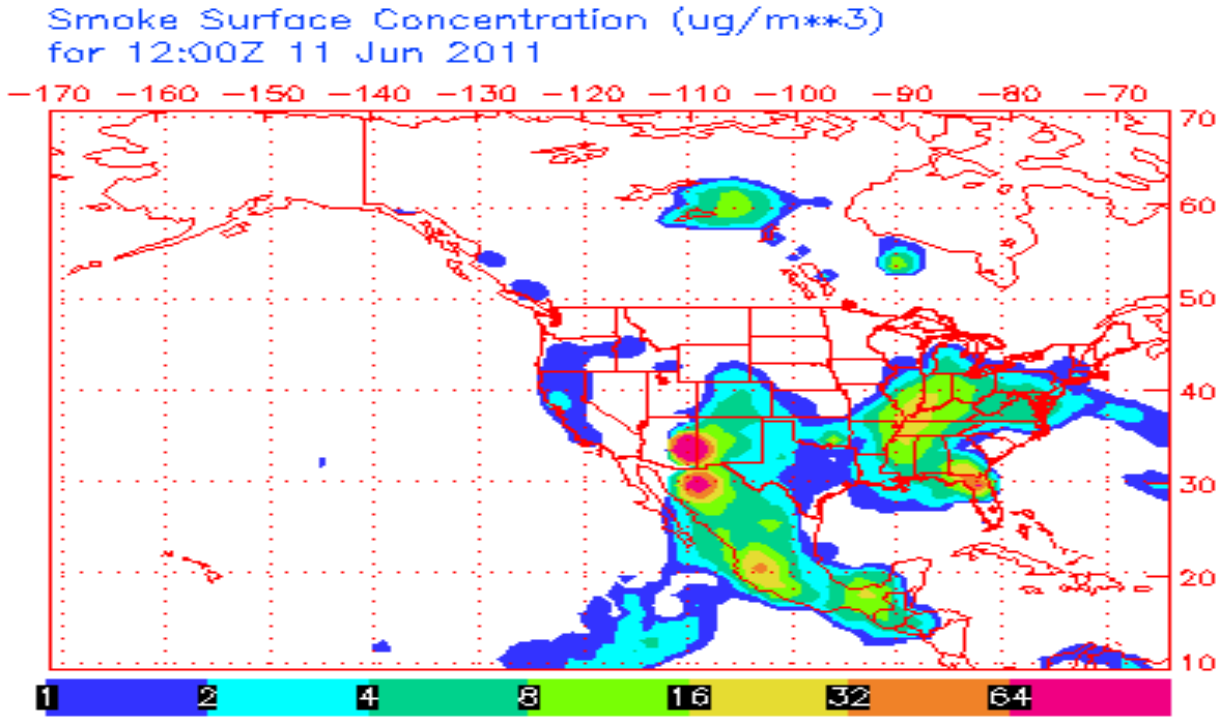

Figure 30-89. NAAPS Smoke Surface Concentration (in micrograms per cubic meter) for June 11, 2011 at 0600 hr. Smoke was also detected at 0000 hr, 1200 hr, 1800 hr and 2400 hr, inferring that smoke was present for the full 24 hours.

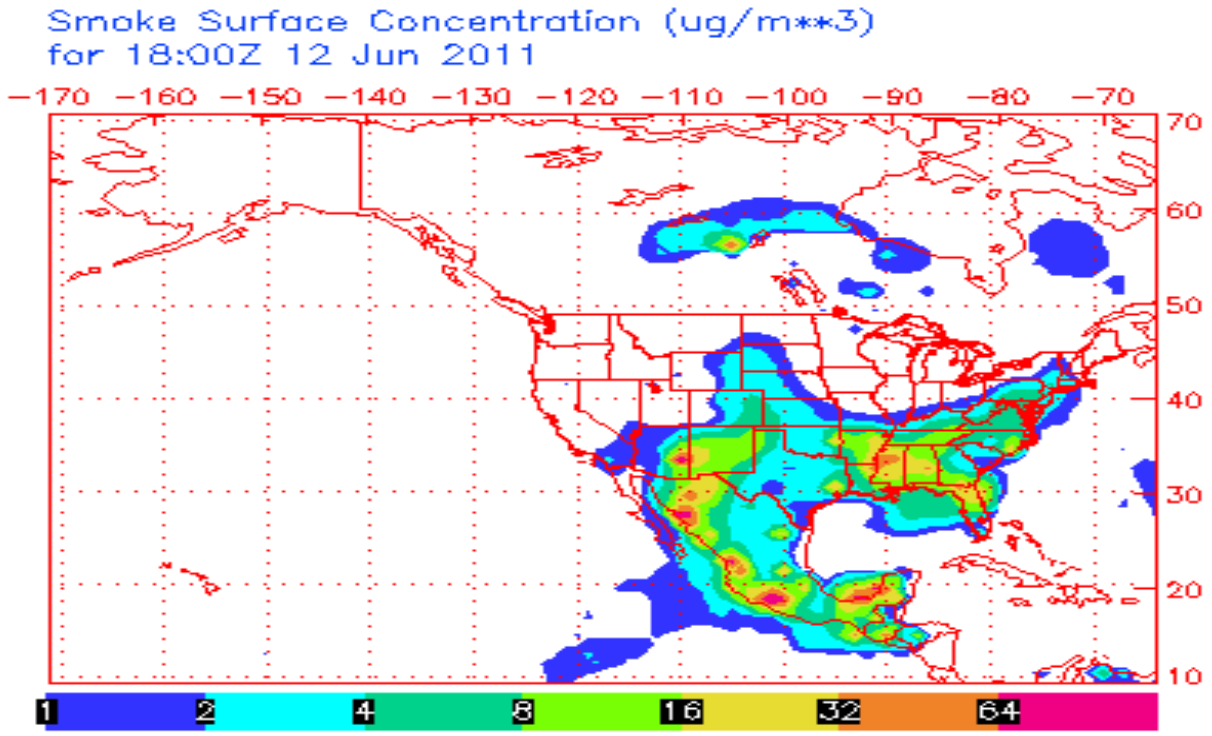

Figure 30-90. NAAPS Smoke Surface Concentration (in micrograms per cubic meter) for June 12, 2011 at 1200 hr MDT. Smoke was also detected at 0000 hr, 0600 hr, 1800 hr and 2400 hr, inferring that smoke was present for the full 24 hours.

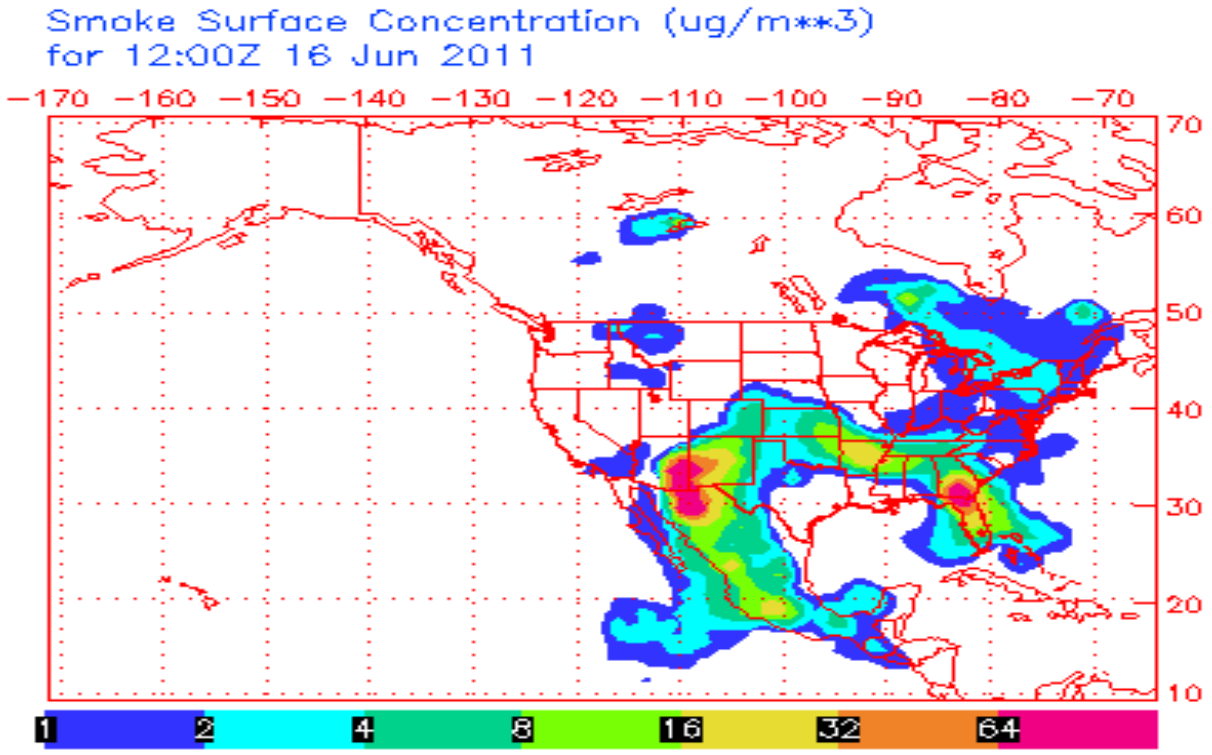

Figure 30-91. NAAPS Smoke Surface Concentration (in micrograms per cubic meter) for June 16, 2011 at 0600 hr MDT. Smoke was also detected at 0000 hr, 1200 hr, 1800 hr and 2400 hr, inferring that smoke was present for the full 24 hours.

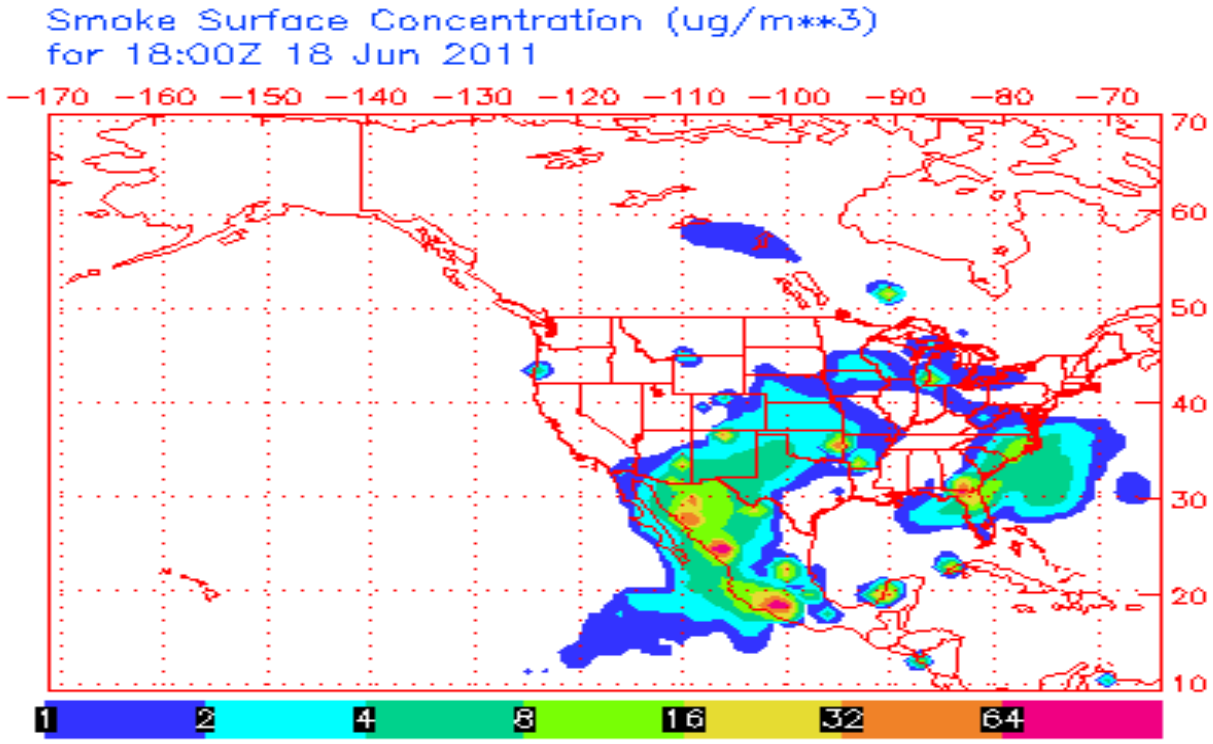

Figure 30-92. NAAPS Smoke Surface Concentration (in micrograms per cubic meter) for June 18, 2011 at 1200 hr MDT. Smoke was also detected at 0000 hr, 0600 hr, 1800 hr and 2400 hr, inferring that smoke was present for the full 24 hours.

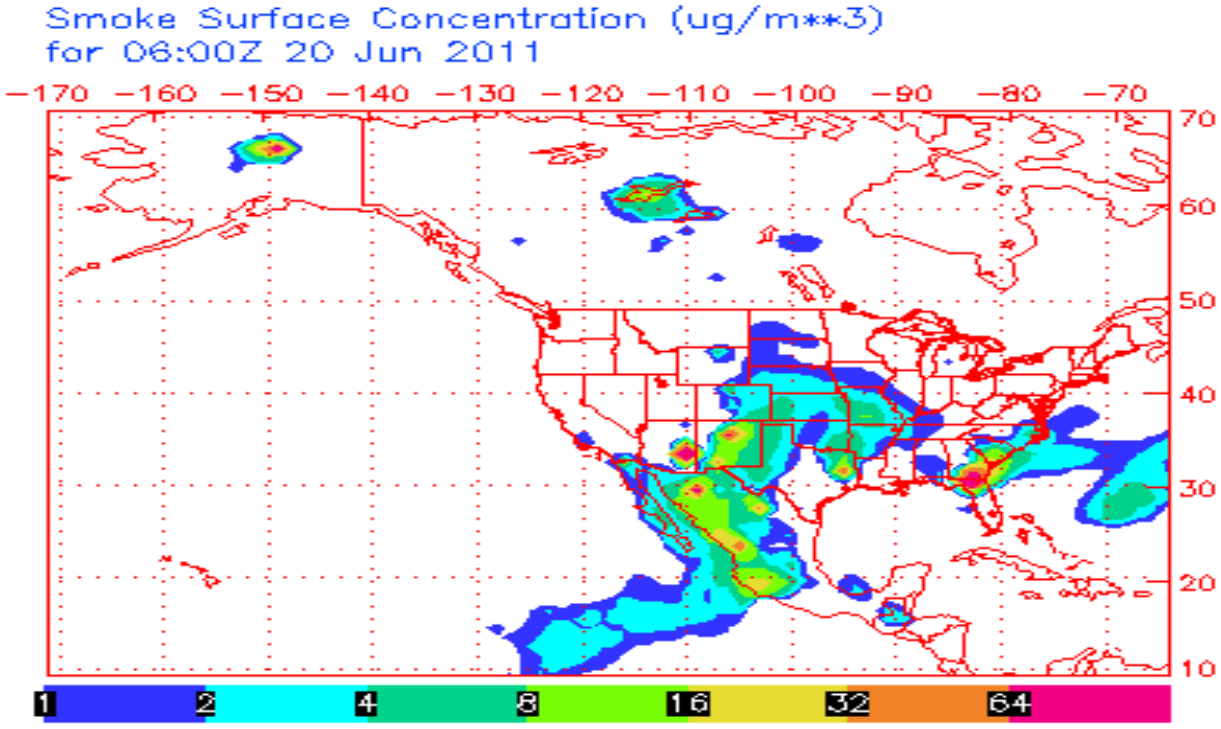

Figure 30-93. NAAPS Smoke Surface Concentration (in micrograms per cubic meter) for June 20, 2011 at 0000 hr. Smoke was also detected at 0600 hr, 1200 hr and 1800 hr, inferring that smoke was present for at least 18 hours.

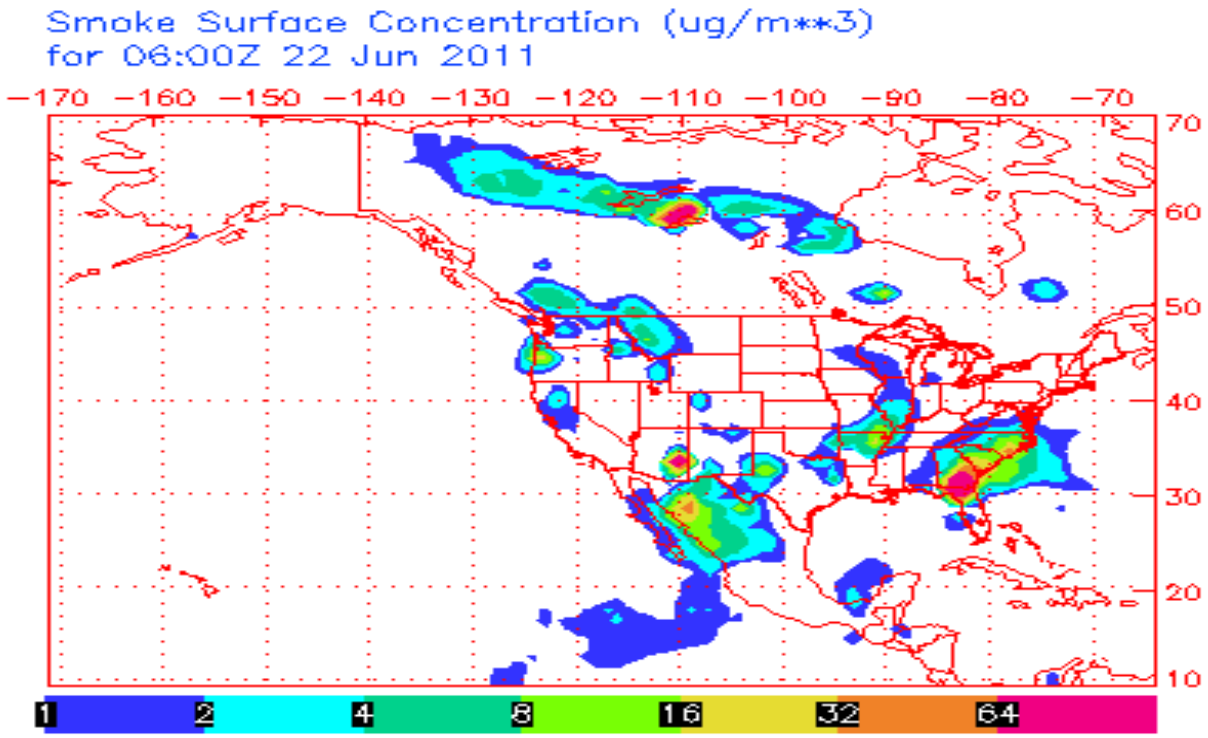

Figure 30-94. NAAPS Smoke Surface Concentration (in micrograms per cubic meter) for June 22, 2011 at 0000 hr MDT. Smoke was also detected at 0600 hr, 1200 hr, 1800 hr and 2400 hr, inferring that smoke was present for the full 24 hours.

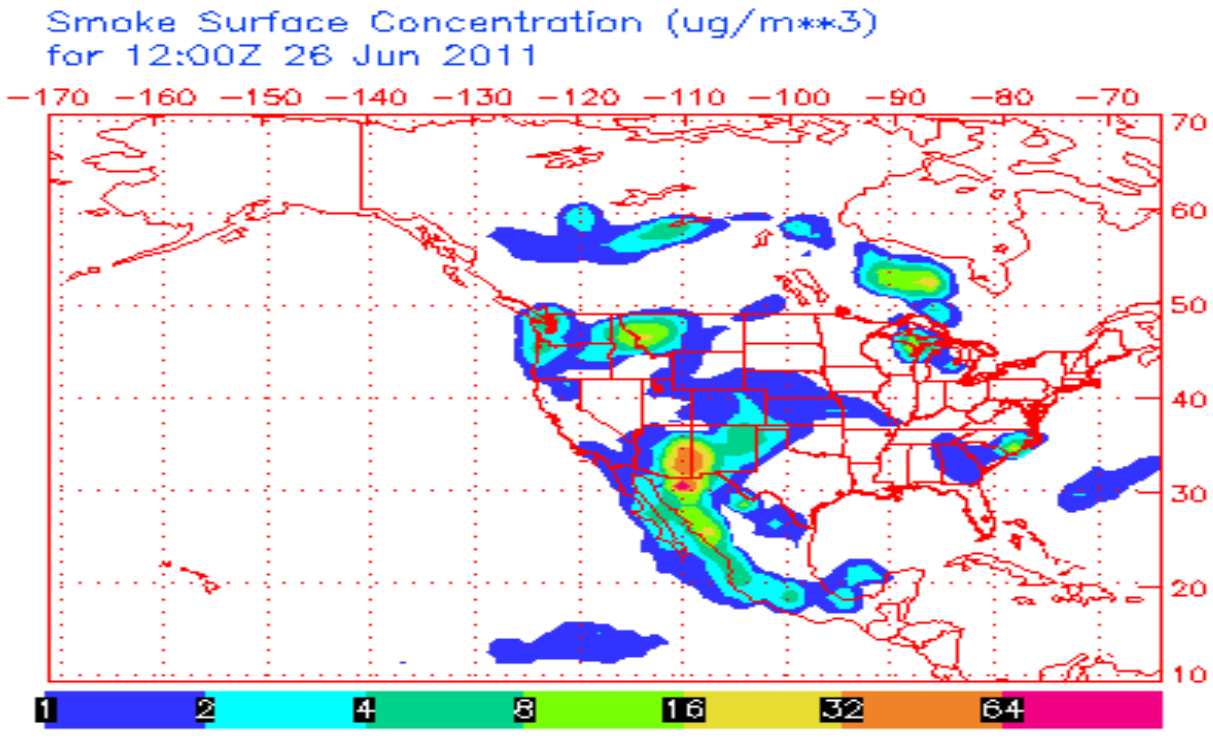

Figure 30-95. NAAPS Smoke Surface Concentration (in micrograms per cubic meter) for June 26, 2011 at 0600 hr. Smoke was also detected at 0000 hr, 1200 hr, 1800 hr and 2400 hr, inferring that smoke was present for the full 24 hours.

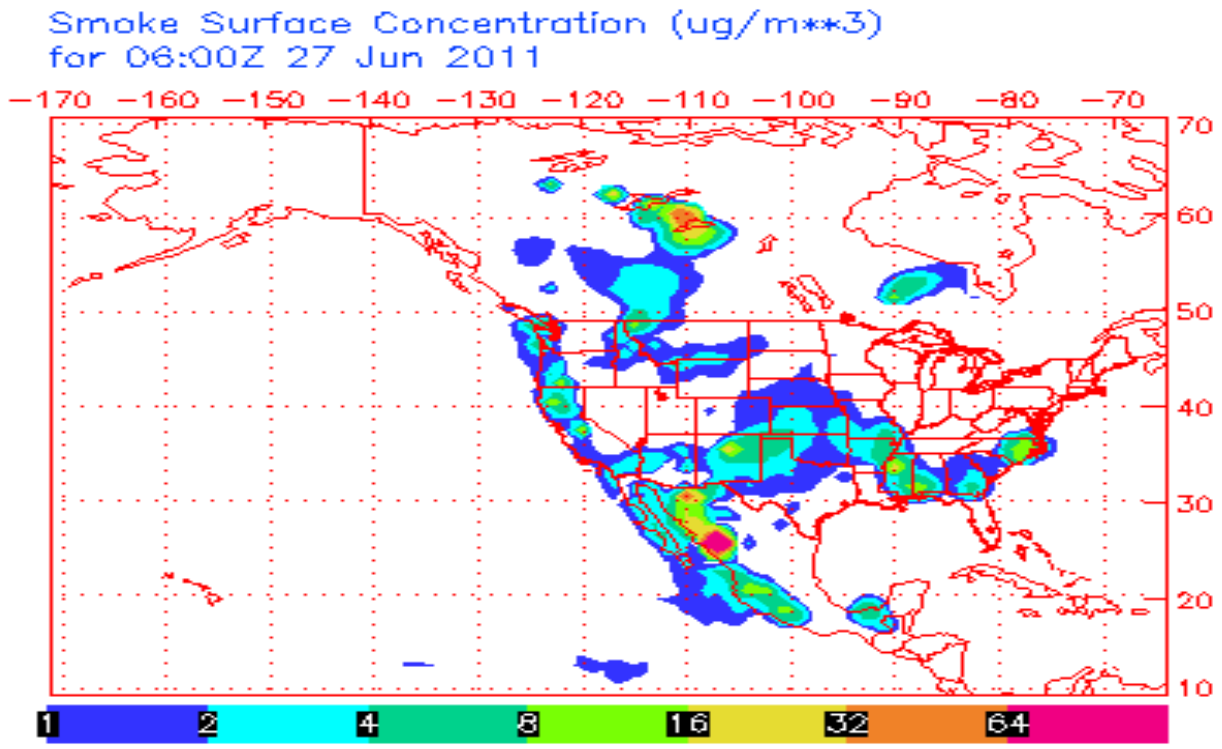

Figure 30-96. NAAPS Smoke Surface Concentration (in micrograms per cubic meter) for June 27, 2011 at 0000 hr. Smoke was also detected at 0600 hr, 1200 hr, 1800 hr and 2400 hr, inferring that smoke was present for the full 24 hours.

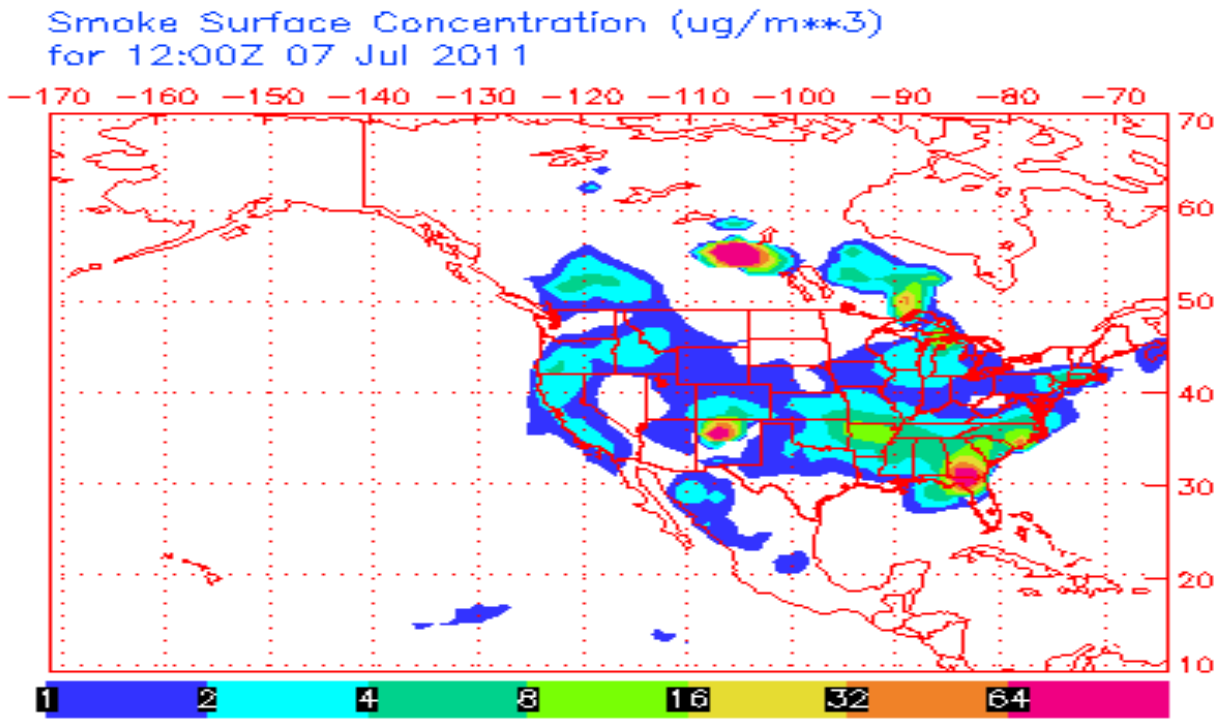

Figure 30-97. NAAPS Smoke Surface Concentration (in micrograms per cubic meter) for July 7, 2011 at 0600 hr MDT. Smoke was also detected at 1200 and 1800 hr, inferring that smoke was present for at least 12 hours.

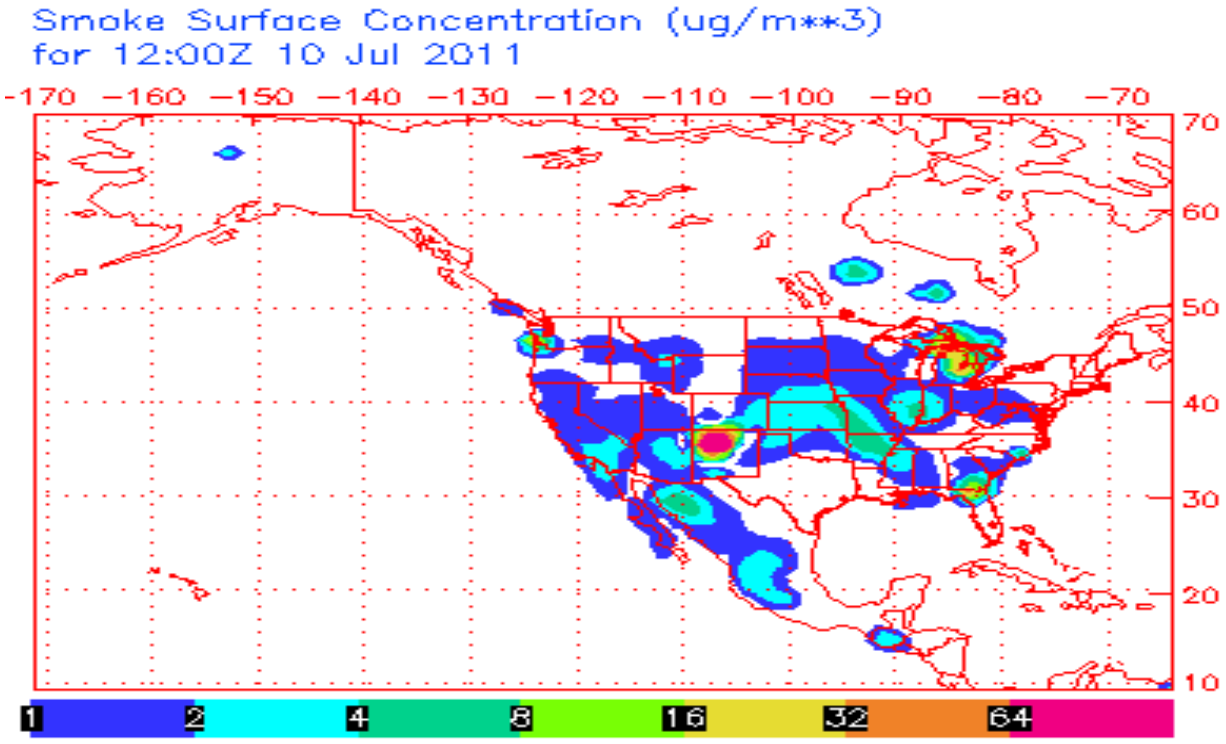

Figure 30-98. NAAPS Smoke Surface Concentration (in micrograms per cubic meter) for July 10, 2011 at 0600 hr MDT. Smoke was also detected at 1200 hr and 1800 hr, inferring that smoke was present for at least 12 hours.

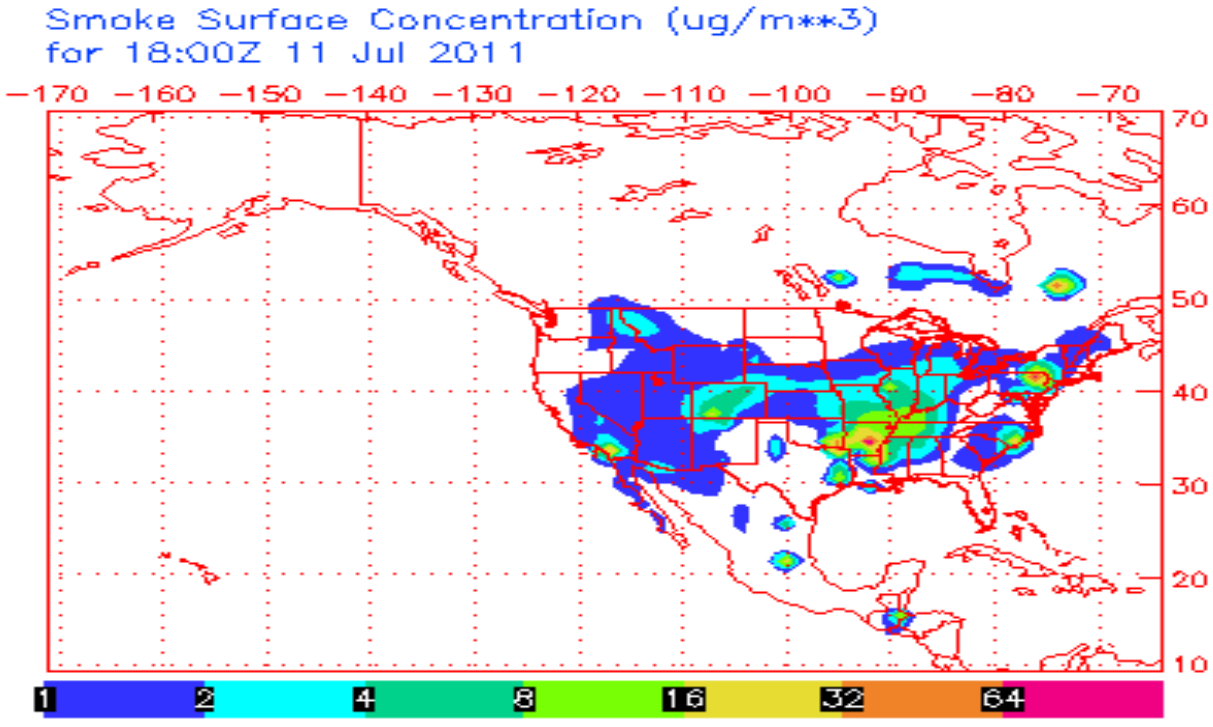

Figure 30-99. NAAPS Smoke Surface Concentration (in micrograms per cubic meter) for July 11, 2011 at 1200 hr MDT.

At night, the land cools quickly, allowing the air just above it to cool relatively quickly as well. During the night and morning hours, when winds are low, cool air descends, carrying with it the smoke that had been aloft. Because the winds are low and $PM_{2.5}$ has a relatively long residence time, the entrained particles concentrate near the ground. When the winds increase somewhat, the smoke may be blown out of the area. For this reason, we see a general inverse pattern between wind speed and $PM_{2.5}$ in the morning and night hours. $PM_{2.5}$ peaks are typically found during periods of very low winds. In general, the reverse applies to midday hours as the land heats the air above it. During the late morning and afternoon hours, when winds increase, $PM_{2.5}$ levels generally increase as smoke is blown in from the surrounding areas, following the terrain into the valley at Sunland Park. When peaks occur during midday, they usually occur when winds increase somewhat. Figures 30-100 to 30-131 show these relationships, using PM_{10} as a proxy, between wind speed and $PM_{2.5}$ concentrations at the SPCY TEOM monitor.

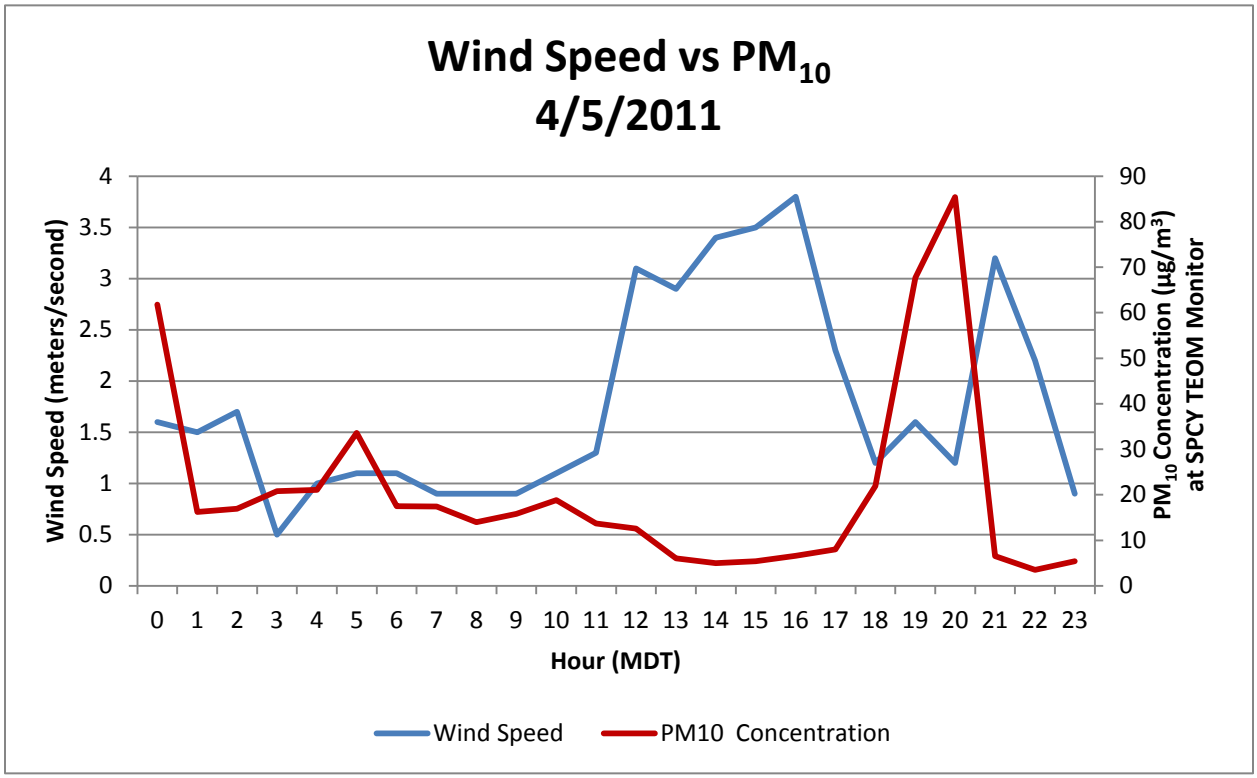

Figure 30-100. Wind speed in meters per second vs. hourly PM_{10} concentrations at the SPCY TEOM monitor. The largest PM_{10} peak occurs in the evening when winds are low. Low wind speed and cooling land mass causes the increase in particles near the ground.

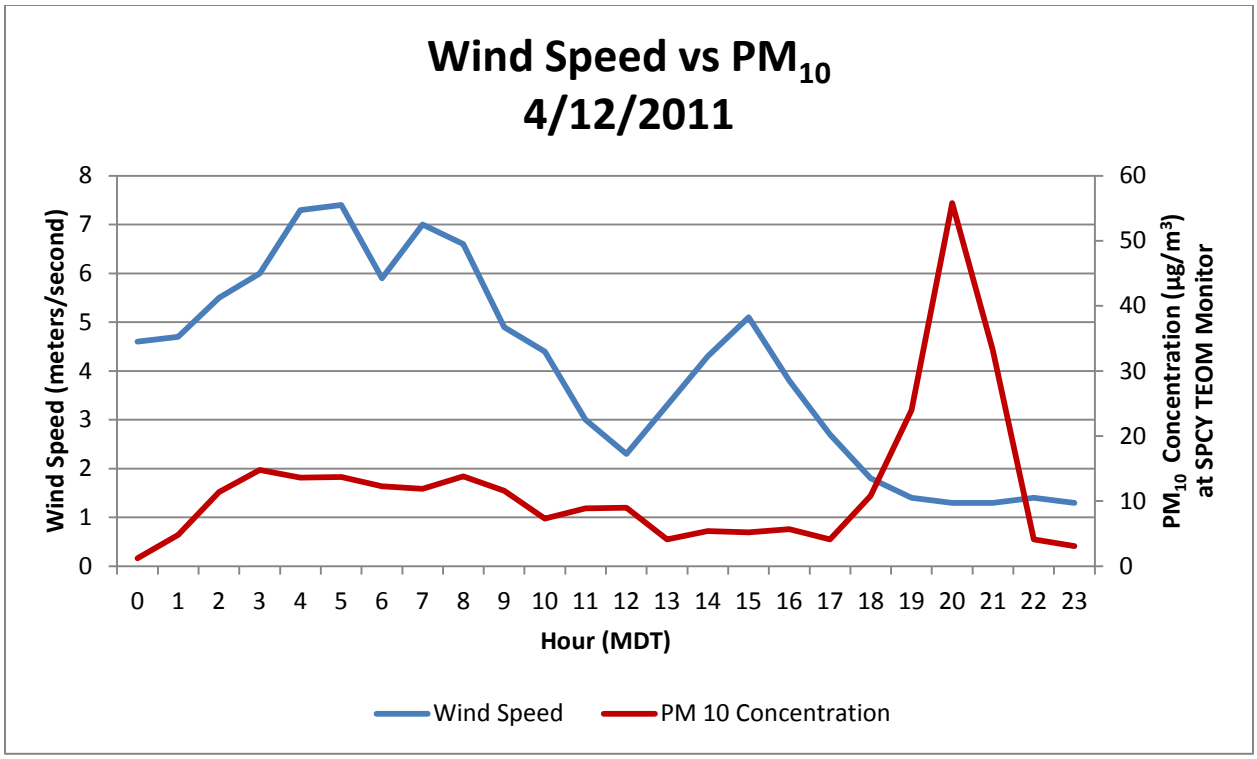

Figure 30-101. Wind speed in meters per second vs. hourly PM_{10} concentrations at the SPCY TEOM monitor. The largest PM_{10} peak occurs in the evening when winds are low. Low wind combined with cooling land mass causes the increase in particles near the ground.

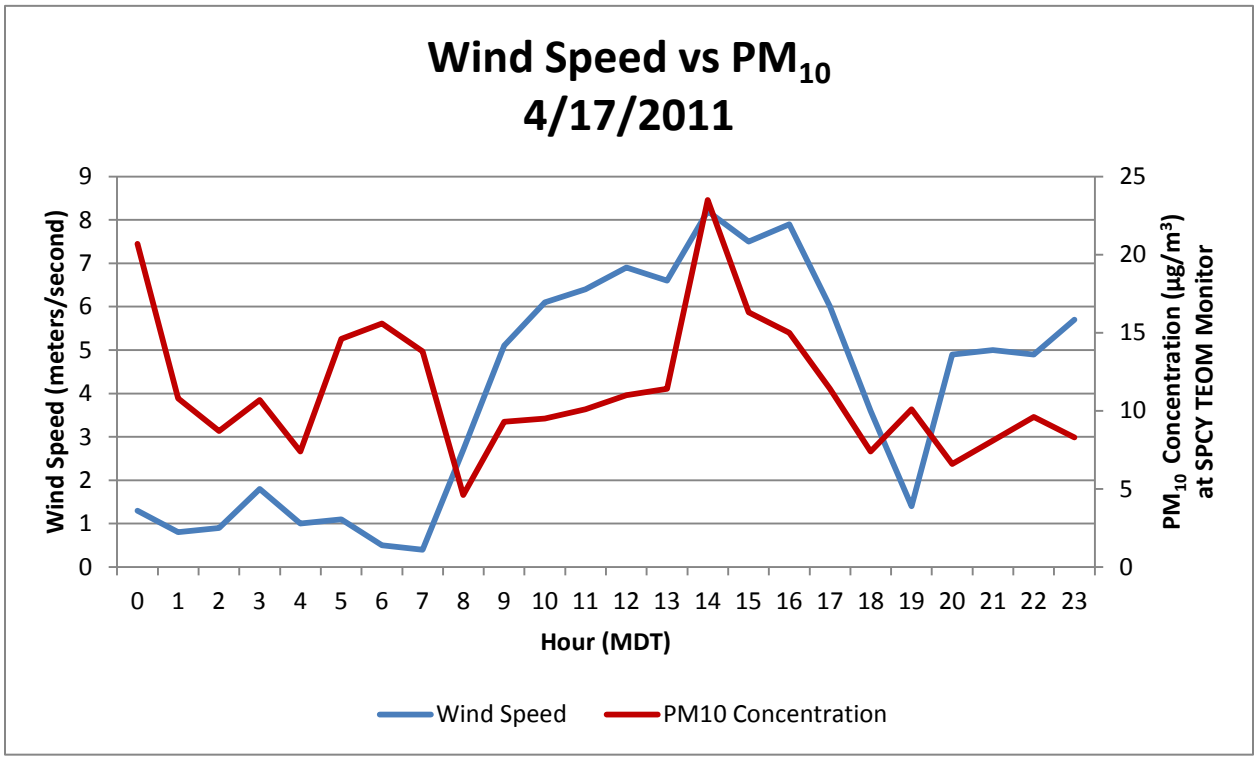

Figure 30-102. Wind speed in meters per second vs. hourly PM_{10} concentrations at the SPCY TEOM monitor. Two PM_{10} peaks occur: one near midnight and the other in the afternoon. The early morning peak shows follows the typical pattern for low wind combined with a relatively cool land mass. The afternoon peak is a result of slightly increased winds allowing smoke to be blown into the valley.

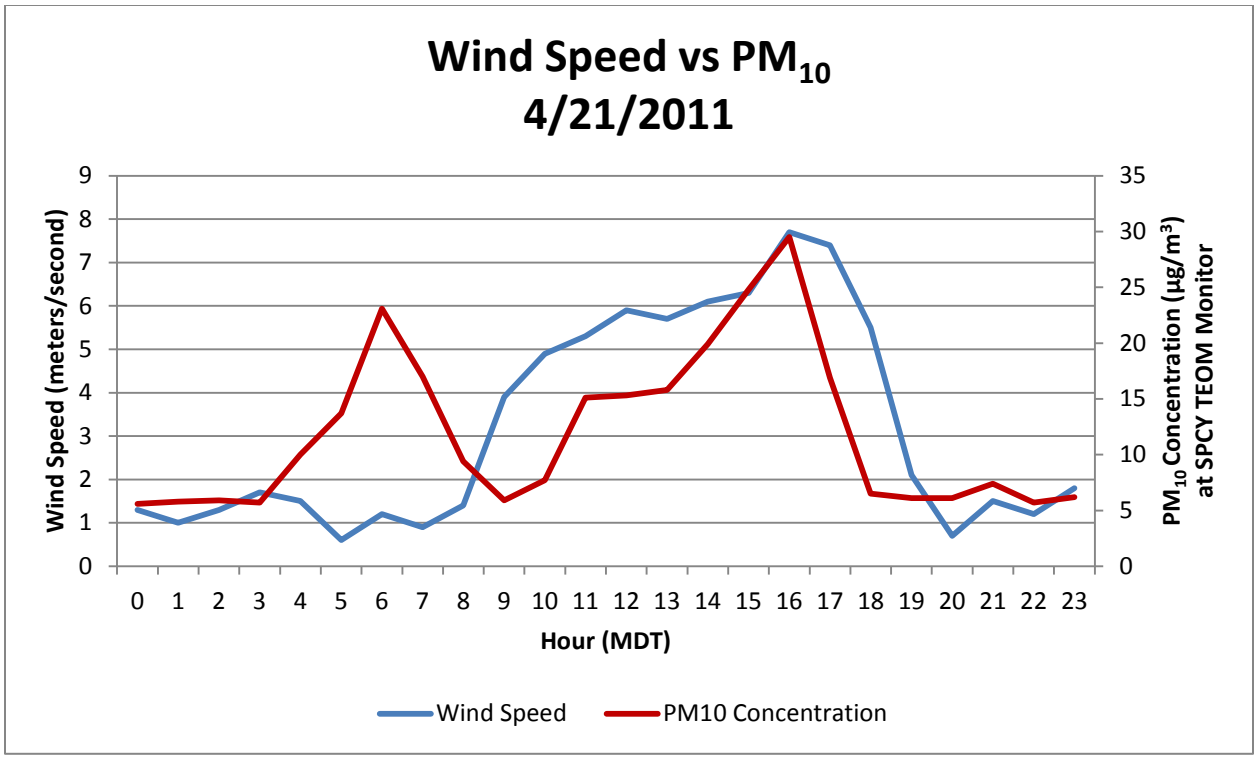

Figure 30-103. Wind speed in meters per second vs. hourly PM_{10} concentrations at the SPCY TEOM monitor. The first PM_{10} peak (in the morning) follows the typical inverse pattern with wind speed while the afternoon peak follows a direct pattern with wind speed as smoke is blown into the valley.

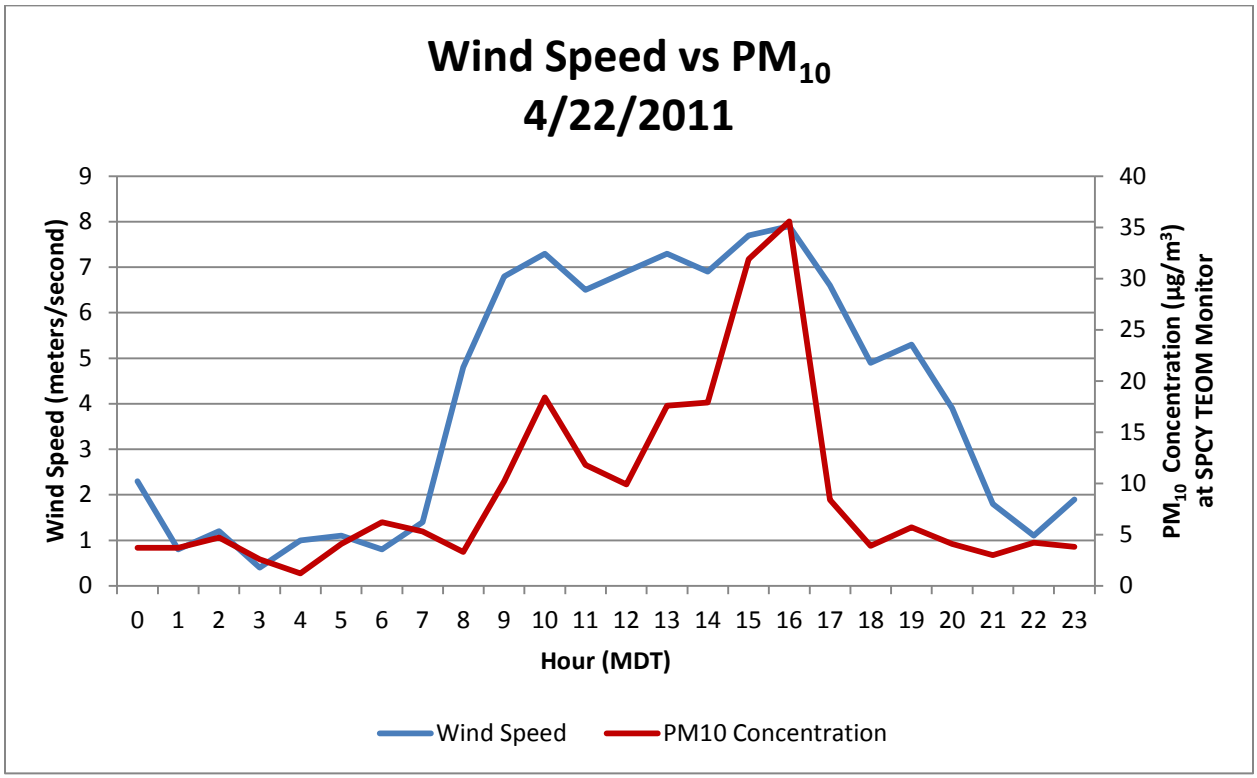

Figure 30-104. Wind speed in meters per second vs. hourly PM_{10} concentrations at the SPCY TEOM monitor. The large afternoon PM_{10} peak follows a direct pattern with wind speed as smoke is blown into the valley.

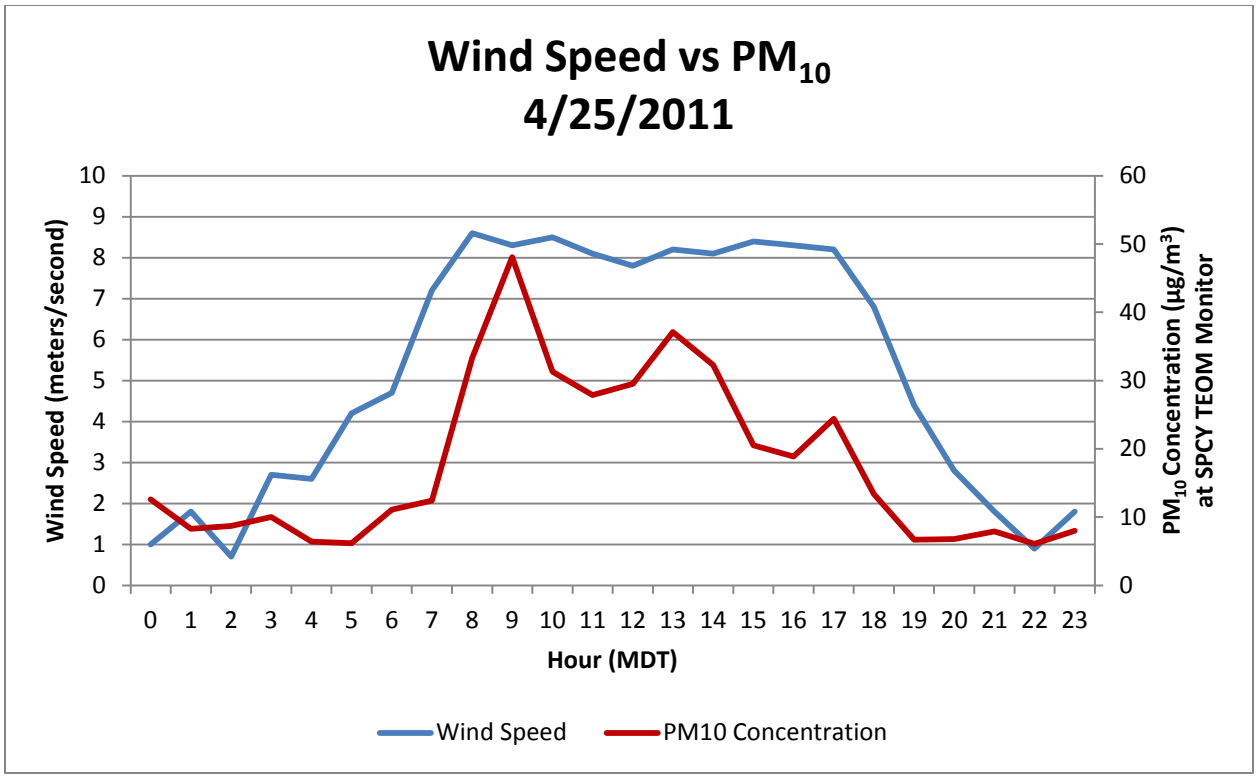

Figure 30-105. Wind speed in meters per second vs. hourly PM_{10} concentrations at the SPCY TEOM monitor. The PM_{10} peaks shown in the middle of the day are generally directly correlated with wind speed as smoke is blown into the valley.

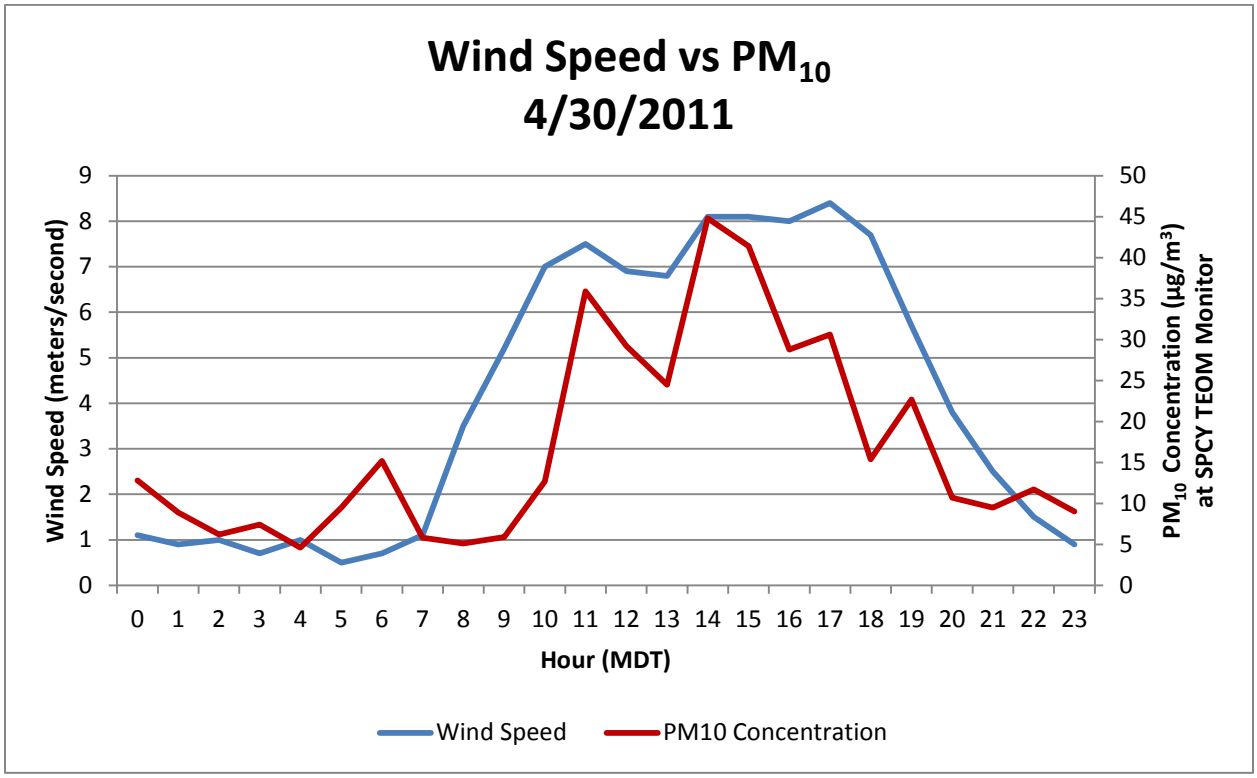

Figure 30-106. Wind speed in meters per second vs. hourly PM_{10} concentrations at the SPCY TEOM monitor. The PM_{10} peaks shown in the middle of the day are generally directly correlated with wind speed as smoke is blown into the valley.

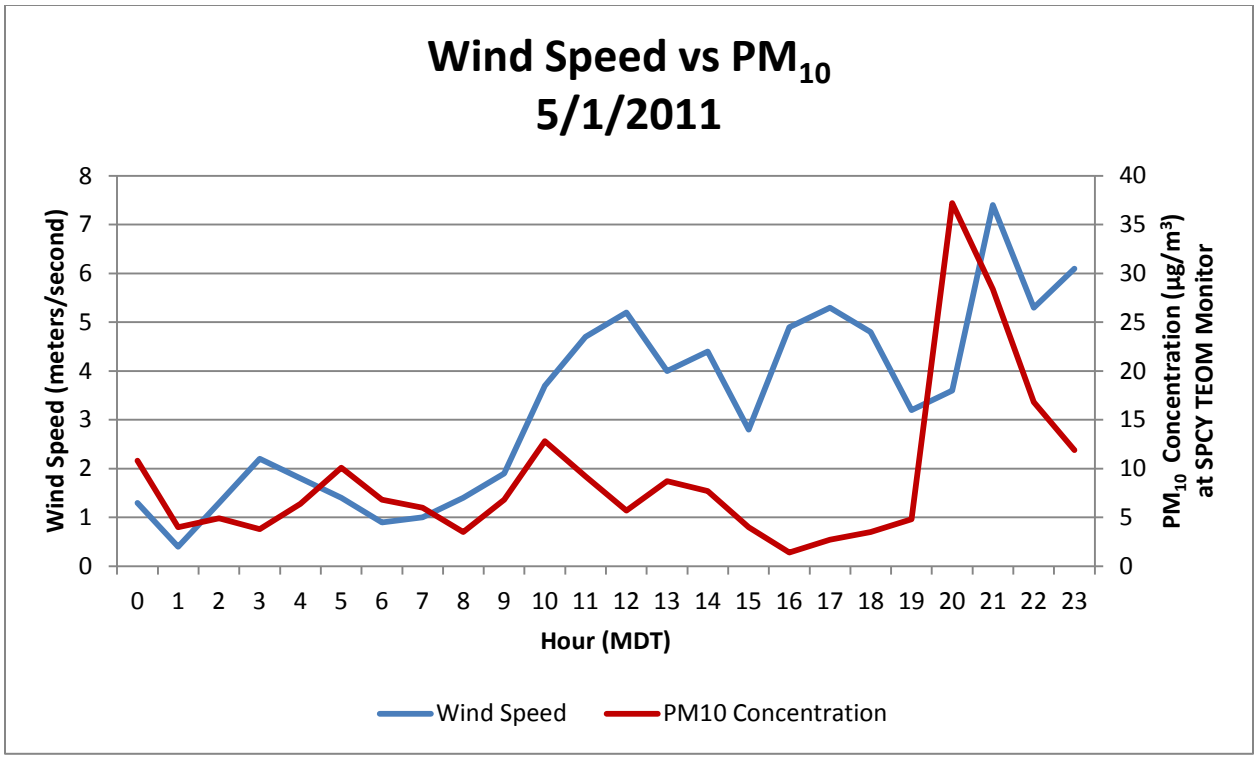

Figure 30-107. Wind speed in meters per second vs. hourly PM_{10} concentrations at the SPCY TEOM monitor. The evening PM_{10} peak occurs approximately when winds slow. Lower winds combined with cooling land mass causes the increase in particles.

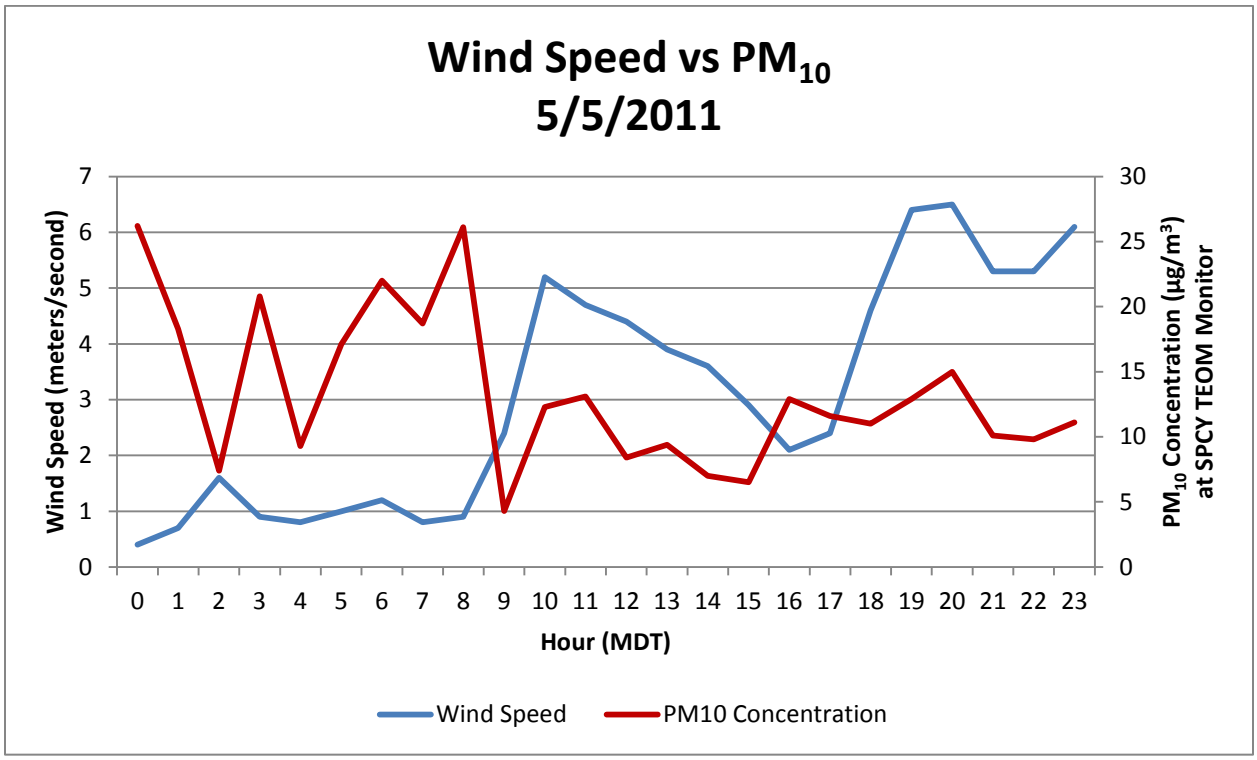

Figure 30-108. Wind speed in meters per second vs. hourly PM_{10} concentrations at the SPCY TEOM monitor. The PM_{10} peaks shown in the morning hours show a roughly inverse relationship with wind speed typical of low winds with a relatively cool land mass.

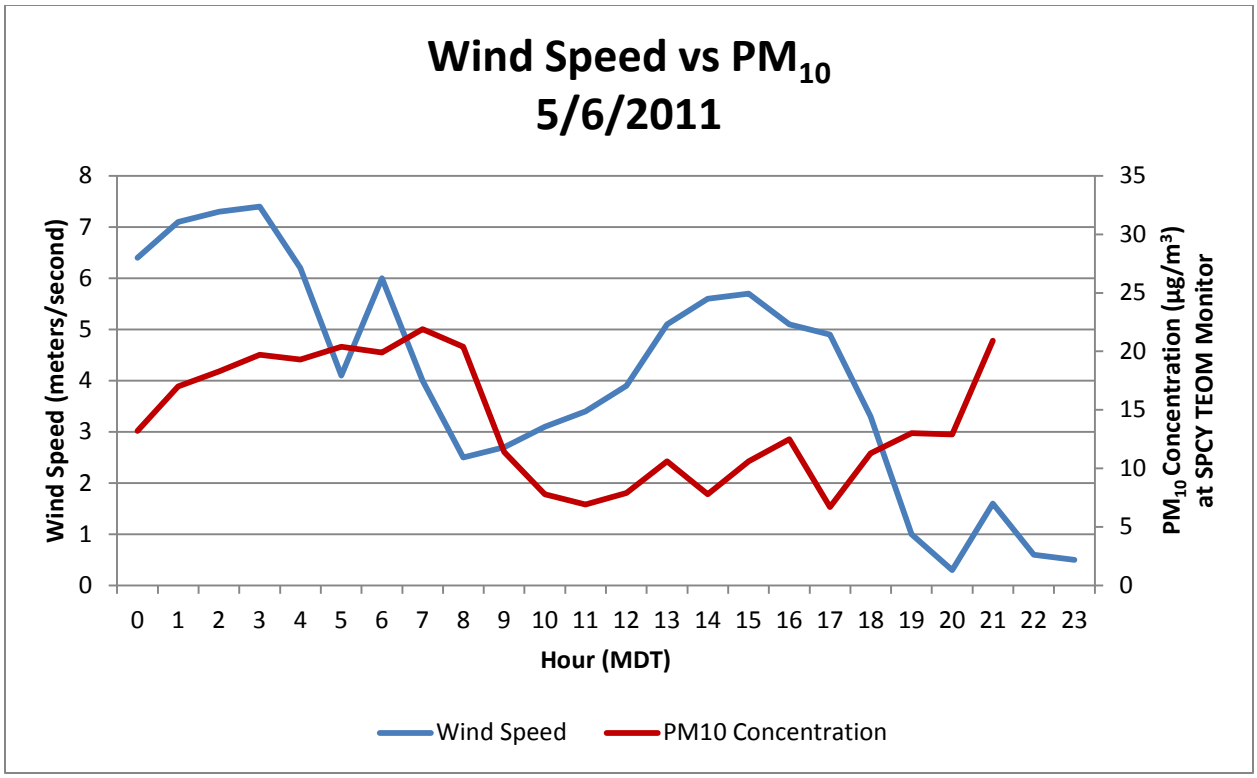

Figure 30-109. Wind speed in meters per second vs. hourly PM_{10} concentrations at the SPCY TEOM monitor. The PM_{10} peaks shown in the morning hours and late evening show a typical, roughly inverse relationship with wind speed.

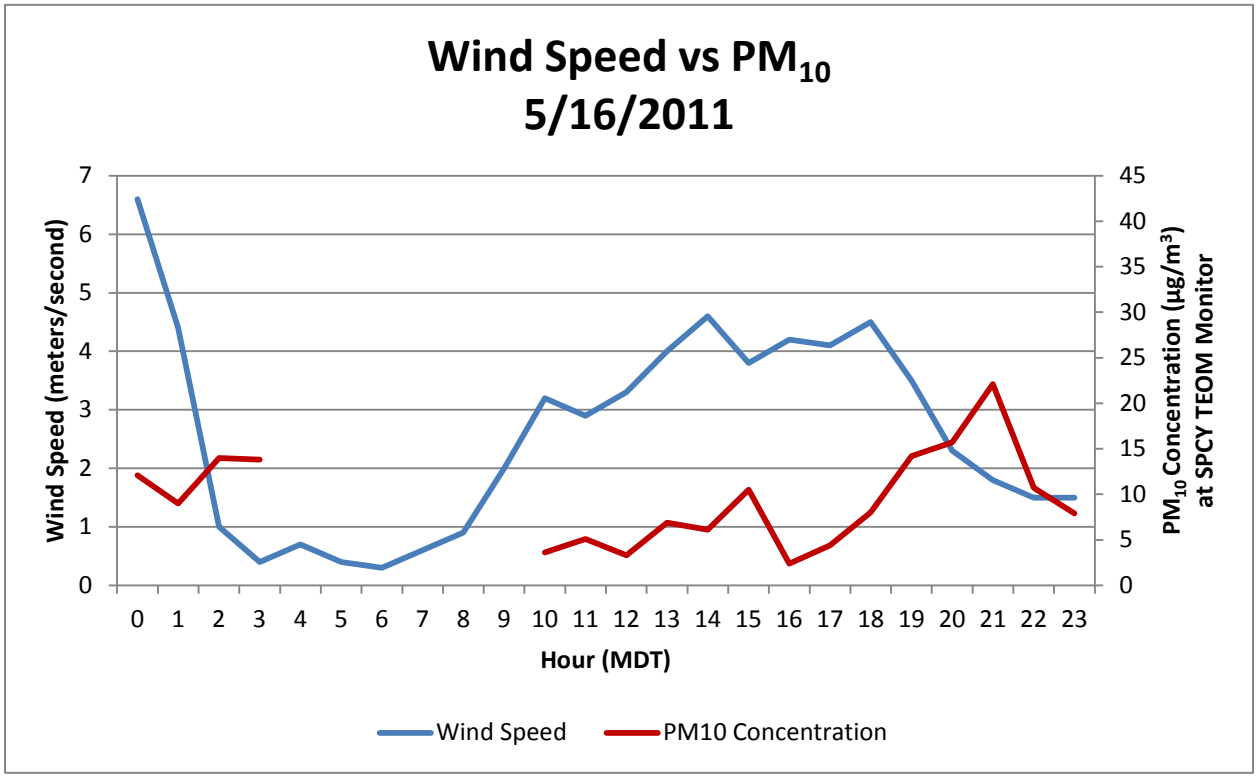

Figure 30-110. Wind speed in meters per second vs. hourly PM_{10} concentrations at the SPCY TEOM monitor. The largest PM_{10} peak in the late evening happens when wind speed is low (and the land mass is cooler).

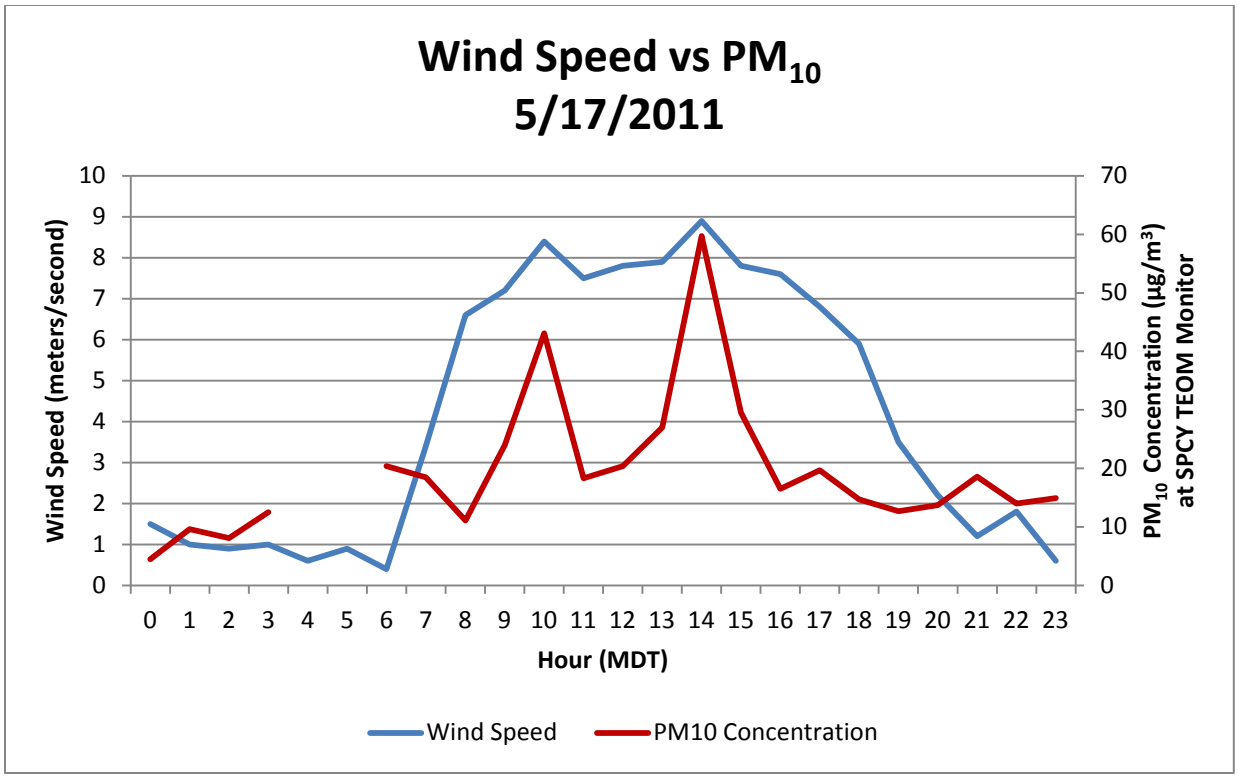

Figure 30-111. Wind speed in meters per second vs. hourly PM_{10} concentrations at the SPCY TEOM monitor. The PM_{10} peaks shown in the middle of the day are generally directly correlated with wind speed as smoke is blown into the valley.

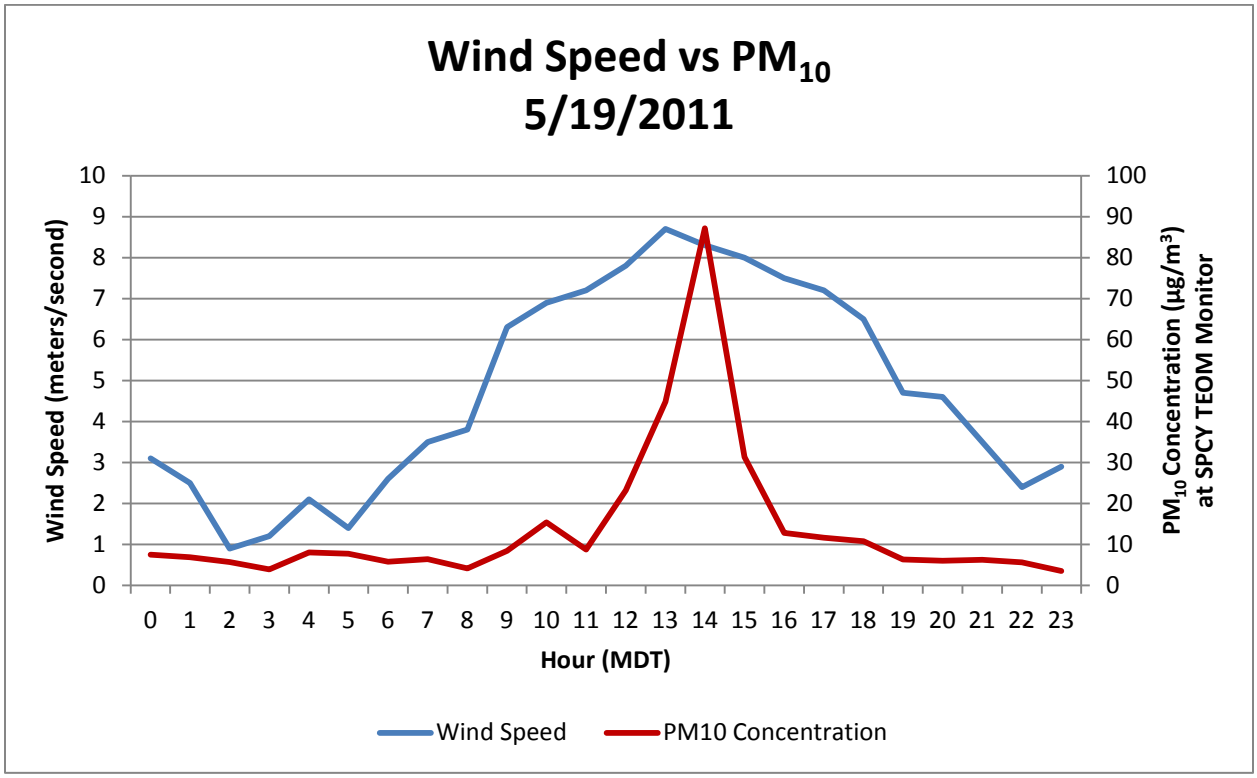

Figure 30-112. Wind speed in meters per second vs. hourly PM_{10} concentrations at the SPCY TEOM monitor. The PM_{10} peak shown in the middle of the day are generally directly correlated with wind speed as smoke is blown into the valley.

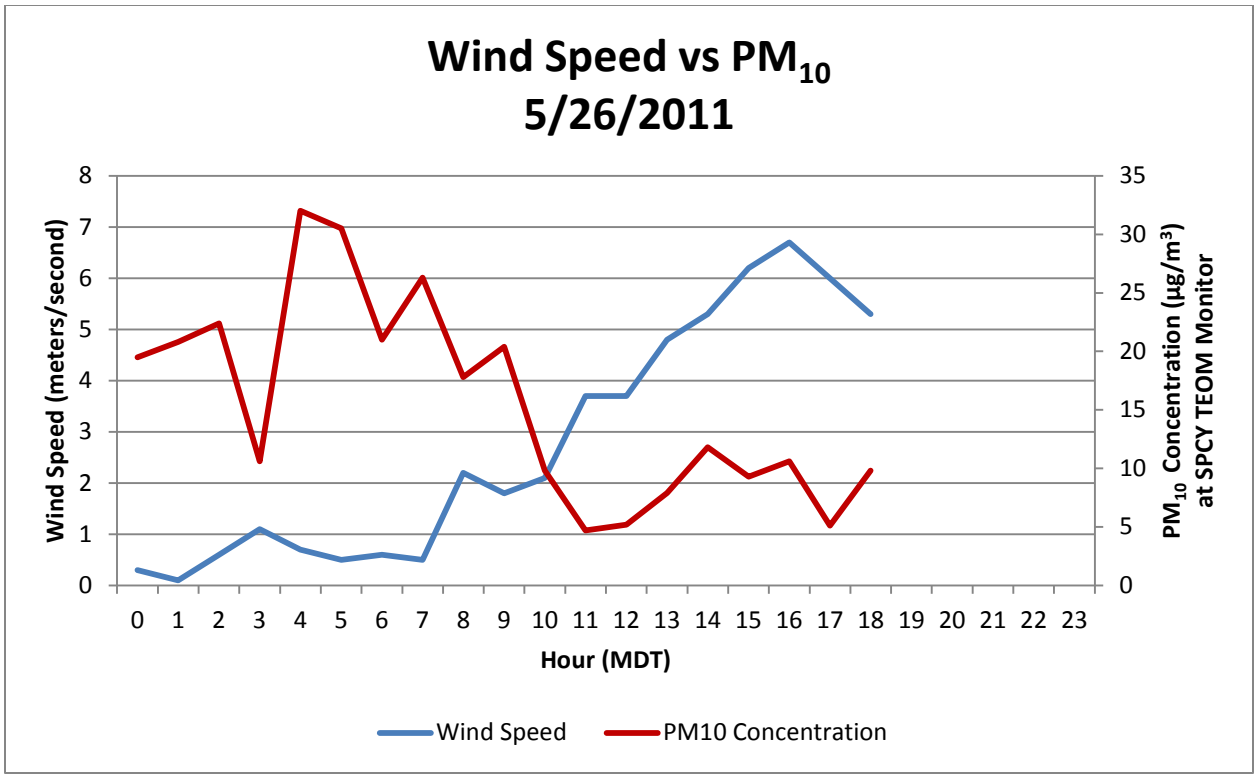

Figure 30-113. Wind speed in meters per second vs. hourly PM_{10} concentrations at the SPCY TEOM monitor. The PM_{10} peaks shown in the morning hours are inversely related to wind speed as low winds and a relatively cool land mass causes an increase in particles.

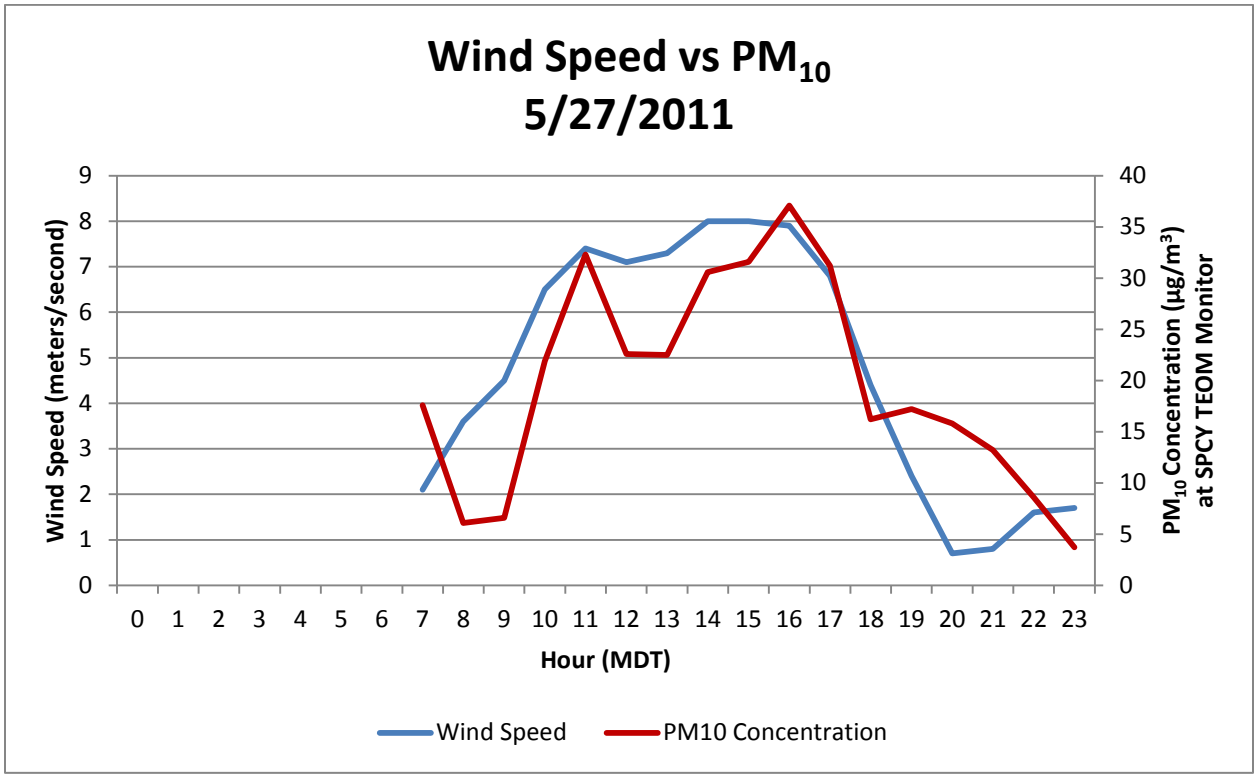

Figure 30-114. Wind speed in meters per second vs. hourly PM_{10} concentrations at the SPCY TEOM monitor. The PM_{10} peaks shown in the middle of the day are generally directly correlated with wind speed as smoke blows into the valley.

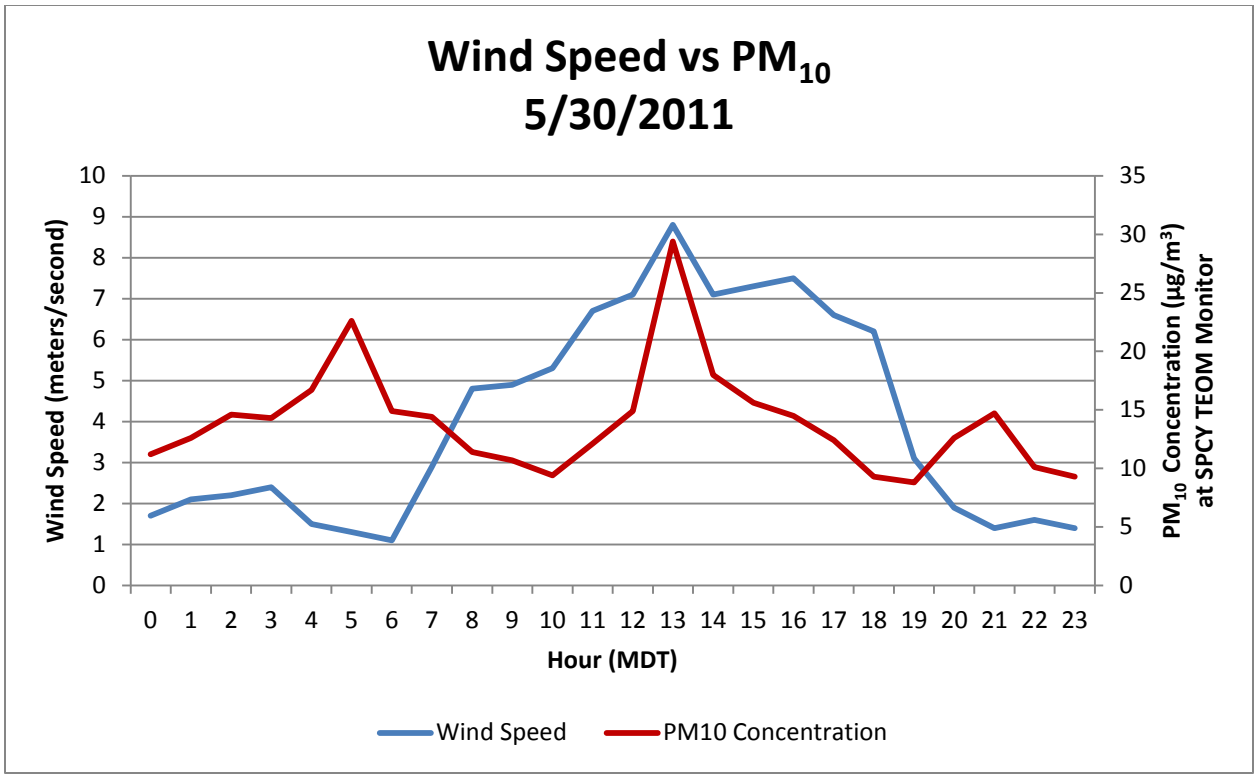

Figure 30-115. Wind speed in meters per second vs. hourly PM_{10} concentrations at the SPCY TEOM monitor. The PM_{10} peak shown in the morning is inversely related to wind speed as usual. The peak shown in the middle of the day is directly correlated with wind speed as smoke is blown into the valley.

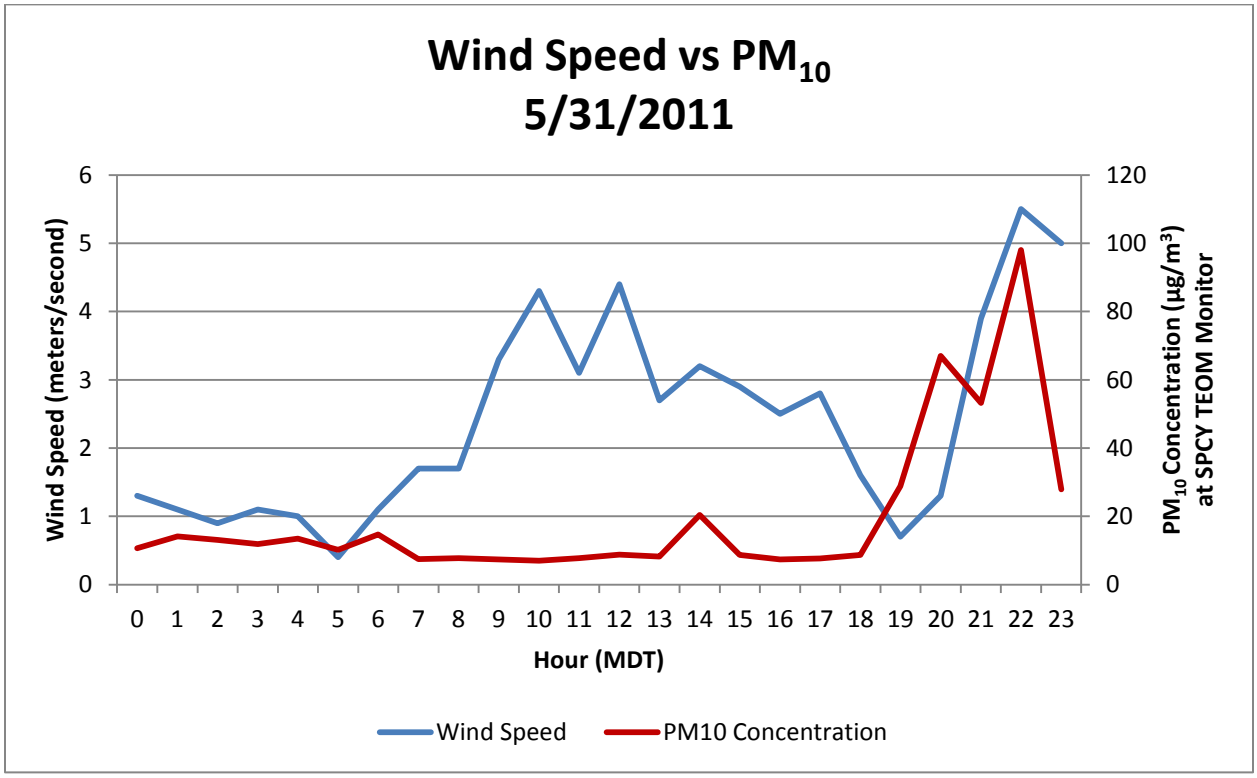

Figure 30-116. Wind speed in meters per second vs. hourly PM_{10} concentrations at the SPCY TEOM monitor. The PM_{10} peaks shown in the evening are roughly directly correlated with wind speed. This is an exception to the general pattern of inverse relationships in the evenings. As Figure 30-132 shows, the winds were southwesterly, blowing from the general direction of the northern Mexico fires.

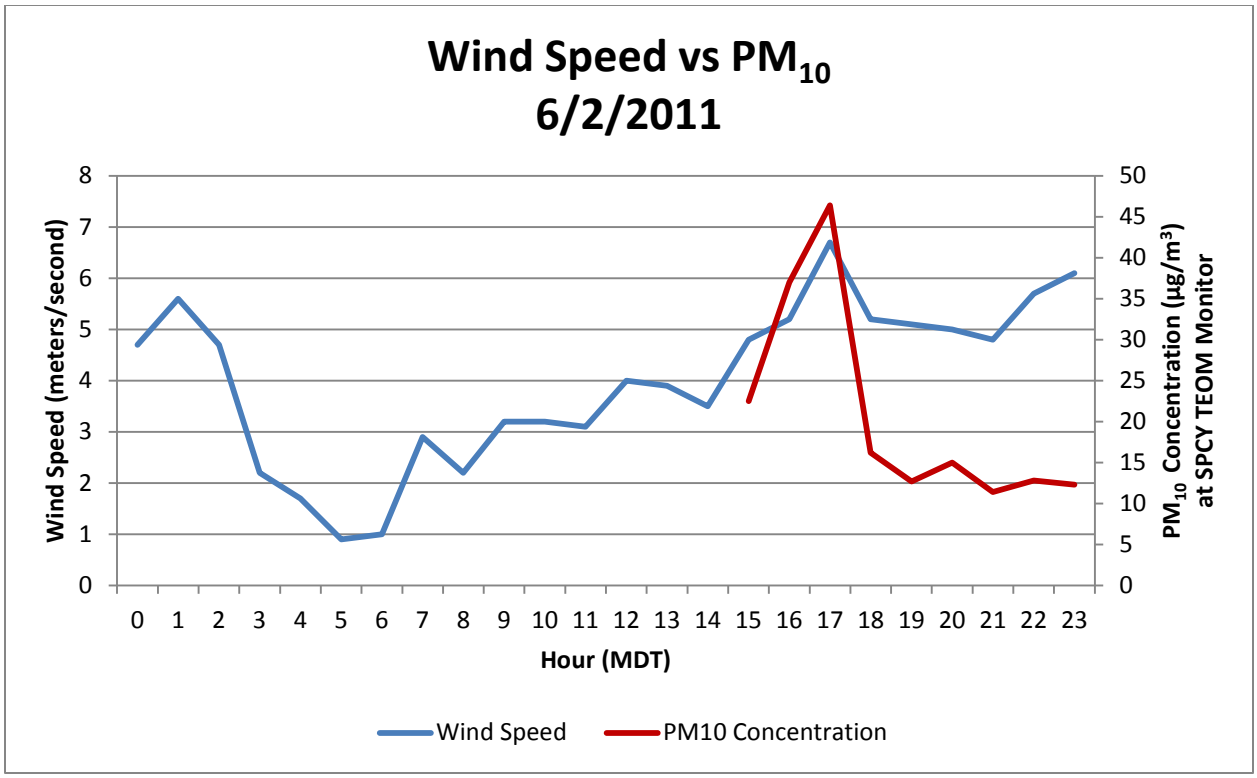

Figure 30-117. Wind speed in meters per second vs. hourly PM_{10} concentrations at the SPCY TEOM monitor. The PM_{10} peak shown in the middle of the day is directly correlated with wind speed as smoke is blown into the valley. PM_{10} data are not available for the first 14 hours of the day.

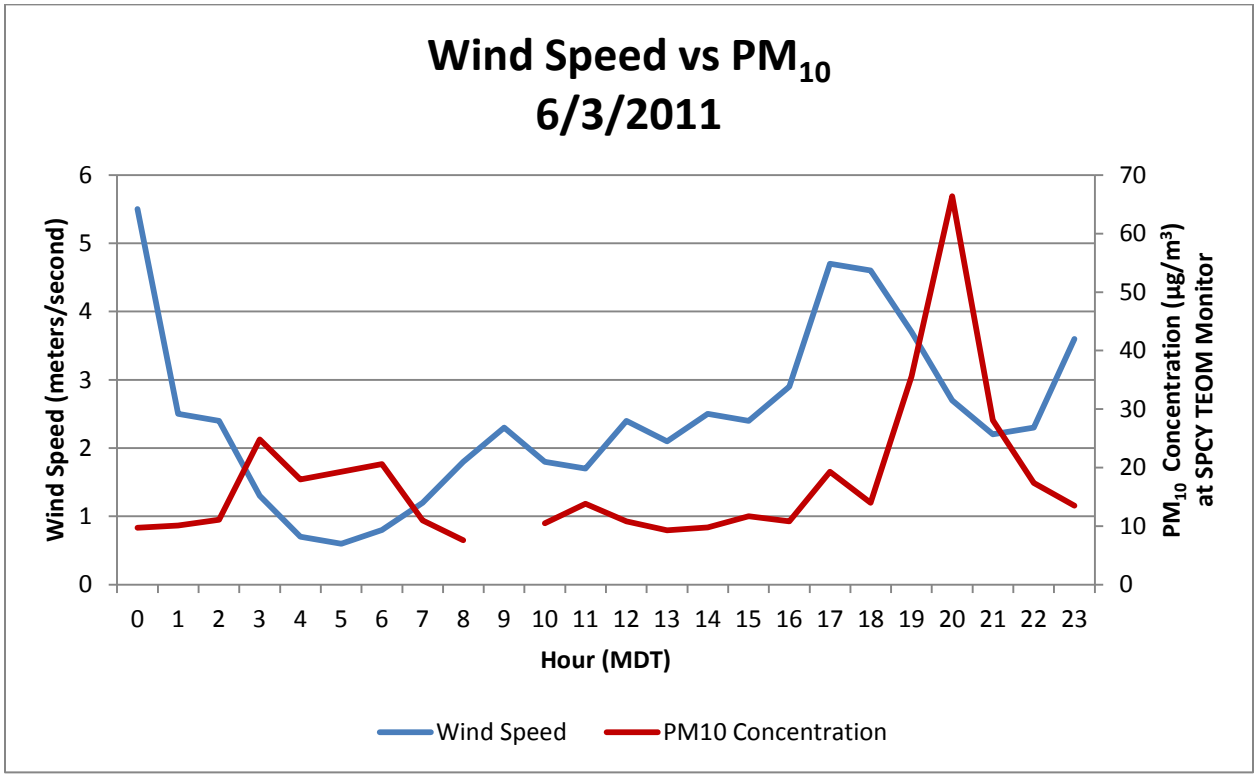

Figure 30-118. Wind speed in meters per second vs. hourly PM_{10} concentrations at the SPCY TEOM monitor. The PM_{10} peak shown in the evening is inversely correlated with wind speed.

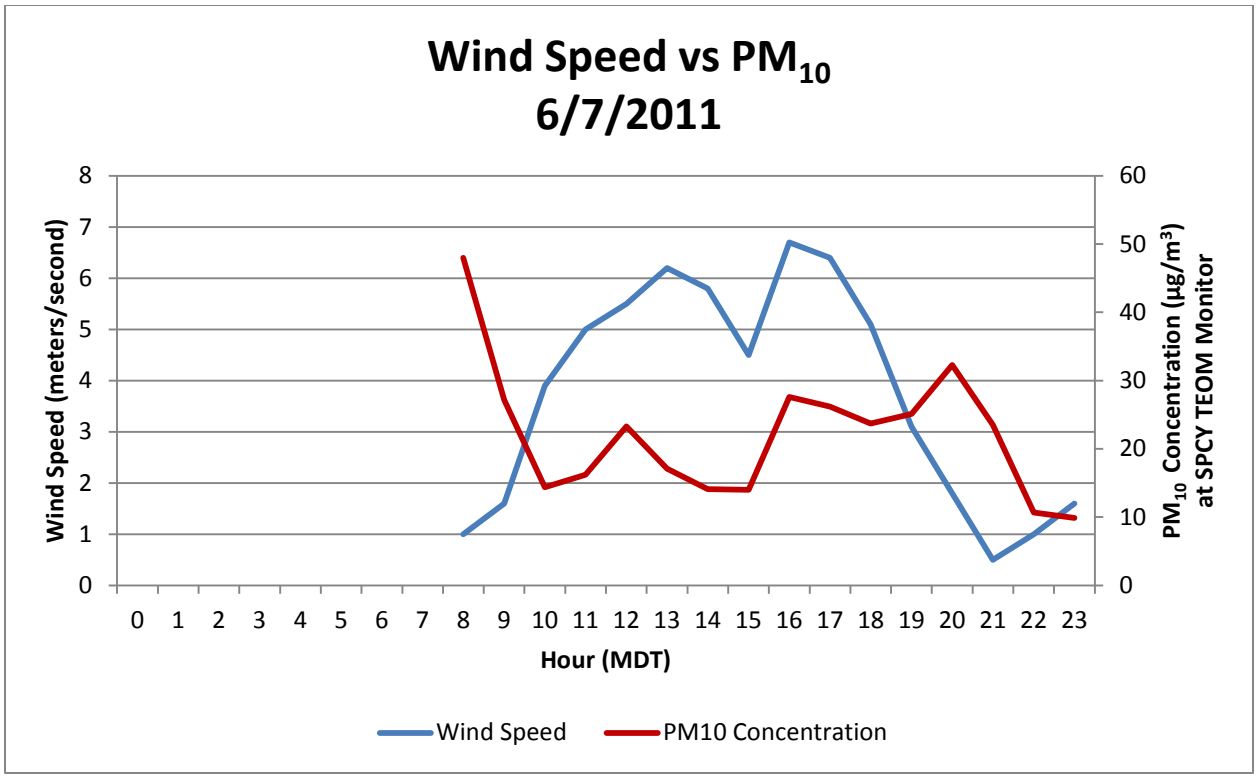

Figure 30-119. Wind speed in meters per second vs. hourly PM_{10} concentrations at the SPCY TEOM monitor. The PM_{10} peaks shown in the morning and evening are inversely correlated with wind speed. The peaks shown in the middle of the day are generally directly correlated with wind speed. Data are not available for the first 7 hours of the day.

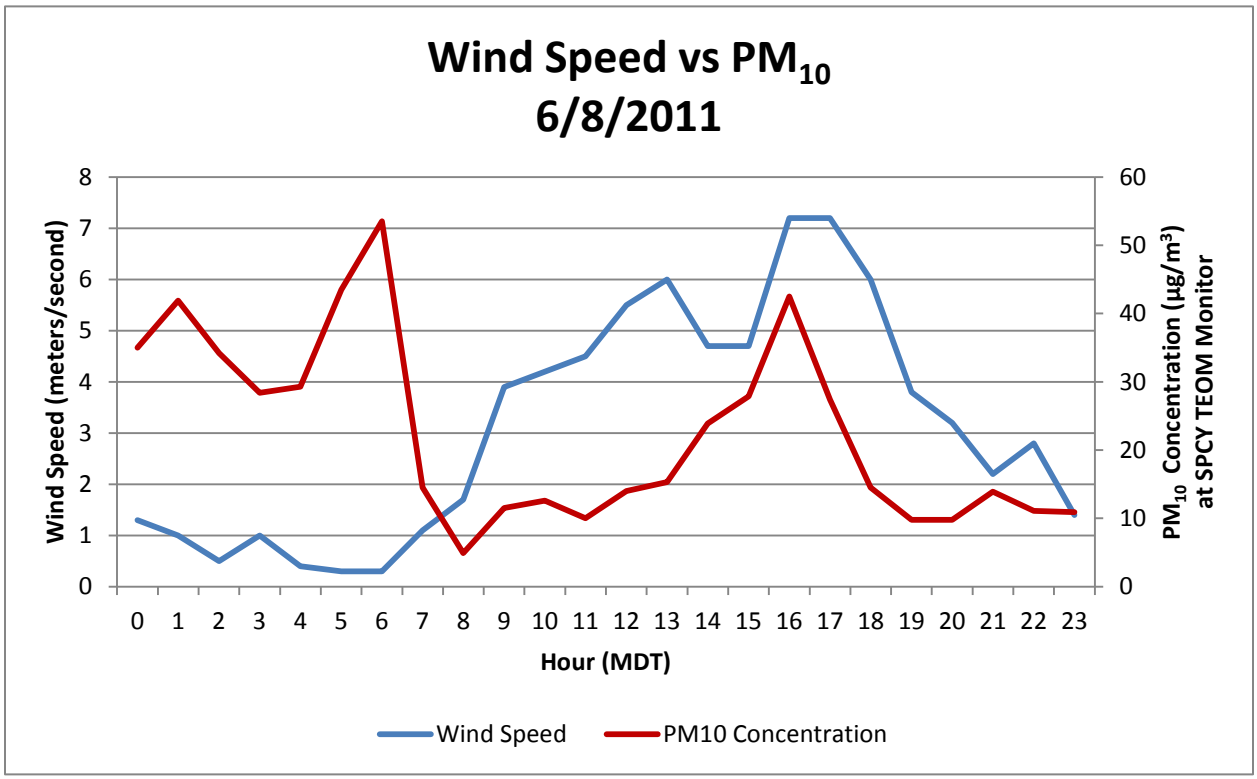

Figure 30-120. Wind speed in meters per second vs. hourly PM_{10} concentrations at the SPCY TEOM monitor. The PM_{10} peaks shown in the morning are inversely correlated with wind speed. The peak shown in the middle of the day is directly correlated with wind speed.

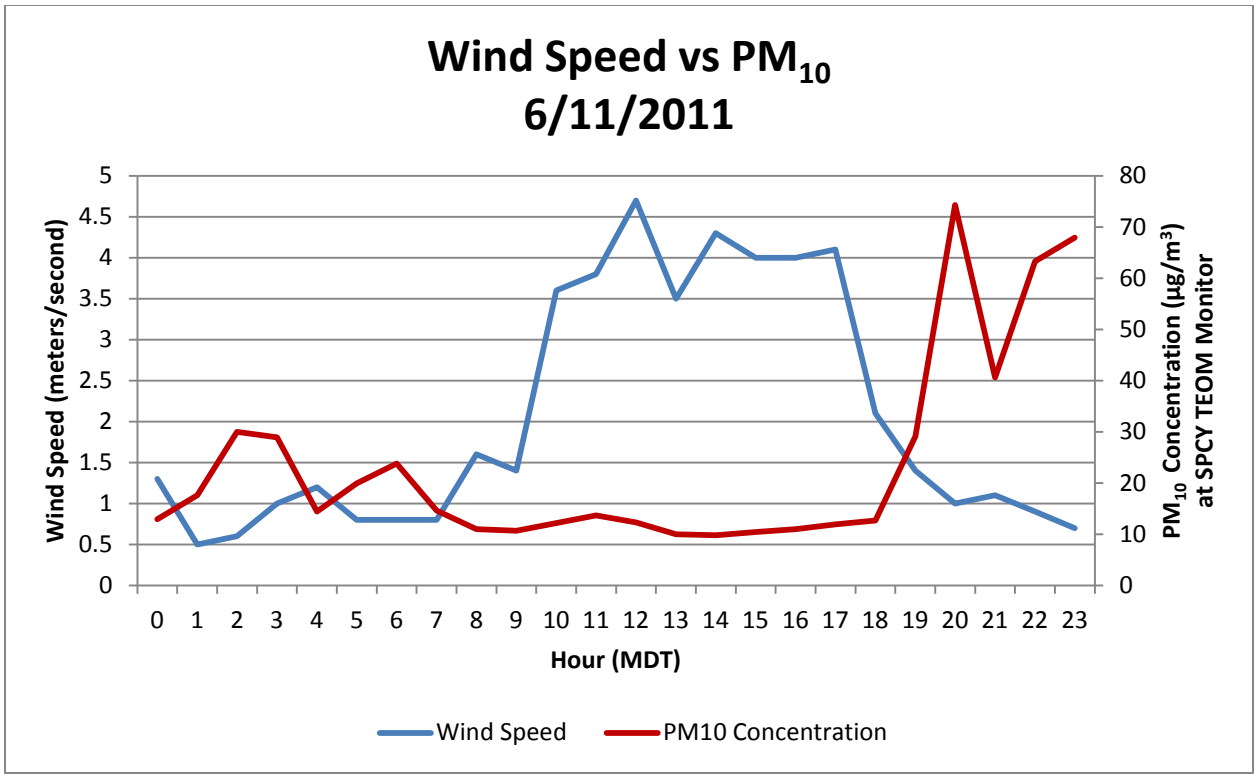

Figure 30-121. Wind speed in meters per second vs. hourly PM_{10} concentrations at the SPCY TEOM monitor. The PM_{10} peaks shown in the morning and evening are inversely correlated with wind speed.

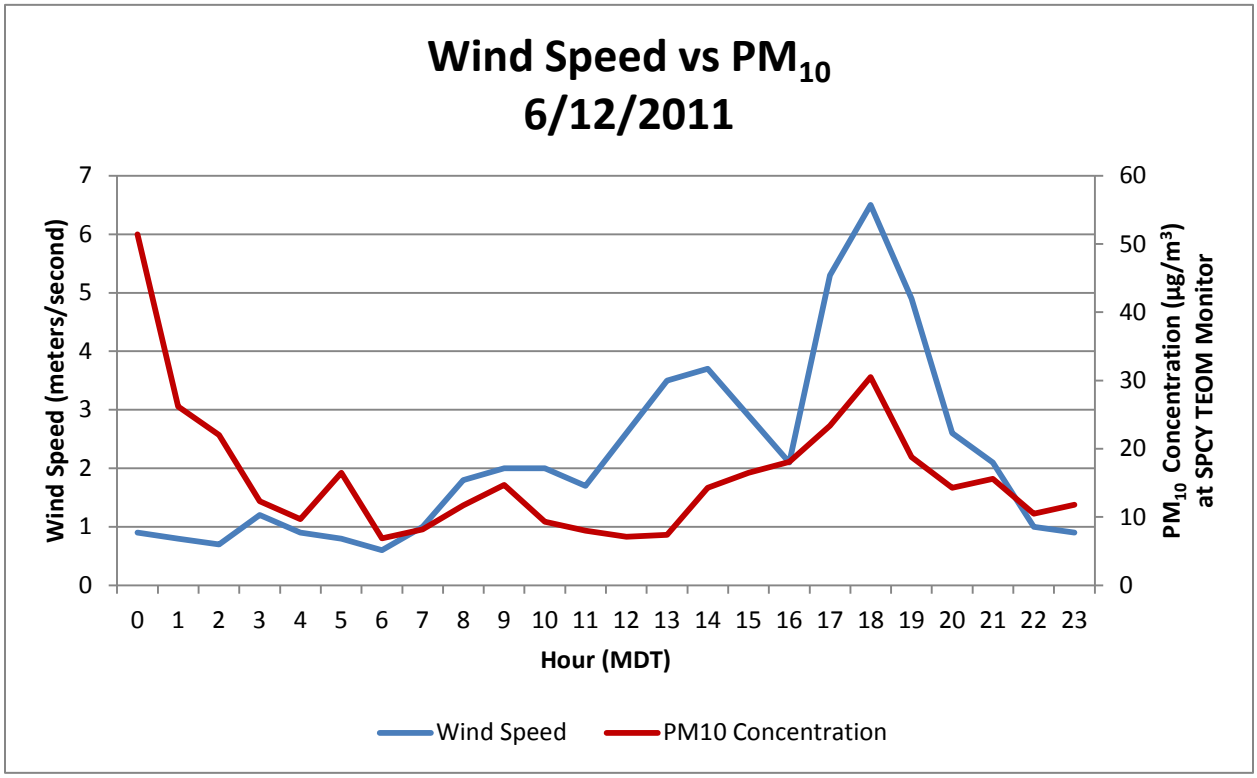

Figure 30-122. Wind speed in meters per second vs. hourly PM_{10} concentrations at the SPCY TEOM monitor. The PM_{10} peak shown in the late afternoon/early evening is generally directly correlated with wind speed. The large peak in the early morning is inversely correlated with wind speed.

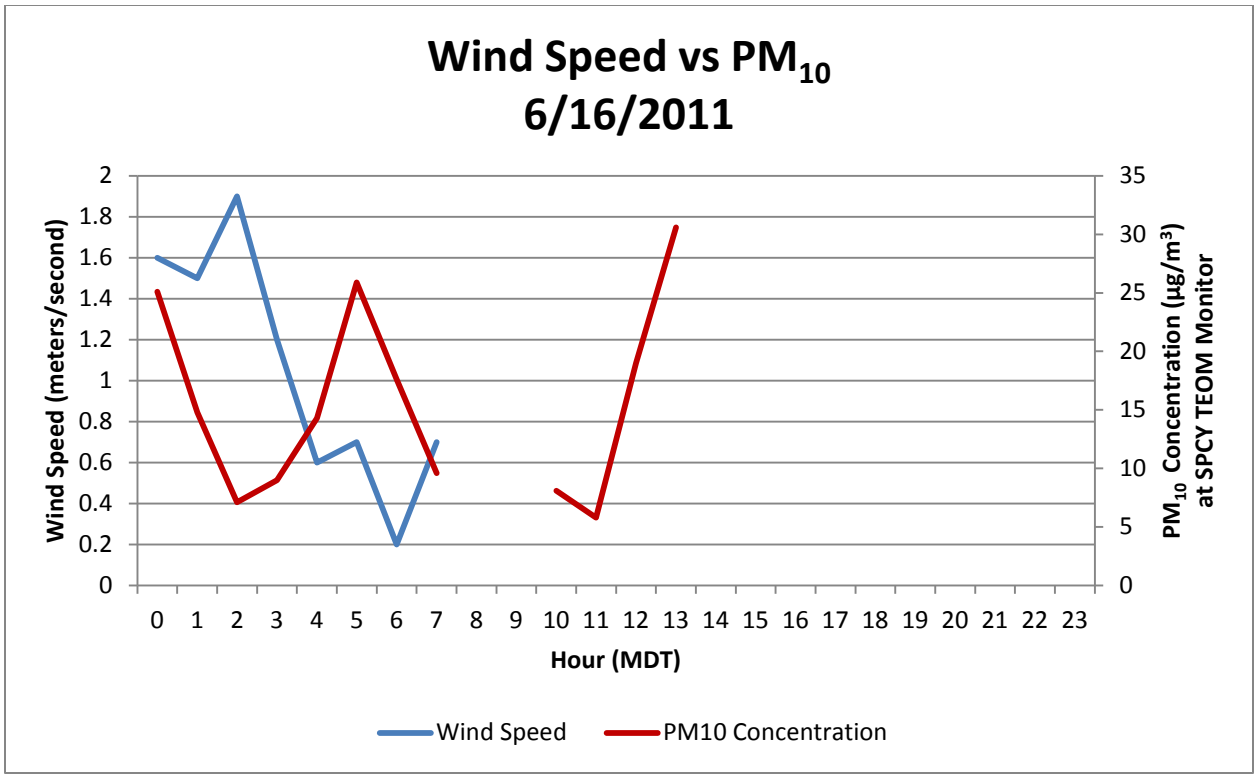

Figure 30-123. Wind speed in meters per second vs. hourly PM_{10} concentrations at the SPCY TEOM monitor. The two PM_{10} peaks shown in the morning correspond to quite low wind speeds and are roughly inversely correlated. No comparison to wind speed can be made for the peak occurring in the afternoon as a significant amount of data is missing.

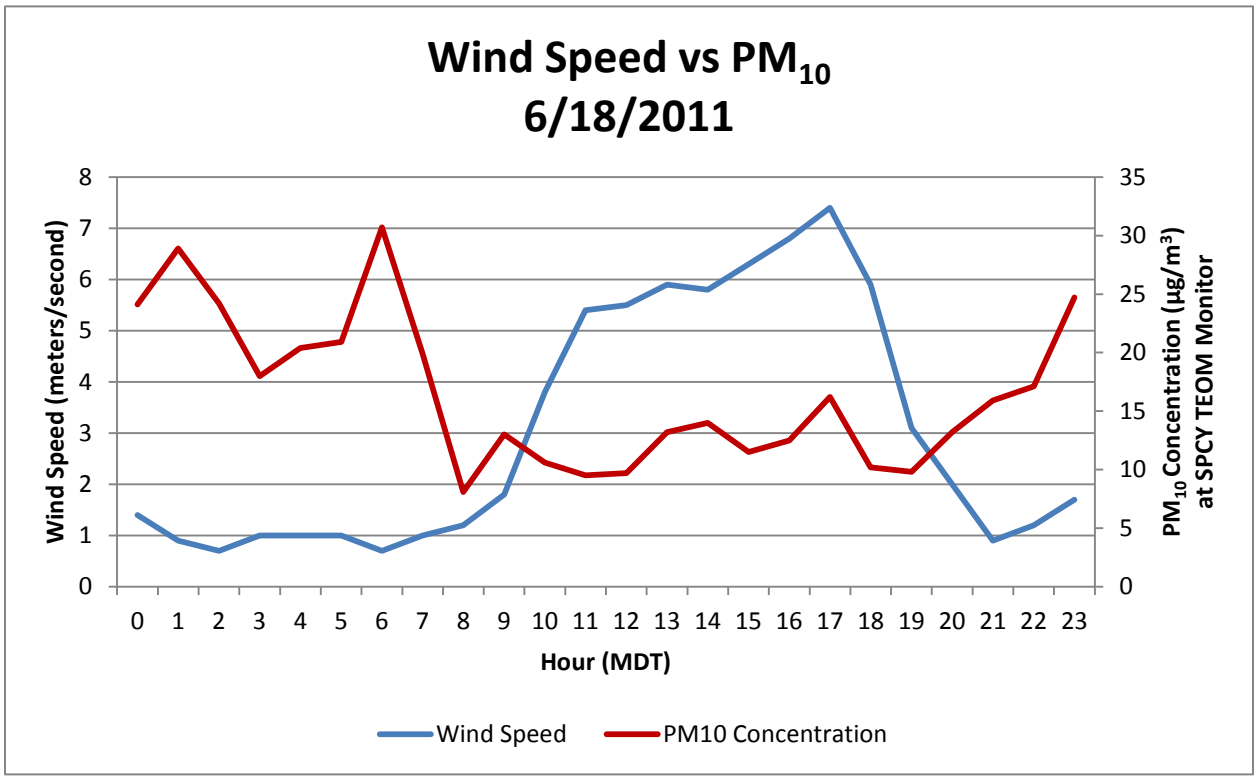

Figure 30-124. Wind speed in meters per second vs. hourly PM_{10} concentrations at the SPCY TEOM monitor. The PM_{10} peaks shown in the morning are inversely correlated with wind speed, as is the peak in the night hours.

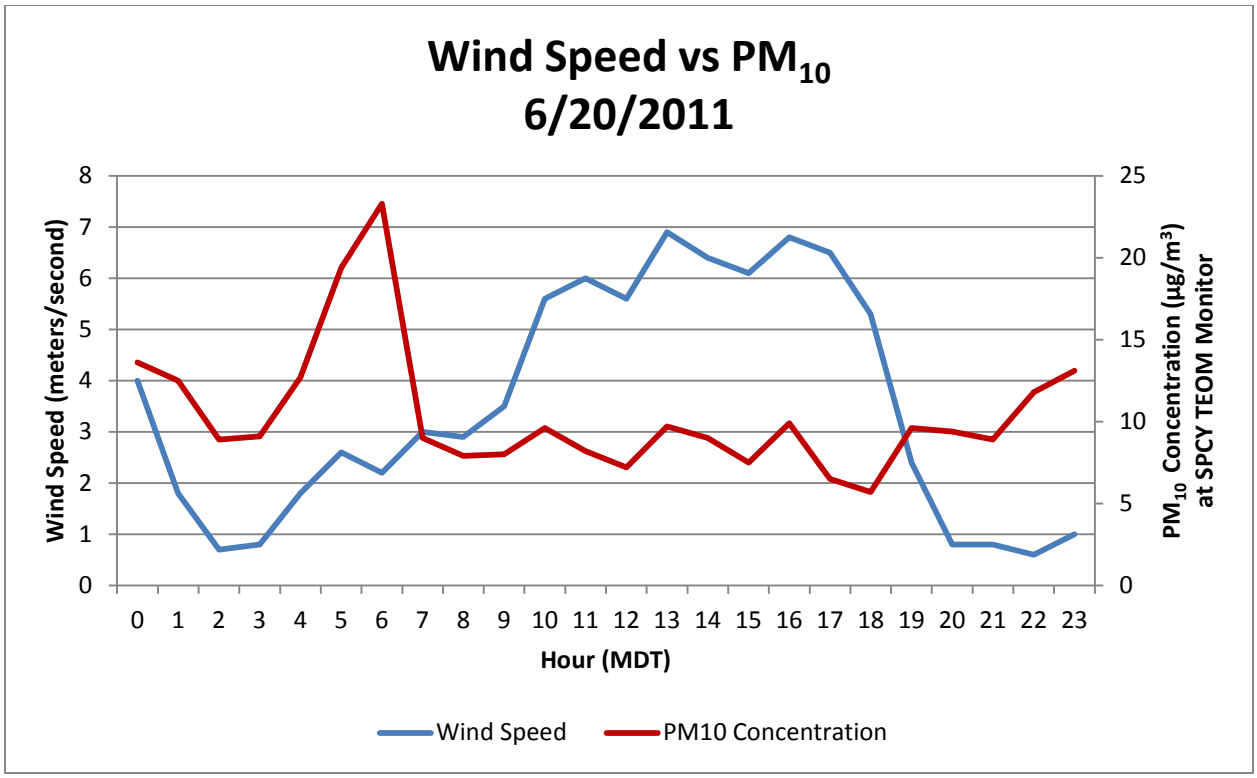

Figure 30-125. Wind speed in meters per second vs. hourly PM_{10} concentrations at the SPCY TEOM monitor. The PM_{10} peaks shown in the morning and late night are inversely correlated with wind speed.

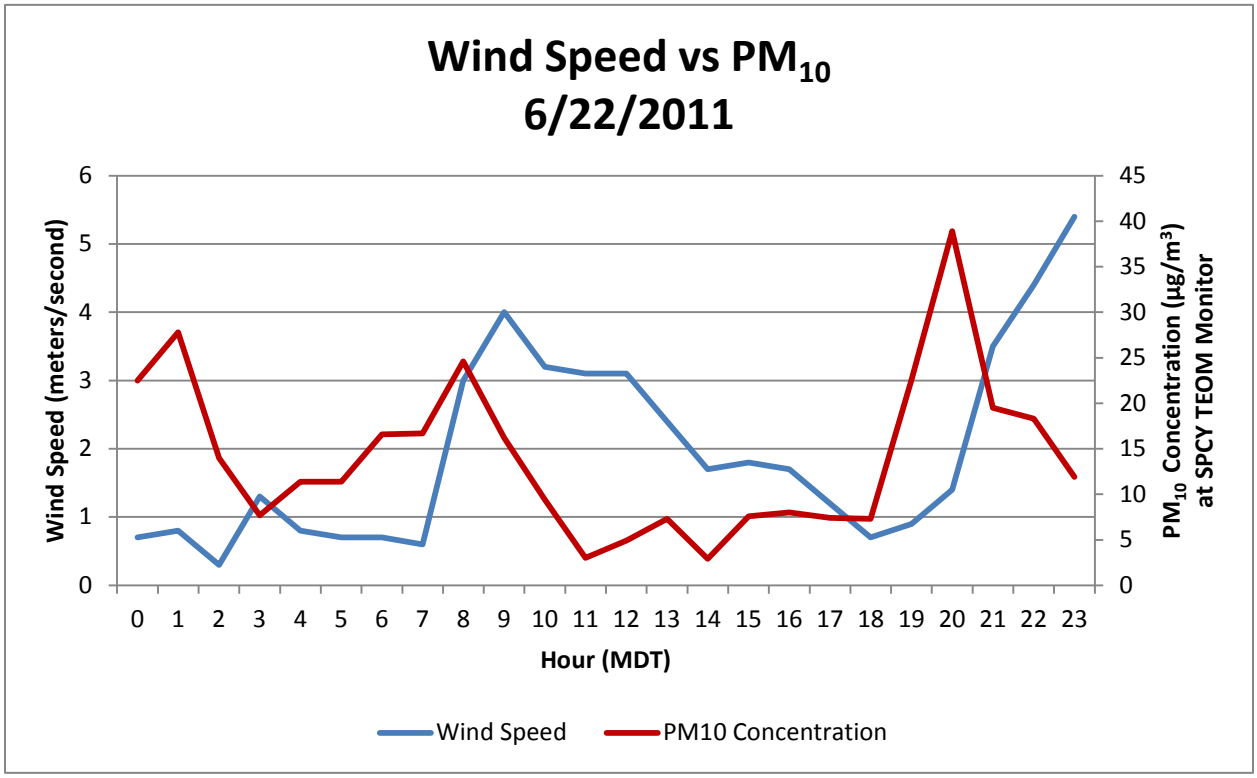

Figure 30-126. Wind speed in meters per second vs. hourly PM_{10} concentrations at the SPCY TEOM monitor. The PM_{10} peaks shown in the morning and evening are inversely correlated.

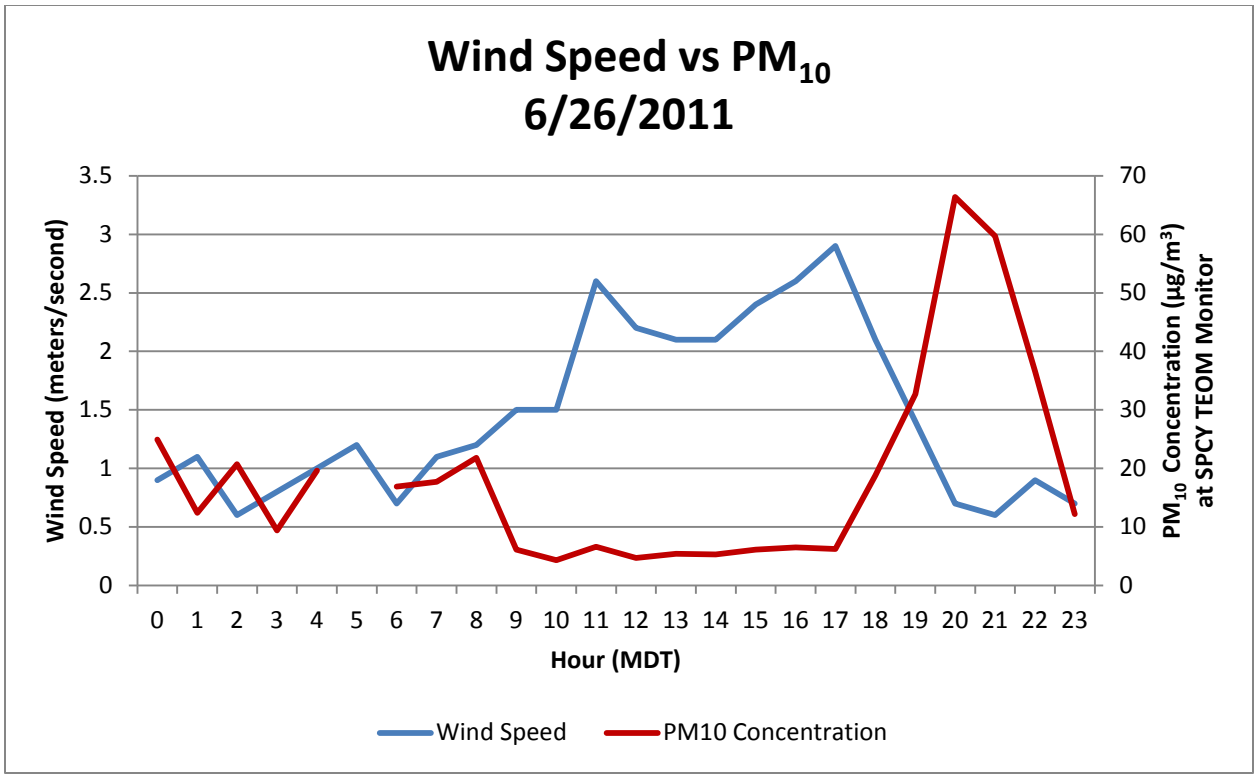

Figure 30-127. Wind speed in meters per second vs. hourly PM_{10} concentrations at the SPCY TEOM monitor. The PM_{10} peaks in the morning and late evening is correlated with wind speed. The small peak in the late morning correlates directly with wind speed.

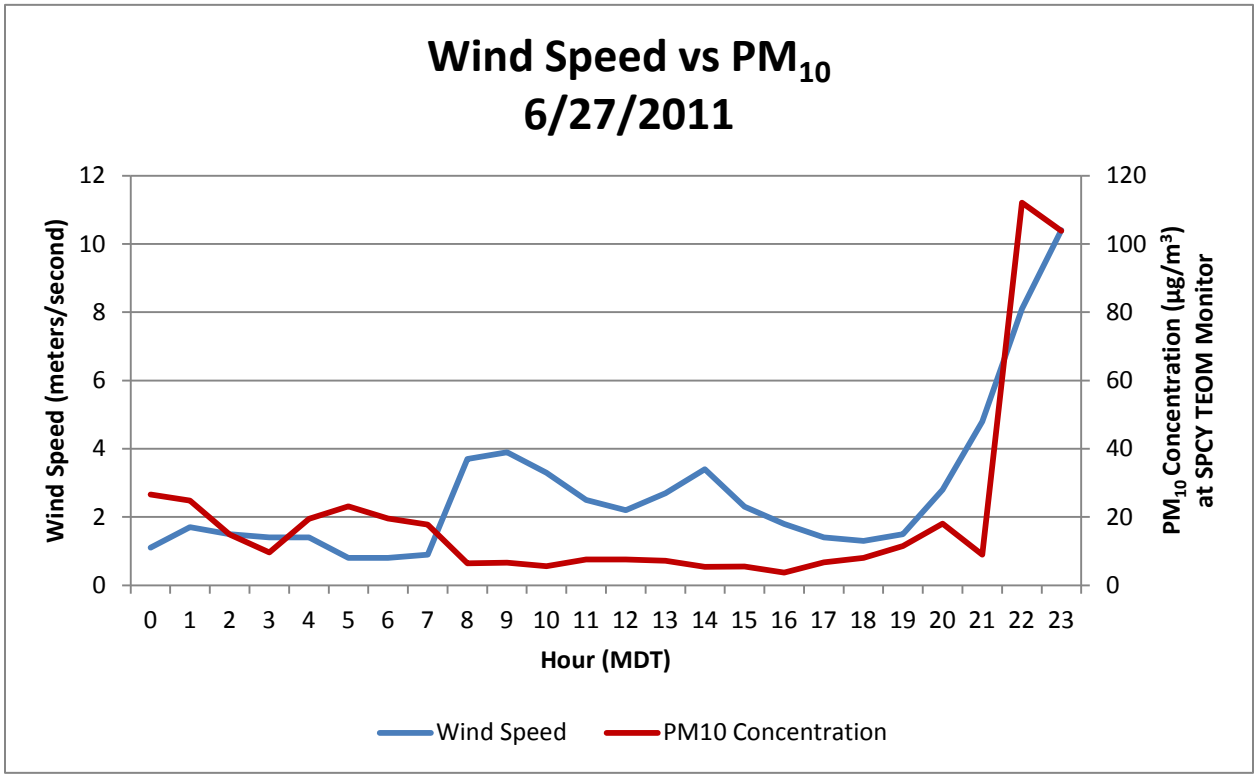

Figure 30-128. Wind speed in meters per second vs. hourly PM_{10} concentrations at the SPCY TEOM monitor. The PM_{10} peak in the late evening is roughly directly correlated with wind speed, which does not follow the expected pattern. As Figure 30-133 shows, the winds were multidirectional, but westerly winds likely blew smoke in from the Horseshoe 2 fire area.

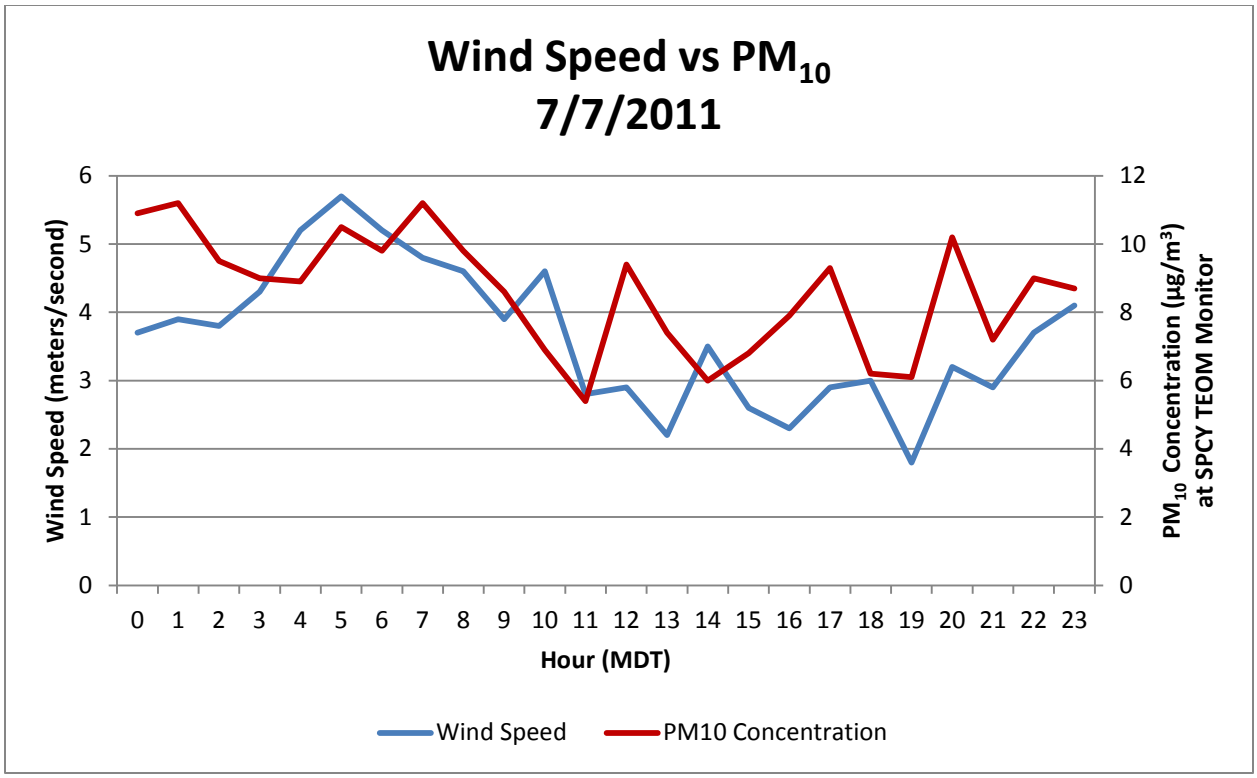

Figure 30-129. Wind speed in meters per second vs. hourly PM_{10} concentrations at the SPCY TEOM monitor. Wind speeds and PM_{10} concentrations are fairly erratic, but are generally directly correlated (except for the early morning hours) but delayed.

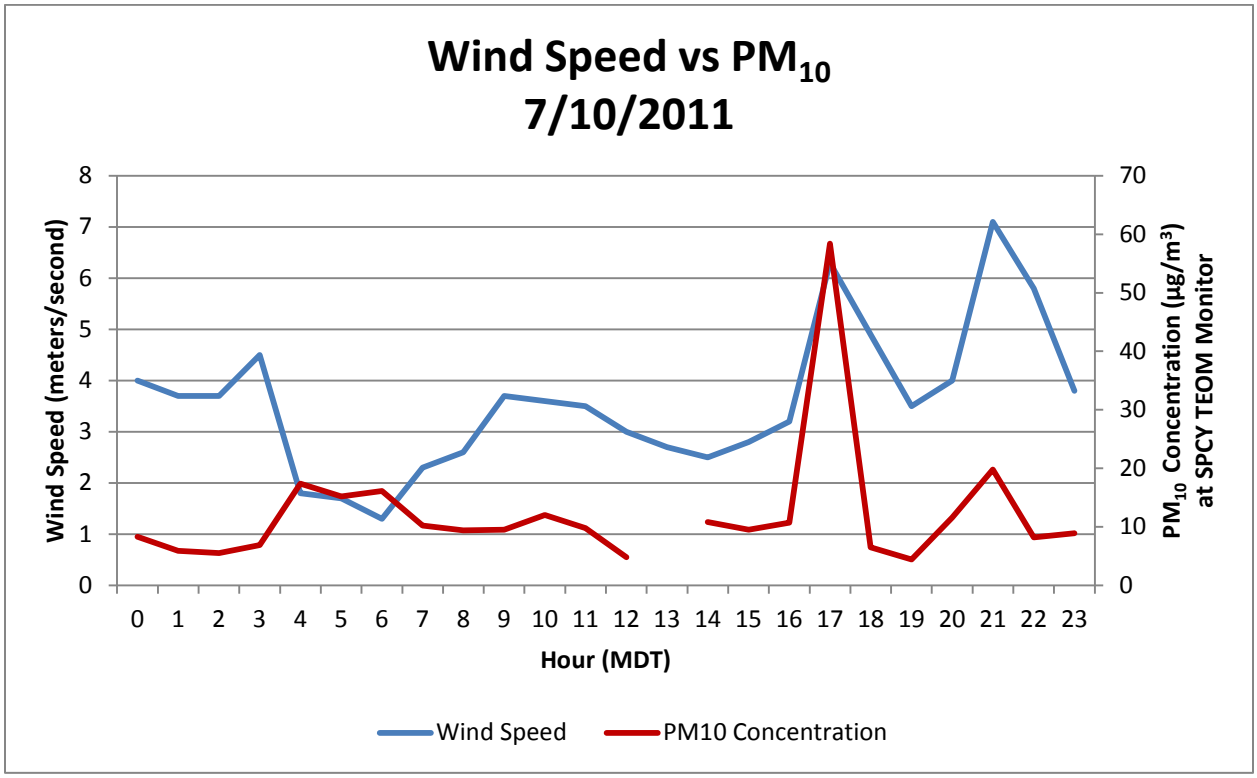

Figure 30-130. Wind speed in meters per second vs. hourly PM_{10} concentrations at the SPCY TEOM monitor. The PM_{10} peak shown in the middle of the day is directly correlated with wind speed.

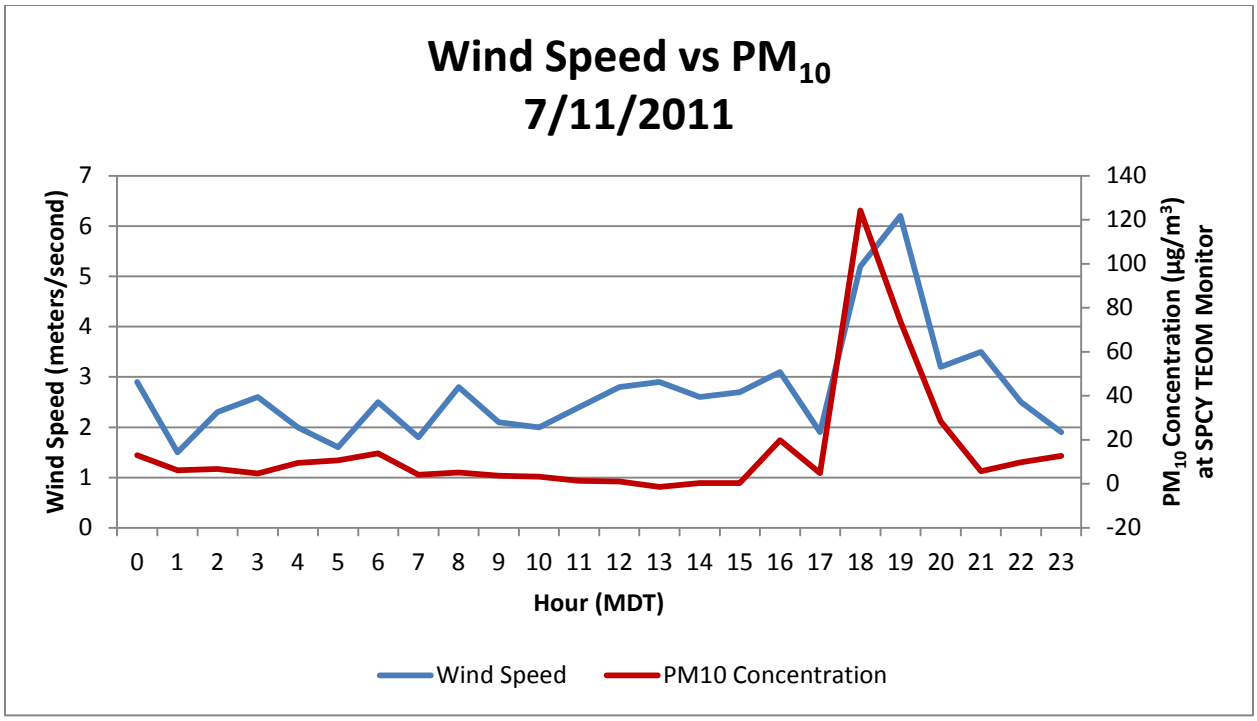

Figure 30-131. Wind speed in meters per second vs. hourly PM_{10} concentrations at the SPCY TEOM monitor. The PM_{10} peak shown in the late afternoon/early evening is directly correlated with wind speed.

The exceptions noted in the captions for May 31 and June 27 can be explained by smoke being blown in from the general direction of fires. 500 mb isobar maps from the National Weather Service are shown in Figures 30-132 to 30-133 for these two dates.

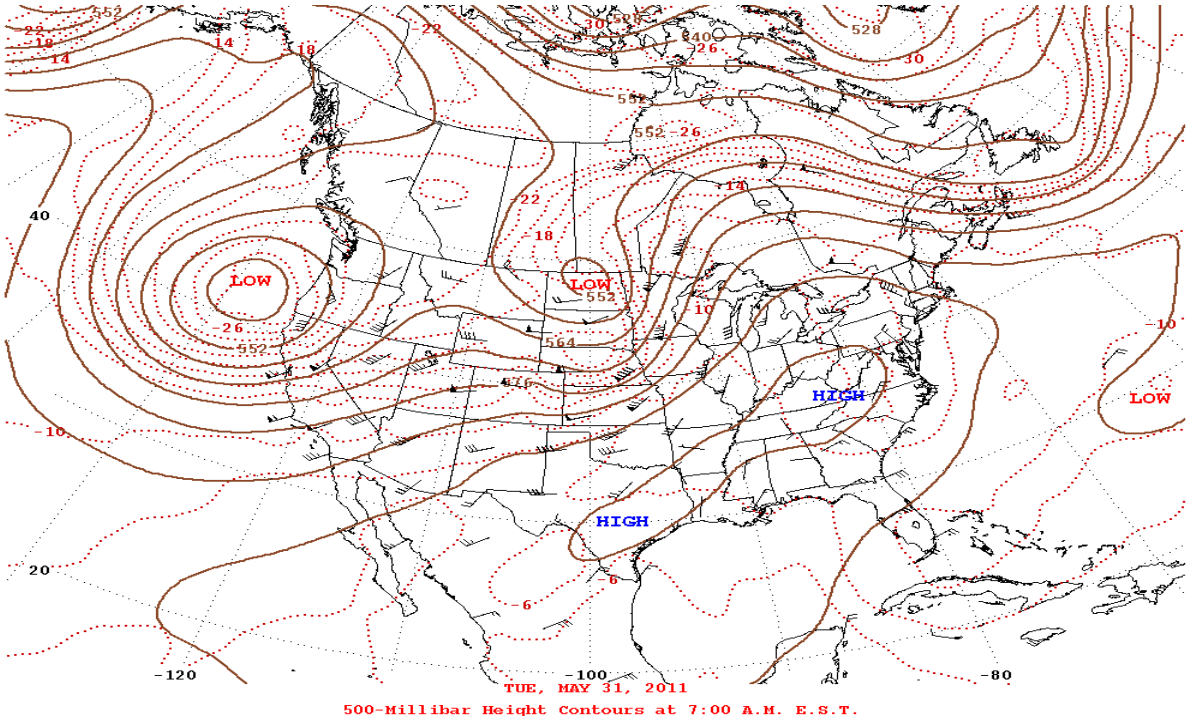

Figure 30-132. National Weather Service map for May 31, 2011, showing southwesterly winds blowing smoke from fire areas in northern Mexico toward the Sunland Park area.

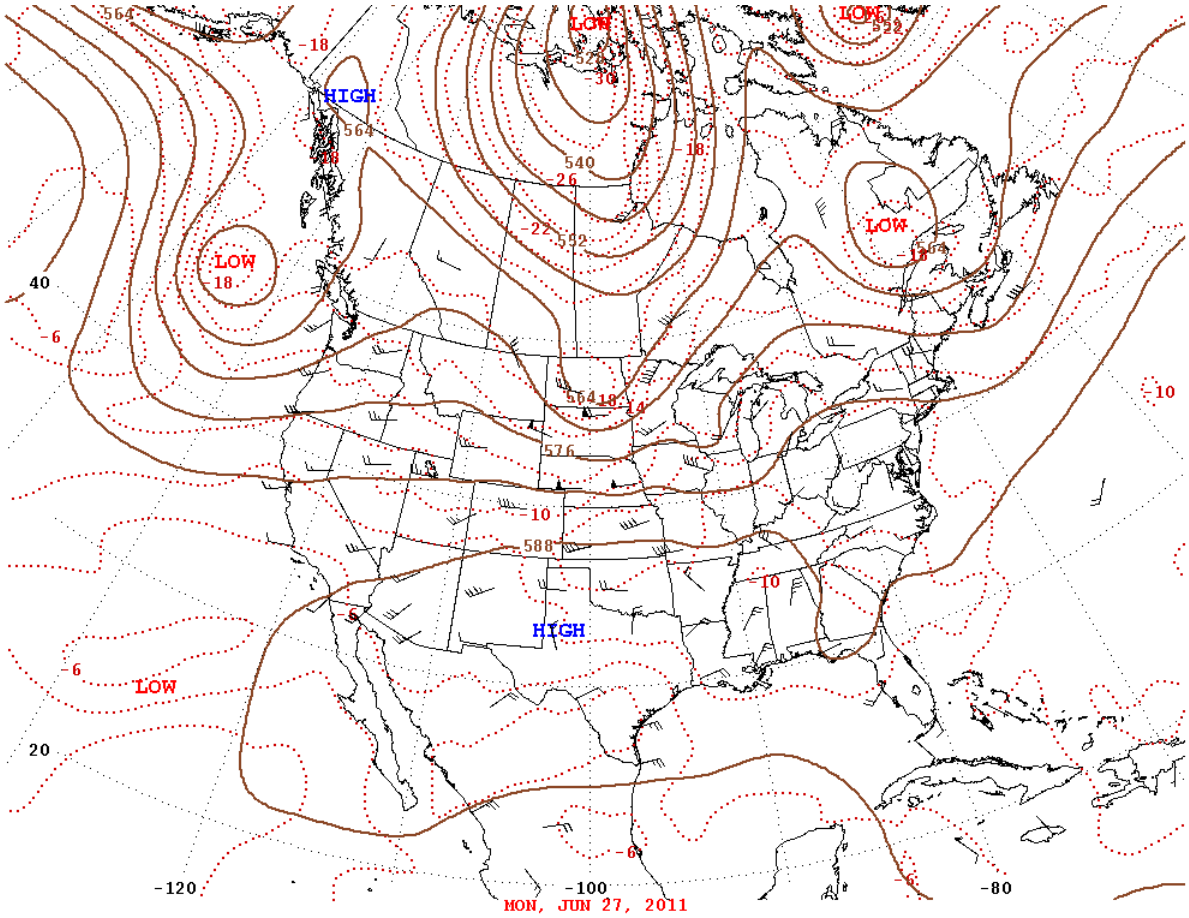

Figure 30-133. National Weather Service 500-mbar map for June 27, 2011 showing multidirectional winds.

30.5 Affects Air Quality

Smoke undoubtedly affected air quality on all dates listed in Table 30-1, as each of these dates had a smoke impact. The NM Border Air Quality Blog confirms that air quality was affected (DuBois, 2011).

30.6 Natural Events

The Clear Causal Relationship and not Reasonably Controllable or Preventable analyses show that these were natural events caused mainly by wildfire smoke. Although 79% of the fires were attributable to human actions, natural conditions (including extreme drought conditions, winds, and remote or rugged terrain) in many fire locations make control of these fires very difficult.

30.7 No Exceedance but for the Event

As the previous sections of this chapter have shown, the exceedances shown in Table 30-1 were caused by natural events of a very active wildfire season in Arizona, New Mexico and northern Mexico, which put significant amounts of smoke (and therefore $PM_{2.5}$) into the atmosphere when low winds and cooling land mass caused increases in particle concentrations near the ground, or

when moderate winds caused smoke to be blown into the valley. The only other possible source for $PM_{2.5}$ would have been from Ciudad Juarez as reports to EPA have previously shown and which were not analyzed for this demonstration. Therefore, the SPCY $PM_{2.5}$ Partisol monitor would have had not recorded these annual exceedances but for the smoke during the fire season.